ADAPTIVE COORDINATED VOLTAGE CONTROL ALGORITHM FOR GRID-TIED PHOTOVOLTAIC INTEGRATION IN A RURAL DISTRIBUTION FEEDER USING THE OPEN DISTRIBUTION SYSTEM SIMULATOR (OPENDSS): A CASE STUDY OF MURANG'A DISTRIBUTION FEEDER

Naomi Muthoni Kamunya

A Thesis Submitted in Partial Fulfillment of the Requirements for the Degree of Master of Technology in Electrical & Electronics Engineering of Murang'a University of Technology

August, 2026

DECLARATION

Student Declaration

I hereby declare that this thesis is my original work and to the best of my knowledge has not been presented for a degree award in this or any other university. I understand what plagiarism is, and I am aware of the university's policy on this. I understand that any false claim regarding this work shall result in disciplinary action in accordance with the University Anti-Plagiarism Policy.

_____ _____

Naomi Muthoni Kamunya Date:

EN400/5795/2022

Supervisor's Approval

The undersigned certify that they have read and hereby recommended for acceptance of Murang'a University of Technology a thesis entitled "**Adaptive Coordinated Voltage Control Algorithm for Grid-Tied Photovoltaic Integration in A Rural Distribution Feeder Using the Open Distribution System Simulator (OPENDSS): A Case Study of Murang'a Distribution Feeder**".

_____ _____

Prof. Eng. Christopher Maina Muriithi, Date:

Department of Electrical and Electronic Engineering,

Murang'a University of Technology.

_____ _____

Dr. David Kimemia, Date

Department of Electrical and Electronic Engineering,

Murang'a University of Technology.

DEDICATION

I dedicate this research thesis to my son John Karoki, a fellow aspiring electrical engineer. May your journey in this noble field be filled with discovery, innovation, and purpose. And to my family, whose endless love and sacrifices made this research possible.

ACKNOWLEDGEMENT

I give thanks to the Almighty God for His mercies, good health, strength, wisdom, and grace which enabled me to successfully complete this Thesis. His faithfulness has sustained me throughout this academic journey.

My sincere gratitude goes to my supervisors, Prof. Eng. Christopher Maina Muriithi and Dr. David Kimemia, for their invaluable guidance, insightful feedback, constructive criticism, and steadfast commitment to this research. Their expertise and mentorship greatly contributed to the successful completion of this work.

I am grateful to my colleagues in the postgraduate Programme Amon, Job, Muragu, Leah, Jonathan and Anthony for the stimulating discussions, shared knowledge, that enriched my studies.

I extend my appreciation to Reverend Joseph Munga for his spiritual guidance, prayers, and words of encouragement, and to my dear friend Gracemary for her friendship, kindness, prayers, and unwavering presence during the demanding moments of my studies.

Above all, I am deeply grateful to my husband, Mr. Gachie, for his love, patience, understanding, and steadfast commitment. I also cherish the love and patience of my children, Sophie, John, and Eunice, whose understanding and encouragement inspired me to persevere and remain focused. Special thanks go to my sisters, Alice, Ruth, and Ann, for their love, prayers, patience, and belief in me. Your constant presence and reassurance have been a source of strength and comfort. Finally, I acknowledge with gratitude everyone who contributed in one way or another to the completion of this Thesis. May the Almighty God richly bless you all.

ABSTRACT

The increasing penetration of photovoltaic (PV) systems into rural distribution networks presents a critical engineering challenge in maintaining statutory voltage performance and grid compliance. The central problem addressed is that uncoordinated high-penetration PV integration on a long, high resistance-to-reactance (R/X) radial feeder induces substantial reverse power flow and daytime voltage rise that generic, voltage-triggered commercial inverter controls do not detect, because the resulting voltages remain below their default activation thresholds. In radial networks such as the 69 km, 11 kV Murang'a distribution feeder in Kenya, high R/X ratios and a temporal mismatch between peak midday solar generation and minimum daytime consumer demand create significant operational stress. Without active control, uncoordinated PV integration exports surplus active power to the primary substation, raises midday nodal voltages towards the upper statutory boundary, and increases the mechanical duty imposed on the substation on-load tap changer (OLTC). To investigate this, a digital twin of the feeder, comprising 158 medium-voltage buses and 92 distribution transformers, was developed in OpenDSS and validated against utility field measurements at three monitored nodes, yielding a mean absolute percentage error (MAPE) of 0.68 % and a root-mean-square error (RMSE) of 0.0066 p.u. (0.70 %), both within the 2 % acceptance criterion adopted in this study. Quasi-Static Time-Series (QSTS) simulations at a one-minute resolution (1,440 steps per 24 h day) evaluated three standardized scenarios: Scenario A (baseline, no PV), Scenario B (3 MW PV, uncontrolled) and Scenario C (3 MW PV, coordinated control). 2Scenario B produced a peak reverse power flow of 0.93 MW at the substation and a maximum nodal voltage of 1.038 p.u., which represents pronounced voltage rise while remaining below the 1.05 p.u. upper limit adopted in this study; the evening minimum voltage of 0.912 p.u. at the feeder extremity is a pre-existing, load-driven condition that occurs when PV output is essentially zero. A context-specific, coordinated Volt-VAR and Volt-Watt smart inverter control strategy was then designed, in which Volt-VAR acts as the primary reactive-power response and Volt-Watt as the secondary active-power response. In Scenario C the coordinated controller reduced peak reverse power flow by 62.3 % (from 0.93 MW to 0.35 MW), limited the maximum nodal voltage to 1.024 p.u., maintained all monitored buses within the adopted 0.95–1.05 p.u. band throughout the PV generation window, and reduced OLTC operations from 28 to 8 per day (71.4 % fewer than Scenario B and 33.3 % fewer than Scenario A). This operational improvement was obtained at a technical energy trade-off of approximately 1,500 kWh of curtailed solar energy per day, that is, renewable energy sacrificed for grid benefit. The study therefore develops and evaluates a coordinated Volt-VAR/Volt-Watt control framework on a validated model of a real Kenyan rural distribution feeder and demonstrates its potential to mitigate reverse power flow, maintain voltage compliance and reduce OLTC operations under the investigated PV scenarios.

TABLE OF CONTENTS

DECLARATION ..... **ii**
DEDICATION ..... **iii**
ACKNOWLEDGEMENT ..... **iv**
ABSTRACT ..... **v**
LIST OF TABLES ..... **ix**
LIST OF FIGURES ..... **x**
ACRONYMS AND ABBREVIATIONS ..... **xi**
CHAPTER ONE: INTRODUCTION **1**
1.1 Background of the study 1
1.1.1 Voltage Regulation (V.R) 1
1.1.2 Voltage Drop 2
1.1.3 Insulation and Clearance Requirements 3
1.1.4 Technical Line Losses and Revenue Degradation 3
1.1.5 Network Anomalies, Variations and Protection Constraints 4
1.1.6 Essence of Coordinated Voltage Control Strategy 5
1.2 Problem statement 6
1.3 Research Objectives 8
1.3.1 Main Objective 8
1.3.2 Specific Objectives 8
1.4 Significance of the Study 8
1.4.1 Practical and Operational Significance 9
1.4.2 Academic and Geographical Contribution 9
1.4.3 Regulatory, Policy and Standard compliance. 10
1.4.4 Socio-Economic Benefit to Consumers 10
1.5 Scope of the Study 10
1.6 Assumptions of the Study 11
1.7 Limitations of the Study 12
1.8 Contributions of the Thesis 12
1.9 Organization of the Thesis 13
CHAPTER TWO: LITERATURE REVIEW **15**
2.1 Introduction 15
2.1.1 Characteristics and Challenges of Rural Distribution Feeders 15
2.1.2 Topological and Structural Differences from Urban Networks 15
2.1.3 The Technical Significance of the High R/X Ratio 16

2.1.4 Power quality challenges in rural feeders 16
2.1.5 Impact of Photovoltaic Integration on Distribution Networks 18
2.1.6 Adverse Impacts and Operational Challenges 19
2.1.7 Overvoltage, the Most Prominent Challenge 19
2.1.8 Voltage Fluctuations from Solar Intermittency 19
2.2 The Concept of Feeder Hosting Capacity 20
2.2.1 Techniques for voltage control in feeders with PV integration 21
2.2.2 Legacy Voltage Control Mechanisms and Limitations 21
2.2.3 Advanced Voltage Control using Smart PV Inverters 22
2.2.4 Coordinated Control Strategies for Active Distribution Networks 23
2.3 Modelling and Simulation Tools for Feeder Analysis 25
2.3.1 Overview of Distribution System Analysis Tools 25
2.3.2 Justification for the Open Distribution System Simulator (OpenDSS) 26
2.3.3 Best Practices for Quasi-Static Time-Series (QSTS) Simulation 27
2.4 Chapter Summary 28
CHAPTER THREE: RESEARCH METHODOLOGY 31
3.1 Introduction 31
3.2 Research Analytical Approach 32
3.3 Research Design 33
3.4 Data Collection and Sources 36
3.5 Problem Formulation – Feeder Modelling and Baseline Analysis 38
3.5.1 Feeder Modelling in OpenDSS 39
3.5.2 Model Validation 42
3.5.3 Development of the Digital twin of Murang'a Feeder 45
3.5.4 Model Validation It involves: 46
3.5.5 Evaluation of Baseline Voltage It involves three areas: 46
3.6 Simulation Scenarios and Baseline Analysis 47
3.6.1 Solution Development – Design of the Voltage Control Scheme 50
3.6.2 Parameterization and Justification of Control Setpoints 52
3.6.3 Volt-VAR Control Design 53
3.6.4 Parameterization of the Volt-VAR Control Law 55
3.6.5 Volt-Watt Control Design 58
3.6.6 Coordination and Curtailment Calculation 60
3.6.7 Implementation in OpenDSS 63
3.7 Validation – Performance Evaluation 64
3.7.1 Definition of Key Performance Indicators (KPIs) 64

3.7.2 Validation Simulation Scenarios 67
3.8 Comparative Analysis 67
3.9 Sensitivity Analysis 68
3.10 Chapter Summary 71
CHAPTER FOUR: RESULTS AND DISCUSSION 72
4.1 Introduction 72
4.2 Baseline Performance and Uncontrolled PV Integration 79
4.2.1 Baseline Feeder Performance (Scenario A, Without PV) 79
4.2.2 Analysis of Baseline Feeder performance 85
4.2.3 Uncontrolled PV Integration Scenario 86
4.3 Diagnosis of the Observed Voltage Sensitivity of the Feeder 87
4.4 Performance of the Adaptive Coordinated Control Strategy 89
4.4.1 Reverse Power Flow Mitigation 89
4.4.2 Voltage Profile Improvement 91
4.4.3 Reactive Power Response 94
4.5 Energy Curtailment Analysis 100
4.6 Legacy Asset Mechanical Duty 103
4.7 Seasonal Robustness Assessment 106
4.8 Rainy Season Performance 107
4.9 Discussion of Results 115
4.9.1 Digital Twin and Baseline Feeder Performance (Objective i) 115
4.9.2 Coordinated Controller Development and Behaviour (Objective ii) 116
4.9.3 Performance under High PV Penetration (Objective iii) 116
4.9.4 OLTC Duty (Objective iv) 117
4.9.5 Integration with Previous Studies 117
4.10 Chapter Summary 121
CHAPTER FIVE: CONCLUSION, RECOMMENDATIONS AND FUTURE WORK 122
5.1 Conclusion 122
5.2 Recommendations 123
5.3 Future Work 124
REFERENCES 126
APPENDICES 135

LIST OF TABLES

Table 3.1: Classification of data sources 36
Table 3.2: Model Validation at Peak load (Hour 18, 15 March 2025) 42
Table 3.3: Definition of the standardized simulation scenarios 47
Table 3.4: Implemented Volt-VAR and Volt-Watt control parameters 55
Table 3.5: Mapping of key performance indicators to the specific objectives 64
Table 3.6: Sensitivity analysis design 68
Table 4.1: Simulation Scenario Matrix and Parameters 72
Table 4.2: Structured and Architectural Parameters of the Validated Rural Feeder 75
Table 4.3: Coordinate points Mapping for OpenDSS Smart Inverter Tracking Curves 77
Table 4.4: Comprehensive Network and Mitigation Metrics 80
Table 4.5: Hourly Powerflow and Midday PV Matrix 83
Table 4.6: Substation OLTC Tap Operations Matrix over a 24-Hour Horizon 104
Table 4.7: Seasonal Sensitivity and Control Performance Metrics 112
Table 4.8: Summary of Research Objective Validation 118

LIST OF FIGURES

Figure 3.1: Research Methodology Flow Diagram 34
Figure 3.2: Single Line Diagram of 11kv Distribution Feeder 40
Figure 3.3: Digital Twin Diagram Of 11KV Feeder 45
Figure 3.4: Volt-VAR Control Characteristic 54
Figure 3.5: Volt-Watt Control Characteristic Curve 59
Figure 3.6: Proposed Coordinated Volt-VAR / Volt-Watt Controller Architecture 62
Figure 4.1: 24 Hour Load Profile of Murang'a Feeder Showing Peak and Minimum Demand 80
Figure 4.2: Coordinated Volt-VAR and Volt-Watt Strategy in Mitigating Substation Reverse Power Flow 90
Figure 4.3: Impact of PV integration and Control on the end of line voltage 92
Figure 4.4: Programmed Smart Inverter Parameter Configurations 95
Figure 4.5: Dynamic Inverter Reactive Power Response (Bus 87) over 24 Hours 98
Figure 4.6: PV Output and curtailment Profile 100
Figure 4.7: Rainy Season PV Bus Voltage Profile 107
Figure 4.8: Substation Power Profile During Rainy Season 109

ACRONYMS AND ABBREVIATIONS

ACSR	Aluminum Conductor Steel Reinforced
ANSI	American National Standards Institute
DER	Distributed Energy Resource
EPRI	Electric Power Research Institute
EPRA	Energy and Petroleum Regulatory Authority (Kenya)
GHI	Global Horizontal Irradiance
HC	Hosting Capacity
IEC	International Electrotechnical Commission
IEEE	Institute of Electrical and Electronics Engineers
KPI	Key Performance Indicator
KPLC	Kenya Power and Lighting Company
MAPE	Mean Absolute Percentage Error
MV	Medium-Voltage
NACOSTI	National Commission for Science, Technology and Innovation
OLTC	On-Load Tap Changer
OpenDSS	Open Distribution System Simulator
PV	Photovoltaic
QSTS	Quasi-Static Time-Series
RMSE	Root-Mean-Square Error
RPF	Reverse Power Flow
R/X	Resistance-to-Reactance Ratio
RDN	Radial Distribution Network
SLD	Single-Line Diagram
TMY	Typical Meteorological Year
VAR	Volt-Ampere Reactive
V.R.	Voltage Regulation
VUF	Voltage Unbalance Factor

CHAPTER ONE
INTRODUCTION

1.1 Background of the study

In rural power systems, voltage instability is a daily operational reality that directly impacts energy quality, system reliability, and consumer satisfaction. In rural and peri-urban distribution feeders operated by the Kenya Power and Lighting Company (KPLC)—such as the representative Murang'a distribution network, fluctuating load profiles and limited real-time regulation capabilities cause severe voltage and current imbalances. Little research has previously quantified these challenges on actual Kenyan feeders using validated time-series simulations. These operational instabilities impair power quality, reduce system efficiency, elevate outage risks, and cause equipment damage and economic losses.

Integrating distributed energy resources (DERs), particularly photovoltaic (PV) systems, presents a viable mitigation strategy to improve voltage performance and reduce grid stress. However, high-penetration PV integration also introduces new system complexities that require proper management to avoid power grid instability [1]. The maximum level of distributed generation that a network can safely accommodate without violating voltage limits or operational constraints defines its Hosting Capacity (HC). Addressing key issues such as voltage variations, current disturbances, and operational inefficiencies on the representative Murang'a feeder requires designing and validating context-specific voltage control strategies [2]. This research achieves this by developing a validated baseline digital twin model to quantify network vulnerabilities and subsequently designing an effective engineering solution to optimize overall grid reliability and performance.

1.1.1 Voltage Regulation (V.R)

As indicated by previous research, voltage supply networks should be maintained within strict limits, typically ±5% of nominal voltage, despite continual changes in load demand [2].

Introducing PV systems at distributed points can support voltage regulation efforts, smoothing potential fluctuations and enhancing acceptable voltage performance and grid compliance early in the operational cycle [3]. However, under fluctuating load demands and highly variable environmental conditions, most rural electrical energy distribution networks exhibit structural deficiencies in maintaining voltage levels within this recommended ±5% tolerance of nominal voltage. It is noted that to maintain efficient equipment operation, the electrical supply must be securely stabilized [3].

The integration of distributed energy resources (DERs) into the localized supplied energy system transforms traditional loads into active power supplies, creating bidirectional power flows [1]. This complexity fundamentally challenges voltage and current control, especially within distribution networks [4]. It is reported that voltage regulation of a line represents the difference between the received end voltage drop under load and the no-load condition reflecting full voltage at sending end [5]. The increase of the transmission voltage level for the same power transfer reduces proportionally with suppression of line impedance (Z) as the voltage regulation improvement ideally decreases [6]. To realize the effect of PV systems potential on grid stability, the current study investigated the dynamically fluctuating voltage to complement load profiles for improved voltage and current regulation.

1.1.2 Voltage Drop

It is noted that as electrical energy flows through transmission and distribution lines, the voltage decreases primarily due to the inherent impedance of the conductors [7]. This voltage drop becomes more significant over longer distances, often resulting in insufficient voltage levels at the consumer end, which can negatively impact electrical devices [8].

Effective mitigation strategies to resolve voltage drops caused by conductor impedance over long transmission distances have historically been inadequate along rural feeders, frequently leading to insufficient end-user voltage and potential degradation of equipment performance efficiency. However, the Incorporation of photovoltaic (PV) systems distributed along the network is found to reduce voltage drops by supplying local power.

This integration significantly improves voltage profiles and reduces the cumulative operational stress on long feeder lines [9].

1.1.3 Insulation and Clearance Requirements

Research indicated that higher operating voltages necessitate enhanced insulation materials and increased clearance between conductors and the ground to prevent electrical arcing and breakdown. Inadequate insulation on rural distribution system increases risks of leakage current fault, energy losses and safety hazards while simultaneously reducing equipment lifespan; and raising infrastructure development and maintenance costs [10].

Localized power delivery provided by the integration of PV sources was found to potentially reduce the necessity for high-voltage infrastructure within specific network sections [11]. This proportionally optimized the insulation resistance, which resonates with varying polarization and moisture levels in the insulation around conducting sections as the aging of the material advances. To resolve these factors, the enhancement of the standardized supply was investigated to monitor the properties of the cylindrical conductor outer insulation resistance (IR)to minimize electrical arcing and insulation breakdown for the protection of human and wildlife safety.

1.1.4 Technical Line Losses and Revenue Degradation

Transmission and distribution line losses are majorly contributed by the current flowing through resistive conductors, which increases as load capacity, transmission distances, conductor sizes, and environmental temperatures rise [12]. IEEE 738 and IEC 60287 provide methodologies for evaluating conductor temperature and current-carrying capacity under various operating conditions. In practical utility asset management, conductor aging is also considered because prolonged thermal and mechanical stresses can gradually affect conductor performance, reliability, and remaining service life [13]. As a fundamental rule of electrical engineering, active power losses in conductors are directly proportional to the square of the line current. These losses can significantly reduce overall system efficiency, particularly in rural distribution networks carrying high currents over extensive radial paths [14]. Conversely, a targeted reduction of line current magnitudes achieved through localized solar PV power injection to supply local consumer

demand directly leads to a substantial drop in technical energy losses and protects utility revenue streams [15].

1.1.5 Network Anomalies, Variations and Protection Constraints

The integration of high-penetration solar photovoltaic (PV) sources near consumer receiving-end locations transforms the traditional unidirectional distribution grid paradigm into a highly complex bidirectional environment [16]. During peak daylight hours, localized solar generation frequently aligns with the rural network's lowest residential demand valley, creating a severe power surplus at the grid extremities [17]. This temporal mismatch forces excess active power to back feed upstream into the primary substation via reverse power flow pathways [18]. This sustained back feeding subjects primary substation transformers to elevated thermal stresses, accelerates insulation aging matrix degradation, and induces severe line sag risks across long overhead distribution conductors [19].

Furthermore, introducing decentralized, inverter-based distributed energy resources fundamentally alters the established fault current profiles and short-circuit capacities across the radial topology [20]. Traditional protection grading schemes rely heavily on predictable, high-magnitude unidirectional fault currents to trip overcurrent relays, fuses, and reclosers [21]. However, modern grid-tied inverters exhibit strict internal current-limiting characteristics during symmetrical and asymmetrical grid faults, contributing transient fault currents that rarely exceed 1.2 to 1.5 times their rated output [22]. This limited fault contribution can cause protective relay blinding, sympathetic tripping of adjacent healthy lines, and desensitization of downstream fuses, directly compromising the overall safety and structural reliability of the utility's protection network [23].

Finally, unequal spatial allocation of single-phase solar PV installations combined with fluctuating consumption profiles across the feeder causes severe voltage and current imbalances between the three individual phases [24]. These systemic phase unbalances force elevated currents to flow continuously through the neutral conductor, increasing localized ground potential rises and aggravating stray voltage risks [25]. Concurrently, uncompensated reactive power components along the 69-kilometer overhead line degrade

the cumulative network power factor, accelerating line capacity utilization and compounding utility revenue losses [26]. Because all of these compounding anomalies ranging from thermal transformer degradation and protection desensitization to neutral current inflation are physically driven by unmanaged voltage profiles at the point of common coupling, implementing a fast-acting, adaptive voltage control framework via smart PV inverters serves as the primary engineering safeguard to stabilize the active distribution system [27].

This research therefore designs and evaluates an OpenDSS-based adaptive coordinated Volt-VAR and Volt-Watt smart inverter control framework to regulate network voltage profiles, suppress reverse power flow and reduce the mechanical duty imposed on the substation OLTC of the Murang'a rural distribution feeder.

1.1.6 Essence of Coordinated Voltage Control Strategy

The essence of the coordinated voltage control strategy is to provide a fast-acting, decentralized "non-wires" safeguard that dynamically balances real and reactive power at the point of common coupling. By prioritizing Volt-VAR reactive power absorption and using Volt-Watt active power curtailment as a secondary layer, the controller prevents voltage rise, mitigates reverse power flow, and reduces mechanical wear on legacy substation tap changers without requiring capital-intensive grid upgrades.

In a grid-connected radial distribution feeder, local active power imbalances between feeder load demand (P_{load}) and distributed PV generation (Pgen) govern the net magnitude and direction of feeder power flow, which directly dictates the localized nodal voltage profile along high resistance-to-reactance (R/X) line segments:

- **Condition 1:** Balance Grid condition ($\boldsymbol{P_{load} = P_{gen}}$) -Local active power generation closely matches consumer demand along the feeder segment. Net feeder active power draw from the primary substation is minimal, resulting in a stable voltage profile within nominal operating bounds. The coordinated smart inverter remains dormant inside its programmed deadband.

- **Condition 2:** Generation Surplus condition $\boldsymbol{P_{gen} > P_{load}}$ – Peak midday solar generation coincides with the low daytime residential demand valley. The local power surplus forces active power to flow in reverse back toward the primary substation. Along high R/X overhead lines, this reverse power flow induces localized voltage rise toward the upper statutory limit. The coordinated controller activates Volt-VAR to absorb reactive power, followed by Volt-Watt active power curtailment if needed, to contain the voltage rise and suppress net power back feed.
- **Condition 3**: Load Exceeds Generation $P_{load} > P_{gen}$ — Occurs during evening peak demand (e.g., Hour 18) when solar generation drops to zero. High consumer demand causes substantial forward active power draw from the primary substation, inducing end-of-line voltage sags along the radial extremity.

1.2 Problem statement

The rapid proliferation of grid-tied solar photovoltaic (PV) systems in Kenya's rural distribution networks has introduced complex operational challenges that traditional grid architectures are ill-equipped to handle. In the context of the Murang'a 11kV rural distribution feeder, the technical problem is threefold:

First, the Murang'a feeder is characterized by a high resistance-to-reactance (R/X) ratio, long radial sections and a relatively weak electrical profile. These characteristics make the feeder more sensitive to changes in active and reactive power injection than a stiff urban distribution network. Consequently, changes in PV output can produce noticeable variations in nodal voltage, particularly at buses located toward the feeder end. In the uncontrolled 3 MW PV scenario, the maximum nodal voltage reached approximately 1.038 p.u. Although this value remained below the 1.05 p.u. upper operating boundary adopted in this study, it demonstrates the feeder's sensitivity to distributed generation and the potential for voltage constraints as PV penetration increases.

Secondly, the integration of distributed PV introduces a mismatch between local electricity generation and feeder demand. When PV generation exceeds the instantaneous local load, the surplus active power is exported upstream toward the primary substation, resulting in reverse power flow. In the uncontrolled 3 MW PV scenario, the peak reverse

power flow reached 0.93 MW. Such upstream power transfer can increase current circulation and technical losses, alter transformer loading patterns and complicate protection coordination. More importantly, the occurrence of substantial reverse power flow while the feeder voltage remains below the conventional upper voltage limit demonstrates that voltage magnitude alone may not adequately indicate the severity of PV-induced operating stress on a long rural feeder. Thirdly, traditional voltage regulation devices, such as On-Load Tap Changers (OLTCs) and switched capacitors, are mechanical in nature and lack the response speed required to mitigate the high-frequency fluctuations of solar irradiance. Excessive reliance on these legacy devices leads to accelerated mechanical wear and increased maintenance costs for the utility. If unresolved, these issues lead to frequent nuisance tripping, customer complaints, and accelerated aging of substation equipment.

To formally ground the problem, baseline time-series load flow analysis of the unmanaged network quantifies the following severe impacts:

- Daytime voltage rise: midday solar generation raises nodal voltages to 1.038 p.u. at the PV injection nodes. This value is below the 1.05 p.u. upper statutory boundary adopted in this study and therefore does not constitute a statutory violation, but it represents movement towards the upper boundary and remains below the default activation thresholds of generic commercial inverter controls (1.04 p.u.), so those controls do not respond.
- Low terminal voltage during the evening demand peak: consumer load peaks depress the voltage at the radial extremity of the feeder to 0.912 p.u. (8.8 % below nominal). This condition is load-driven and occurs when PV output is essentially zero, and it therefore exists in the baseline network independently of PV integration.
- Active power back feed: the temporal load–generation mismatch drives a peak reverse power flow of 0.93 MW through the substation during the peak irradiance window. Reverse power flow, rather than statutory overvoltage, is therefore the dominant PV-induced operating stress on this feeder under the investigated 3 MW scenario.

Consequently, there is an urgent need to design and validate a “non-wires” engineering solution. This research addresses this gap by developing an OpenDSS-based adaptive control framework that utilizes coordinated Volt-VAR and Volt-Watt smart inverter functions to stabilize the voltage profile and align PV output with real-time consumer demand, thereby mitigating reverse power flow, containing daytime voltage rise and reducing OLTC mechanical duty.

1.3 Research Objectives

1.3.1 Main Objective

To design and validate an adaptive coordinated voltage control framework using OpenDSS to improve the voltage performance and operational stability of the Murang’a rural distribution feeder integrated with solar photovoltaic systems.

1.3.2 Specific Objectives

i. To develop and validate a digital twin model of the Murang’a 11 kV rural distribution feeder in OpenDSS and evaluate its baseline voltage performance under PV integration.

ii. To develop an adaptive coordinated control algorithm utilizing smart inverter Volt-VAR and Volt-Watt functions to mitigate daytime voltage rise and reverse power flow and maintain nodal voltages within the limits recommended by IEEE Standard 1547 and the Kenyan Grid Code.

iii. To simulate and evaluate the performance of the proposed control algorithm under high PV penetration scenarios using Quasi-Static Time-Series (QSTS) simulations in OpenDSS.

iv. To assess the impact of the proposed control strategies on the mechanical duty cycle of the substation On-Load Tap Changer (OLTC).

1.4 Significance of the Study

This research is justified by providing an end-to-end engineering framework to mitigate voltage volatility and tap-changer degradation in high-penetration rural distribution

feeders. The significance of this study lies in its dual impact: it delivers actionable operational strategies for distribution utilities while advancing power system control theory through the quantitative validation of localized PV inverter control schemes using OpenDSS co-simulation. Furthermore, it establishes a benchmark for network compliance under grid-code constraints typical of developing distribution infrastructures.

1.4.1 Practical and Operational Significance

From a practical standpoint, this research addresses an immediate operational need for power utilities. By developing a validated model and formally quantifying the performance issues of the Murang'a feeder, this study provides the utility with invaluable, data-driven insight into a real-world network's vulnerabilities. The subsequent design of an effective control scheme using existing smart inverter technology presents a viable and cost-effective ‘’non-wires’’ alternative to traditional grid reinforcement. By leveraging optimized control schemes, the study demonstrates a viable method to contain daytime voltage rise while simultaneously reducing reverse power flow and the mechanical duty imposed on the substation On-Load Tap Changer (OLTC). This approach offers the potential to defer or eliminate the need for immediate capital-intensive infrastructure upgrades such as transformer uprating or conductor replacement. By deploying these custom-tuned droop settings, utilities can effectively defer capital expenditures for rural feeder upgrade.

1.4.2 Academic and Geographical Contribution

This research contributes to power distribution engineering by modeling and validating localized PV voltage control strategies under the high R/X ratios, low short-circuit levels, and severe voltage drops characteristic of long, weak radial feeders. While existing literature predominantly focuses on tightly regulated urban or European/North American networks, this study quantifies the dynamic interaction between smart inverter volt-var/volt-watt response and legacy On-Load Tap Changers (OLTCs) on a rural Kenyan distribution topology. The resulting co-simulation framework in OpenDSS serves as a generalized benchmark for analyzing renewable integration and asset degradation in weak distribution grids across sub-Saharan Africa and similar developing regions.

1.4.3 Regulatory, Policy and Standard compliance.

The findings are highly crucial for policy and regulatory bodies by providing empirically validated data on the performance of strategic inverter functions (such as Volt-VAR and Volt-Watt droop parameters) in high resistance-to-reactance (R/X) ratio grids. This alignment ensures that the utility is provided with a tangible, verifiable engineering solution that meets both local regulatory requirements and international best practices for grid-tied photovoltaic systems. This data-driven framework is essential for the effective enforcement and potential future updating of national grid codes and IEEE 1547-based interconnection standards for decentralized distributed energy resources

1.4.4 Socio-Economic Benefit to Consumers

Ultimately, the study establishes a framework for enhanced power quality and reliability for consumers connected to the Murang'a feeder network. By demonstrating practical methods to maintain stable voltage profiles within statutory bounds, the research directly contributes to a reduction in unplanned utility outages and prevents voltage-related equipment damage, thereby supporting the broader socio-economic stability of the peri-urban region.

1.5 Scope of the Study

The geographical and technical boundaries of this research are strictly delimited to ensure depth and analytical rigor. Geographically, this study is confined to the 11 kV Murang'a rural distribution feeder, spanning an approximate radial length of 69 kilometers. Technical modeling and time-series load flow simulations are conducted exclusively using the OpenDSS (Open Distribution System Simulator) environment. To maintain a focused investigation into medium-voltage grid dynamics, the structural scope is bounded by the following parameters:

- Voltage Level Boundaries: This research is restricted to the primary medium-voltage (MV) distribution network. The study does not model individual low-voltage (LV) consumer circuits or internal household wiring; it terminates at the MV side of distribution transformers. All simulated extremities, including the designated end-of-

line nodes such as Bus 158, are strictly medium-voltage entities within the primary distribution topology.

- Hardware Implementation Exclusions: The development and evaluation of the adaptive control framework are limited to software-based algorithmic validation and time-series co-simulation. Physical hardware implementation, laboratory prototyping of inverter power electronic topologies, and real-time hardware-in-the-loop (HIL) testing fall outside the scope of this study.
- Economic and Financial Exclusions: While the technical strategies developed herein present an inherent "non-wires alternative" capable of deferring capital infrastructure spending, this study does not include formal techno-economic modeling. Detailed net present value (NPV) evaluations, simple payback periods, solar market tariff structures, and utility billing financial analyses are explicitly excluded from the research scope. Consequently, the curtailed PV energy reported in this thesis is presented strictly as a technical energy trade-off and is not monetised.
- Hosting Capacity Exclusion: this study does not determine a formal maximum hosting capacity for the feeder. PV capacity is varied only as a sensitivity parameter around the investigated 3 MW scenario, and no constrained optimization of the maximum admissible PV capacity is performed.

1.6 Assumptions of the Study

This study was conducted under the following assumptions. First, the secondary data supplied by the utility (feeder topology, conductor parameters, distribution-transformer ratings, 24-hour load records and substation measurements) are accurate and representative of the actual operating conditions of the Murang'a 11 kV feeder, and the accuracy of the metering equipment used by the utility is consistent with its stated accuracy class. Second, the OpenDSS solver is assumed to model the unbalanced, multi-phase power flow of the network with numerical accuracy sufficient for distribution-level studies, and its results are comparable to measured field readings within the ±2 % validation tolerance adopted in Section 3.5.2. Third, the aggregated load and PV generation profiles are assumed to be representative of typical daily and seasonal behavior, and the smart-inverter models are assumed to respond to their programmed

Volt-VAR and Volt-Watt control curves without significant communication or measurement delay. Fourth, the irradiance data adopted from the Typical Meteorological Year record for Murang'a County are assumed to be representative of the dry-season and rainy-season days simulated in this study. Finally, the three 1 MW PV plants are assumed to be three-phase, grid-tied installations whose inverters are capable of the Volt-VAR and Volt-Watt functions specified in IEEE Standard 1547-2018.

1.7 Limitations of the Study

The following are limitations of this thesis:

i. No formal maximum hosting capacity was computed. PV capacity was varied only as a sensitivity parameter about the investigated 3 MW case, and no constrained optimization of the admissible PV capacity was performed.
ii. All results are simulation results obtained from a model validated against measurements at three monitored nodes at a single recorded operating point. They are not field-trial results, and the controller was not tested in hardware.
iii. The load and irradiance records were available at hourly resolution and were interpolated to the 1-minute simulation step, so the 1-minute resolution of the results reflects the simulation, not measured 1-minute field data.
iv. The curtailment figure is the mean of five representative dry-season days and is not an annual value.
v. No economic analysis was performed, so the curtailment result is reported strictly as a technical energy trade-off.
vi. The evening minimum voltage at the feeder extremity is a pre-existing, load-driven condition that lies outside the reach of PV inverter control and is therefore unresolved by the proposed framework.

1.8 Contributions of the Thesis

This study contributes to power systems engineering by developing and evaluating a coordinated Volt-VAR/Volt-Watt smart inverter control framework on a validated model of a real Kenyan rural distribution feeder, and by demonstrating its potential to mitigate

reverse power flow, maintain voltage compliance and reduce OLTC operations under the investigated PV scenarios.

The research also quantifies, for this feeder, a limitation of default commercial inverter voltage settings: at the investigated 3 MW penetration level the voltage rise remains below their default activation thresholds, so that substantial reverse power flow occurs without triggering any control response. This provides an evidence-based argument for feeder-specific threshold tuning on structurally weak, high-impedance networks.

Finally, this thesis establishes a reproducible, seasonally aware time-series methodology for evaluating coordinated smart-inverter control on a rural feeder while preserving the integrity of existing electrical distribution assets.

1.9 Organization of the Thesis

This thesis is organized into five chapters. Chapter One introduces the study by presenting the background to photovoltaic integration in rural distribution networks, the problem statement, the main and specific objectives, the significance, scope, assumptions, limitations and contribution of the study. Chapter Two reviews the relevant literature, examining the characteristics and challenges of rural distribution feeders, the impacts of high photovoltaic penetration, the concept of feeder hosting capacity, the modelling and simulation tools available for feeder analysis, and the voltage control strategies reported in prior work, culminating in a synthesis that identifies the research gap addressed by this study. Chapter Three presents the research methodology, describing the analytical approach and research design, the data collection and sources, the formulation and validation of the OpenDSS digital twin of the Murang'a 11 kV feeder, the definition of the simulation scenarios, the configuration of the adaptive coordinated Volt-VAR and Volt-Watt control algorithm, and the comparative and sensitivity analyses used for performance evaluation. Chapter Four presents and discusses the results of the quasi-static time-series simulations, covering the baseline and uncontrolled photovoltaic cases, the diagnosis of the voltage sensitivity of the feeder, the performance of the proposed coordinated control strategy in mitigating voltage rise and reverse power flow, the associated energy curtailment, the mechanical duty of the substation on-load tap changer,

the seasonal robustness of the control scheme, and the contributions to knowledge arising from these findings. Chapter Five concludes the thesis by drawing conclusions against each of the specific objectives and offering recommendations for utility practice and for further research. The references and appendices, which contain the OpenDSS model scripts, control definitions and supporting data, are provided at the end of the thesis.

CHAPTER TWO
LITERATURE REVIEW

2.1 Introduction

This chapter provides a critical review of the existing literature to establish the context for integrating photovoltaic (PV) systems into challenging rural distribution networks. The discussion begins by outlining the inherent technical challenges of these feeders, followed by an analysis of the impacts of PV integration. Furthermore, it evaluates modern voltage control strategies that inform the proposed solution and justifies the choice of analytical software. This review demonstrates a clear gap in the literature regarding the design and validation of context-specific PV integration scheme for a representative Kenyan feeder.

2.1.1 Characteristics and Challenges of Rural Distribution Feeders

Rural electrical distribution feeders exhibit distinct topological and electrical characteristics that differentiate them from their urban counterparts, leading to a unique set of power quality and reliability challenges. These inherent characteristics are fundamental to understanding the operational problems that this research addressed.

2.1.2 Topological and Structural Differences from Urban Networks

The most defining feature of a rural distribution network is its structural configuration. While urban centers often utilize meshed or ring-main configurations to provide built-in redundancy and multiple paths for electricity to flow, rural grids are predominantly designed as long, sprawling radial lines [28].

In a radial design, which typically originates from a single busbar substation, power flows along a single primary path to downstream branches. While this is a cost-effective method for serving sparsely populated areas, it lacks the resilience of urban loop systems. Consequently, a fault on a radial feeder often results in sustained outages for all downstream customers, as there is no alternative path for energy delivery [29]. This inherent structural vulnerability is the primary source of many power quality issues prevalent in these networks.

2.1.3 The Technical Significance of the High R/X Ratio

Beyond the physical layout, the electrical behavior of a rural feeder is characterized by its high resistance-to-reactance (R/X) ratio. Due to the vast distances covered, rural feeders require long conductors which, for economic reasons, are often of a smaller cross-sectional area than those used in dense urban centers. The direct consequence is that the electrical resistance (R) of the line becomes significantly larger in proportion to its inductive reactance (X) [28].

This characteristic fundamentally alters the voltage stability of the feeder. In high-voltage transmission lines, where reactance dominates, voltage is primarily managed through the control reactive power. However, in high R/X rural feeders, the voltage level becomes highly sensitive to the flow of real power. This implies that any fluctuation in electricity consumption or generation along the line can cause dramatic swing in the voltage profile, making the entire system inherently difficult to stabilize without advanced control mechanisms.

2.1.4 Power quality challenges in rural feeders

The intersection of extended, radial topologies and high R/X ratios creates a significant technical environment for chronic power quality degradation. These issues are not merely transient anomalies but represent persistent operational conditions that negatively impact both the utility infrastructure and the end-user experience.

The high sensitivity of these networks to active power flow implies that even minor fluctuations in load or generation can lead to severe deviations from nominal voltage levels. Furthermore, the lack of redundancy inherent in the radial structure means that voltage instability at any point along the primary feeder can propagate downstream, affecting the entire service area. These challenges necessitate a robust control framework to ensure that the distribution of electrical energy remains within the strict regulatory tolerances required for modern equipment and consumer satisfaction.

2.1.4.1 Chronic Voltage Drop and Profile Issues

The most prevalent technical challenge associated with rural feeders is poor voltage. As electricity travels down the long, resistive lines, the voltage steadily decreases—a phenomenon known as voltage drop [30]. This principle is formally governed by the approximate voltage drop equation for a distribution line.

For rural feeders, which are defined by a high resistance-to-reactance (R/X) ratio, the active power term, P and Resistance R becomes the dominant factor in the expression. This provides an engineering basis why these networks are so susceptible to severe voltage drops and why their voltage profiles exhibit high sensitivity to fluctuations in real power (P) flow, such as those introduced by PV systems.

Furthermore, rural networks are often plagued by voltage imbalances between the three phases. These imbalances increase the operational stress on distribution equipment and in severe cases, establish hazardous operating conditions that compromise system safety [31].

2.1.4.2 High Technical Power Losses

A significant consequence of the high line resistance inherent in rural feeders is the excessive loss of energy. This energy dissipates as heat as it flows through the long conductors, a process formally defined as Joule heating. The fundamental principle governing these technical losses, is commonly referred to as I^2R losses.

Power loss is proportional to the square of the current. This mathematical relationship demonstrates that even a modest reduction in the current drawn from the substation, for instance, by supplying loads with a local PV system, can result in a substantial and highly desirable decrease in total energy losses [28]. These losses represent a direct economic drain for the utility and are often exacerbated by phase imbalances common in rural networks [32].

2.1.5 Impact of Photovoltaic Integration on Distribution Networks

The integration of distributed photovoltaic (PV) systems is frequently proposed as a direct solution to the chronic voltage and loss issues that plague rural feeders. By generating power closer to the points of consumption, PV can indeed offer significant benefits.

However, the introduction of active generation into a passive network designed for one-way power flow creates a new set of complex challenges. This section will explore this dual nature of PV integration, exploring both its positive contributions to grid performance and the adverse impacts that arise, particularly as penetration levels increase. The transition from a radial, one-way system to a bidirectional active network necessitates a sophisticated understanding of how these decentralized energy sources interact with existing grid infrastructure.

2.1.5.1 Positive Impacts on Feeder Performance

When implemented under optimal conditions, the integration of PV systems can directly counteract the fundamental technical weaknesses inherent in rural distribution feeders. Research demonstrates that distributed PV installations can effectively reduce network power losses and improve the overall voltage profile [33]. The underlying mechanism is based on the reduction of power flow from the upstream source, by supplying local loads, the PV system reduces the amount of current that must be drawn from the distant substation. This reduction in current flow along the feeder's long, resistive lines directly leads to a decrease in I^2R losses and a mitigation of the severe voltage drop.

Crucially, the effectiveness of these benefits is highly dependent on the strategic placement of the PV systems within the network topology. Studies confirm that the greatest improvements in both voltage support and loss reduction are achieved when the PV installations are located closer to the far ends of the feeder, where the power quality issues are most severe [33]. This finding indicates that a targeted, engineering-led approach rather than haphazard, approach to PV deployment is essential to maximize its positive contributions.

2.1.6 Adverse Impacts and Operational Challenges

While integration of distributed generation offers clear technical benefits at low levels, increasing the amount of PV on a feeder can introduce significant problems. If left unmanaged, these issues can be more disruptive than the original ones. These challenges threaten the stable and safe operation of the entire distribution network.

2.1.7 Overvoltage, the Most Prominent Challenge

The most prevalent and critical issue arising from high PV penetration is overvoltage [34]. This phenomenon typically occurs during periods of peak solar irradiance that coincide with low local electricity demand. When the power generated by the PV systems exceeds the local consumption, the excess power begins to flow in reverse, back towards the substation. This reverse power flow, particularly on the highly resistive lines of a rural feeder, can push the local voltage above the statutory upper limits, a condition known as overvoltage.

This is not a benign issue; it can trigger protective devices, cause unnecessary disconnections, and potentially damage both utility equipment and consumer appliances [34]. Furthermore, the severity of overvoltage is strongly linked to the self-consumption ratio of the prosumers; lower self- consumption means more power is exported to the grid, exacerbating both overvoltage and grid power losses [35].

2.1.8 Voltage Fluctuations from Solar Intermittency

Beyond the steady-state issue of overvoltage, the inherently variable nature of solar power introduces dynamic stability challenges. The intermittent output of PV systems, primarily driven by transient meteorological factors such as cloud cover, can lead to rapid and significant voltage fluctuations across the grid [36], [37]. These swings can cause the voltage to violate both upper and lower limits over short periods, a condition that is difficult for traditional, slow-acting voltage regulation equipment to manage. This increased volatility places immense stress on legacy devices. For instance, On-load tap changers (OLTCs) at the substation, for instance, are forced to operate much more frequently to try and compensate for these swings, leading to increased mechanical wear and a shortened operational lifespan [38]. Consequently, the reliance on traditional

mechanical regulation alone is insufficient for maintaining power quality in high-penetration PV scenarios, necessitating the integration of fast-acting, inverter-based control solutions.

2.2 The Concept of Feeder Hosting Capacity

To mitigate the adverse impacts, the engineering concept of "Hosting Capacity" (HC) has become central to grid planning. Hosting capacity is formally defined as the maximum threshold of distributed generation that can be integrated into a feeder without necessitating significant infrastructure upgrades or compromising the fundamental safety, reliability, and power quality of the network [39], [40].

The assessment of hosting capacity is a complex, multi-faceted analysis. The primary limiting factors, or performance indices, typically evaluated include:

- Voltage magnitude violations (both overvoltage and undervoltage),
- Thermal limits of conductors and transformers, and
- Protection system issues [39], [41].

A variety of analytical methodologies are employed, ranging from deterministic and time-series approaches to more advanced stochastic and optimization techniques, each with varying levels of accuracy and computational demand [40]. Understanding a feeder's hosting capacity is the critical first step in developing an effective and sustainable PV integration plan.

A critical comparison of these methodologies reveals distinct trade-offs. Deterministic methods evaluate hosting capacity for a single worst-case snapshot and are computationally cheap, but they overestimate risk by ignoring temporal load– generation diversity. Probabilistic (stochastic) methods capture uncertainty in irradiance, load and PV siting through Monte Carlo sampling, yielding more realistic capacity envelopes at high computational cost. Time-series (QSTS) approaches explicitly resolve the temporal coincidence between peak generation and minimum demand and can therefore expose

reverse power flow and tap-hunting phenomena that snapshot methods miss, while 17ptimization-based approaches embed the hosting-capacity question inside an objective function to co-optimize inverter setpoints and network constraints. Because the core vulnerability of the Murang'a feeder is a temporal generation–demand mismatch rather than a single static peak, the time-series (QSTS) approach is adopted in this study, and this justifies the methodological choice made in Chapter 3.

2.2.1 Techniques for voltage control in feeders with PV integration

The integration of photovoltaic (PV) systems, while operationally beneficial, introduces significant voltage regulation challenges that render conventional control methods insufficient on their own [42]. The stochastic nature of PV generation, characterized by high-power injection during low-load periods, can interfere with the operation of legacy regulation devices and cause frequent over voltages [43]. Consequently, the literature extensively focused on a range of advanced control strategies, transitioning from autonomous inverter functions to sophisticated coordinated schemes, to maximize the benefits of renewable generation.

2.2.2 Legacy Voltage Control Mechanisms and Limitations

Historically, voltage control in distribution networks has relied upon centralized slow-acting, mechanical devices, primarily On-Load Tap Changers (OLTCs) located at the substation and switched capacitor banks along the feeder. An OLTC maintains the secondary bus voltage by physically modulating the transformer's turns ratio. While these mechanisms are effective for managing slow, predictable load variations, they are fundamentally ill-equipped to handle the rapid, localized voltage fluctuations caused by solar intermittency.

The operation frequency required to track these changes scales almost linearly with PV penetration, leading to significant mechanical wear and accelerated depreciation of the asset's operational lifespan [38], [44]. Such inherent limitation necessitates a transition towards faster, more flexible power-electronic-based solutions which can provide the sub-cycle response times required for modern, active distribution networks.

2.2.3 Advanced Voltage Control using Smart PV Inverters

Modern Photovoltaic systems are integrated into the grid through smart inverters, which are power electronic interfaces with significant computational capabilities. These inverters are programmed to perform a variety of "grid-support functions" to actively manage local grid conditions, moving beyond their basic role of DC-to-AC power conversion.

The transition from passive to smart inverters represents a paradigm shift in distribution grid management. These interfaces provide a high-bandwidth, software-defined response to grid disturbances, allowing for real-time adjustments to active and reactive power injection at the Point of Common Coupling (PCC). In the context of rural feeders, this computational autonomy is critical; it enables the inverter to act as a decentralized regulation asset that can mitigate voltage violations at the source, significantly reducing the operational burden on upstream legacy control devices.

2.2.3.1 Volt-VAR Control- Autonomous Reactive Power Management

The most widely adopted smart inverter function for voltage control is the Volt-VAR (QV) control strategy. This autonomous function enables a smart inverter to regulate its terminal voltage by modulating the injection or absorption of reactive power (Q) in response to real-time local voltage measurements (V) [45].

The control law is defined as a piecewise linear function that relates the reactive power output to the measured grid voltage.

This function allows the inverter to act as a dynamic, localized voltage regulator. If voltage rises, the inverter absorbs reactive power to pull it down, effectively mitigating overvoltage issues during periods of high PV generation [46]. Studies have shown that these distributed Volt-VAR strategies can resolve voltage violations while minimizing the reactive power burden on the main substation [45].

2.2.3.2 Volt-Watt Control: Active Power Curtailment

In operational scenarios where reactive power support is insufficient to prevent overvoltage, the Volt-Watt function provides a direct method of control by curtailing

active power. When the terminal voltage exceeds a predefined threshold, the inverter modulates its real power output according to a defined droop characteristic.

While highly effective, from a technical point, the implementation of active power curtailment implies that potential renewable energy generation is wasted, leading to financial losses for the prosumer [47].

2.2.3.3 The Challenge of Control Equity

Research highlights a significant fairness and equity issue inherent in standard Volt-Watt control schemes. Because voltage rise is physically most severe at the distal ends (the far sections) of a radial feeder, the smart inverters located there reach their voltage limits much sooner than those located near the substation. [48]. Consequently, the Volt-Watt function is typically categorized as a secondary control measure, to be activated only when the Volt-VAR capacity is exhausted or insufficient to maintain grid compliance [49].

2.2.4 Coordinated Control Strategies for Active Distribution Networks

While autonomous inverter functions provide robust localized regulation, the most effective solutions involve the coordinated control of multiple assets across the feeder. However, relying purely on decentralized, uncoordinated control loops introduces significant operational vulnerabilities that are often overlooked in simplified grid models. In rural distribution networks characterized by high resistance-to-reactance (R/X) ratios, uncoordinated Volt-VAR droop settings can trigger severe hunting oscillations, where adjacent smart inverters continuously counteract each other's reactive power contributions in a destabilizing feedback loop [50]. Furthermore, uncoordinated control loops suffer from severe structural fairness issues; because voltage rise is compounded along the line, distal inverters located at the radial extremities are forced to curtail significantly more active power than upstream units near the stiff substation bus [48]. These critical localized control instabilities, capacity allocation inequities, and rapid voltage fluctuations are not explored in generic test feeder studies, yet they significantly accelerate the degradation of power electronic switching components and penalize remote clean energy yield [51]

Furthermore, decentralized control schemes inherently introduce structural fairness issues across radial topologies [52]. Because voltage rise is cumulative along a line, distal inverters located at the radial extremities of long rural feeders experience significantly higher localized voltage stress than upstream units situated closer to the primary substation [53]. Consequently, when autonomous Volt-Watt functions are triggered to suppress overvoltage violations, these downstream inverters bear a disproportionate burden, curtailing a vast majority of their active power output to protect the network while upstream assets continue to generate unhindered [54]. These critical structural limitations ranging from dynamic control hunting to systemic curtailment unfairness are rarely explored in generic, stiff test feeder studies, thereby directly highlighting the necessity of designing an adaptive, coordinated framework tailored to the unique physical constraints of weak rural infrastructures. These strategies aim to establish a cohesive system where modern smart inverters and traditional legacy equipment are integrated to work together intelligently.

2.2.4.1 Coordinated Control Architectures/mechanisms

The literature classified these coordination mechanisms into several distinct architectures, including centralized, decentralized, distributed, and local approaches. Each architecture presented inherent trade-offs regarding communication infrastructure requirements, computational overhead, and global optimality of performance [55], [56].

A primary focus of contemporary research is the hierarchical coordination between distributed smart inverters and the substation On-Load Tap Changer (OLTC).

By using the fast-acting reactive power support from inverters as the primary regulation layer, the slow-moving and mechanically limited OLTC was engaged less frequently. This reduced mechanical stress and preserved the lifespan of the tap changer while maintaining a stable voltage profile [44],[57].

2.2.4.2 Advanced Predictive and Supervisory Control

Recent advancements in the field incorporated solar forecasting and Model Predictive Control (MPC) to proactively modulate both inverter setpoints and regulator tap positions.

These proactive strategies aimed to prevent voltage deviations before they manifested, rather than merely reacting to them [58]. Such supervisory Volt-VAR schemes demonstrated the significant benefits of an integrated, system-level approach to voltage regulation in modern distribution networks [59].

Recent research has extended autonomous smart-inverter functions well beyond the basic Volt-VAR and Volt-Watt droop laws. Studies have investigated adaptive and self-tuning droop slopes that adjust to local short-circuit strength, coordinated Volt-VAR/Volt-Watt schemes that explicitly sequence reactive-power support ahead of active-power curtailment, and data-driven controllers that anticipate irradiance ramps. A consistent finding across these works is that a single fixed manufacturer setting is rarely optimal for weak, high R/X feeders, and that context-specific tuning is required to balance voltage regulation against curtailment losses. This directly motivates the 22 parameter, feeder-specific control 22 parameterization developed in this thesis.

2.3 Modelling and Simulation Tools for Feeder Analysis

The analysis of modern distribution feeders, with their complex, unbalanced loads and the variable nature of integrated renewables, required the utilization of sophisticated simulation tools. The selection of an appropriate software platform represented a critical methodological step that directly impacted the validity and accuracy of the research findings. This section provided an overview of the available simulation tools and presented a robust justification for the selection of the Open Distribution System Simulator (OpenDSS) for this thesis.

2.3.1 Overview of Distribution System Analysis Tools

Historically, the literature identified several industry-standard software packages for power system analysis, including MATPOWER, ETAP, and DIgSILENT PowerFactory. While these tools offered significant capabilities for high-voltage transmission studies, many presented limitations when applied to the unique requirements of active distribution networks. For instance, traditional methods like Newton-Raphson often struggled with the unbalanced, four-wire nature of rural feeders or lacked the specialized models required for sophisticated smart inverter control functions [60].

Research indicated that the increasing complexity of distributed energy resource (DER) integration necessitated a transition toward tools capable of performing high-resolution Quasi-Static Time-Series (QSTS) simulations. Earlier studies suggested that static snapshot analyses were insufficient for capturing the voltage volatility induced by solar intermittency, leading to the widespread adoption of more dynamic modelling environments in the academic community [61]. Consequently, the evaluation of available platforms highlighted the need for a simulator that combined robust power flow solvers with extensible control interfaces.

2.3.2 Justification for the Open Distribution System Simulator (OpenDSS)

For the specific task of analyzing distribution feeders with high PV penetration, the Open Distribution System Simulator (OpenDSS) emerged as an industry-standard and highly capable tool. Developed by the Electric Power Research Institute (EPRI), OpenDSS was an open- source platform specifically designed to model and analyses the complexities of modern distribution networks. The literature strongly supported its selection for several key reasons.

2.3.2.1 Suitability for Unbalanced, Multi-phase Distribution Systems

Unlike many simulators that were optimized for balanced, high-voltage transmission networks, OpenDSS was built from the ground up to handle the unbalanced, multi-phase circuits that were characteristic of distribution feeders. This made it ideal for accurately modelling the real- world conditions of the Murang'a network and assessing critical issues such as voltage unbalance [62].

2.3.2.2 Advanced Capabilities for Quasi-Static Time-Series (QSTS) Analysis

The most significant advantage of OpenDSS for this research was its powerful engine for performing Quasi-Static Time-Series (QSTS) simulations. A QSTS analysis simulated the system's behavior over extended periods of time such 24 hours or a full year, by running a sequence of power flows at specific time intervals ranging from minutes to seconds.

This methodology was essential for accurately capturing the time-dependent impacts of PV generation, including midday overvoltage conditions and rapid fluctuations induced by cloud cover [63]. Furthermore, QSTS allowed for the comprehensive assessment of multiple performance metrics, such as overvoltage, thermal loading, and reverse power flow, which made it the definitive method for hosting capacity analysis [62],[64].

2.3.2.3 Precedent Studies Utilizing OpenDSS for PV Integration

The suitability of OpenDSS for this type of research was well-established in the literature. Numerous recent studies successfully utilized OpenDSS to perform analyses directly comparable to this thesis. Researchers employed the tool model large-scale, real-world feeders with high renewable penetration [65], to analyze the voltage profile impacts of PV insertion using actual utility data [66], and to conduct hosting capacity assessments that confirmed voltage as the primary limiting constraint [64].

Furthermore, OpenDSS was frequently co-simulated with other platforms such as MATLAB to implement and test advanced control and optimization algorithms. This demonstrated the platforms flexibility and its central role in cutting-edge distribution system research [67],[68]. This strong academic and industrial precedent provides high confidence in OpenDSS as the appropriate and robust choice for the simulation tasks to be undertaken in this work.

2.3.3 Best Practices for Quasi-Static Time-Series (QSTS) Simulation

To accurately evaluate the high-frequency operational dynamics of high-penetration solar PV integration, power system modelling must move beyond standard deterministic snapshot evaluations and implement Quasi-Static Time-Series (QSTS) simulations [69].Standard guidelines from structural framework institutions, including the Electric Power Research Institute (EPRI) and Sandia National Laboratories, emphasize that the fidelity of a QSTS model relies heavily on three core parameters: time-step selection, irradiance variability matching, and strict solver convergence criteria[70] . Selecting an inappropriate time-step can mask fast-acting voltage deviations and underestimate localized legacy voltage device wear. According to the foundational modelling frameworks established by [71] a high-resolution time-step typically ranging from 1

second to 1 minute is mandatory to capture the rapid ramp rates caused by cloud cover and local environmental changes.

Furthermore, these simulation environments require high-fidelity time-synchronous irradiance profiles that match historical load variation matrices rather than relying on smoothed hourly averages [72]. This high-frequency irradiance variability ensures that the simulation accurately triggers smart inverter control functions, such as Volt-VAR and Volt-Watt loops, under volatile weather conditions [73]. Consequently, robust solver convergence criteria are required within the OpenDSS environment to maintain numerical stability and ensure the reliability of the simulation results [74]. Tolerances must be set tightly (typically between 10-4 and 10-6 p.u. control error limits) to avoid false solutions or artificial numerical damping during extreme reverse power flow conditions [75]. Adhering to these industry-vetted modelling frameworks guarantees that the digital twin of the rural network remains highly dependable and reproducible during dynamic voltage stability analyses [76].

2.4 Chapter Summary

The body of literature reviewed in this chapter confirmed a broad consensus on several key points. It was well-established that rural distribution feeders were inherently weak due to their radial topology and high R/X ratio, making them prone to significant voltage drop and power loss issues [28],[29]. It was also undisputed that the uncoordinated, high-penetration integration of photovoltaic (PV) systems exacerbated these issues, primarily through overvoltage phenomena and voltage instability caused by solar intermittency [34],[36]. To address these problems, the literature presented a suite of advanced solutions, with smart inverter functions such as Volt-VAR and Volt-Watt control, often in coordination with legacy devices like OLTCs, emerging as the most effective technical strategies [44],[45]. Furthermore, simulation platforms like OpenDSS were recognized as the standard and appropriate tools for modelling and analyzing these complex interactions [65].

However, a critical analysis of the existing research revealed a significant and persistent gap between the theoretical validation of these advanced solutions and their practical,

context- specific application, particularly within the developing world and Sub-Saharan Africa. First, while numerous studies demonstrate the effectiveness of advanced inverter controls, they are often validated using standardized IEEE test feeders [28] , which completely fail to replicate the electrical stiffness, severe phase imbalances, or extreme reverse power flow intensity characteristically observed along a weak, 69 km radial Kenyan rural feeder [77].

The literature explicitly confirmed this gap. Researchers in [78] and [79] highlighted that weaker low-voltage networks, coupled with challenges in data availability and communication infrastructure, were significant barriers to implementing advanced control strategies in developing countries. The need for cost-effective, reliable control strategies specifically designed for developing country contexts was a recurring theme [78], [80]. While the potential of local, autonomous inverter control was recognized [79] , there was a clear call for further development and validation of these methods on actual, operational feeders.

Furthermore, studies focusing on the Sub-Saharan African context pointed to critical deficiencies in existing grid codes and technical regulations needed to properly manage and coordinate smart inverter functions [81],[82]. This underscores the importance of not just designing a control strategy, but also validating its performance against internationally recognized standards like IEEE 1547, thereby providing a clear, evidence-based framework to inform future grid code updates in Kenya.

Therefore, the specific research gap that this work addressed was the lack of a comprehensive, simulation-based design and validation of a smart inverter voltage control scheme for a specific, real-world, data-driven model of a Kenyan rural distribution feeder. This study moved beyond generic models by first formally quantifying the unique voltage challenges inherent to the Murang'a feeder. Following this problem formulation, the research designed an effective and practical control solution utilizing established smart inverter functions such as Volt-VAR and Volt-Watt coordination. Finally, it rigorously validated the performance of this solution, ensuring it both resolved the feeder's specific operational constraints and complied with the stringent requirements of international

engineering standards. By addressing this gap, this research will provide a tangible, context-specific, and standards-compliant engineering framework directly relevant to Kenyan utilities contributing to the broader body of knowledge on effective renewable energy integration in developing regions.

CHAPTER THREE
RESEARCH METHODOLOGY

3.1 Introduction

This chapter presents the detailed and systematic methodology employed to achieve the objectives of this research. The primary goal of this study is to design and validate an effective voltage control scheme for the Murang'a rural distribution feeder. To accomplish this, a quantitative, simulation-based approach is utilized, ensuring that the findings are both replicable and grounded in established engineering principles. The research methodology is logically structured to mirror the three core objectives outlined in Chapter 1. It follows a sequential, three-phase engineering framework: first, a comprehensive Problem Formulation through detailed system modelling and baseline analysis; second, the Solution Development, which involves the design of an advanced control strategy and finally, a rigorous validation of the proposed solution against the quantified baseline and established industry standards. This chapter provided a step-by-step blueprint of the simulation procedures and analytical techniques used in each of these distinct phases.

Research framework employed a simulation-based approach to investigate adaptive coordinated voltage control in the Murang'a 11 kV photovoltaic-integrated rural distribution feeder. A digital twin was developed and validated in OpenDSS to assess baseline voltage performance under PV integration. An adaptive coordinated control algorithm incorporating smart-inverter Volt-VAR and Volt-Watt functions was developed to mitigate daytime voltage rise and reverse power flow in accordance with IEEE Standard 1547 requirements. QSTS simulations evaluate the control strategy under varying high-photovoltaic-penetration conditions, considering generation and feeder-load variations. The Framework presents impacts assessment of the proposed control strategies on technical energy losses and OLTC mechanical duty cycles, thereby establishing their overall effectiveness and performance.

The methodology was structured according to the four specific objectives. Objective (i) was addressed through acquisition of utility feeder data, development and validation of the OpenDSS digital twin, and baseline network analysis (Sections 3.4–3.5). Objective (ii) was addressed through the design and implementation of the coordinated Volt-

VAR/Volt-Watt controller (Section 3.6). Objective (iii) was addressed through QSTS simulation, comparative performance evaluation and sensitivity analysis under varying PV and loading conditions (Sections 3.7–3.9). Objective (iv) was addressed by quantifying OLTC tap operations under the defined operating scenarios (Sections 3.7.1).

3.2 Research Analytical Approach

The study adopted a simulation-oriented research methodology centered on the development and analysis of a digital twin of the Murang'a 11 kV rural distribution feeder using the Open Distribution System Simulator (OpenDSS). Operational data and information were obtained and applied to construct a virtual representation of the physical feeder, incorporating its network topology, conductor and line parameters, transformer specifications, demand profiles, photovoltaic generation, and voltage-regulation equipment. The developed OpenDSS model represented the key electrical characteristics and operating conditions of the physical distribution network, thereby providing the foundation for the digital twin. OpenDSS power-flow analysis was conducted to reproduce and evaluate feeder behavior under different operating conditions, with particular emphasis on voltage profiles, power flows, feeder loading, and technical energy losses. Photovoltaic penetration levels were subsequently varied within the digital twin, as a sensitivity study, to establish how the feeder voltage profile and reverse power flow respond to increasing PV capacity; no formal maximum hosting capacity was computed, as explained in Section 1.5. Simulation outputs were analysed to characterize the electrical performance of the physical feeder and identify operating conditions associated with elevated voltages and increased photovoltaic penetration. The digital twin model was subsequently validated by comparing simulated results with utility field measurements at three monitored nodes to establish its accuracy and representativeness of the physical network. Consequently, OpenDSS served as the principal analytical platform for developing, simulating, and validating the digital twin and for evaluating the electrical behavior of the Murang'a 11 kV rural distribution feeder under the investigated PV scenarios.

3.3 Research Design

The research is designed as a quantitative, simulation-based case study. This approach is deliberately preferred over a purely analytical or a field-experimental approach for three reasons: (i) it permits repeatable, controlled evaluation of high-penetration and control scenarios that cannot be imposed on a live utility feeder without risk to supply security; (ii) it captures the full unbalanced, time-varying behavior of a 158-bus radial feeder, which closed-form analytical models cannot represent; and (iii) it is markedly more cost-effective and safer than hardware prototyping while still producing standards-referenced, verifiable results. The case study is centered on the Murang'a distribution feeder, utilizing real-world data to ensure the findings are context- specific and practically relevant to the challenges faced by Kenyan utility providers.

The primary analytical tool for this research is the Open Distribution System Simulator (OpenDSS). OpenDSS is an industry-standard, open-source software specifically engineered for the detailed analysis of unbalanced, multi-phase distribution systems and is exceptionally well-suited for performing the Quasi-Static Time-Series (QSTS) simulations required to capture the time-varying impacts of PV generation. All modelling, simulation and analysis are conducted within this software environment [83]. The overall research process, from modelling through to final validation, is illustrated in the flow diagram in Figure 3.1.

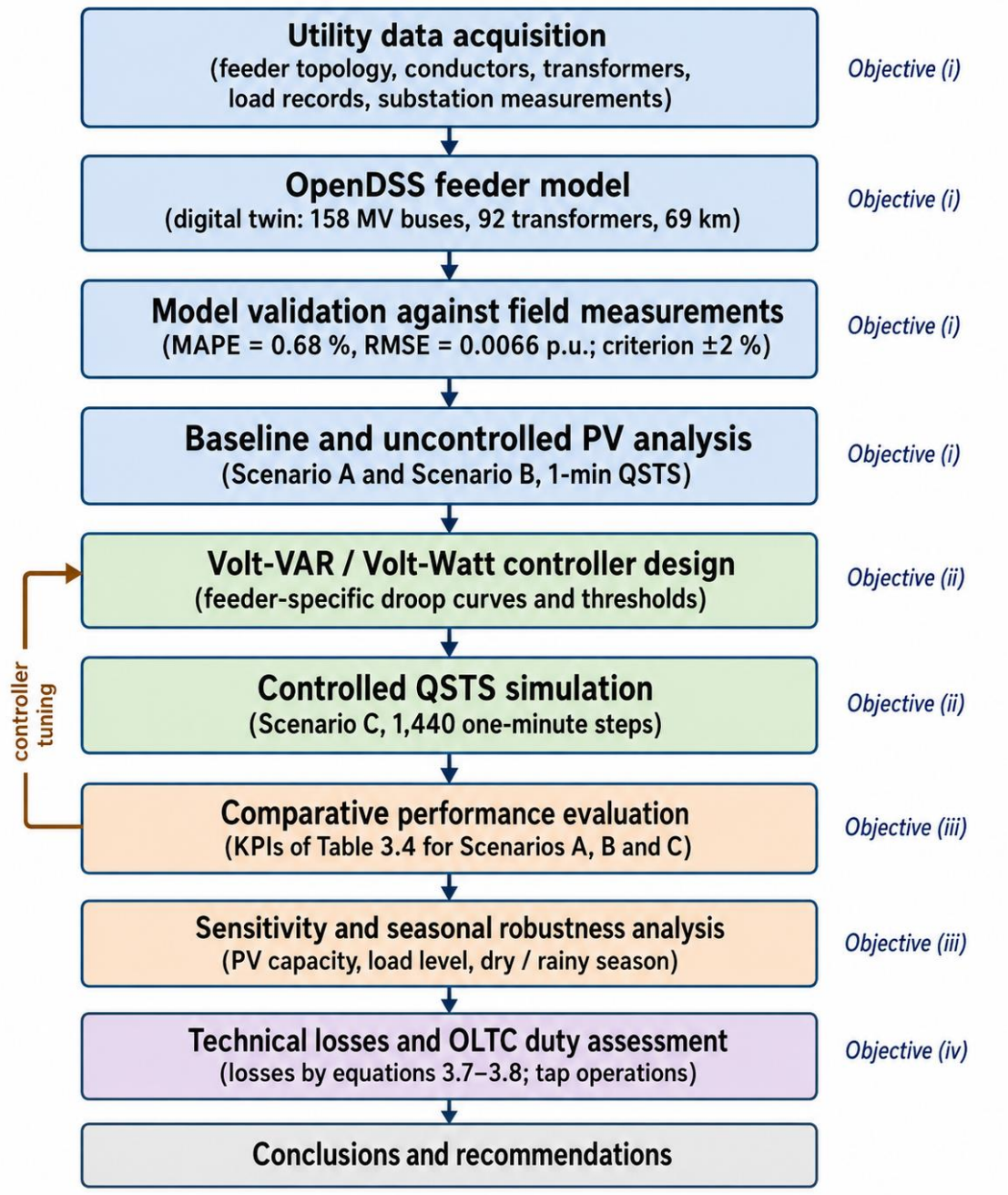

Figure 3.1: Research Methodology Flow Diagram

Analysis of Figure 3.1: Research Methodology Flow Diagram

Key observations

Sequential three-phase structure: the flow diagram resolves the research into problem formulation (data acquisition, OpenDSS feeder modelling and validation), solution development (design and parameterization of the coordinated Volt-VAR and Volt-Watt

controller) and validation (QSTS simulation, comparative evaluation and sensitivity analysis), with each phase feeding the next as a single directed path.

Explicit objective mapping: every block of the diagram corresponds to one of the four specific objectives, so that Objective (i) is served by the modelling and baseline blocks, Objective (ii) by the control-design block, Objective (iii) by the QSTS and comparative-evaluation blocks and Objective (iv) by the OLTC duty count.

Common simulation platform: all analytical blocks reside inside the OpenDSS environment at a 1-minute time step, so the same validated circuit is reused for the baseline, uncontrolled and controlled cases.

Peculiar features

A validation gate precedes control design: the model-acceptance test (percentage error, MAPE and RMSE against field measurements) is positioned before the controller is designed, so no control parameter is tuned on an unverified network. This ordering is deliberate and is not a feature of the conventional design-then-verify workflow.

The robustness branch re-enters the validation phase: the seasonal and sensitivity cases are drawn as a return path into the validation phase rather than as a separate terminal branch, which reflects the decision reported in Section 4.7 to treat them as additional operating cases of Objective (iii) rather than as a fifth objective.

Conclusions and findings

Methodological replicability: the diagram establishes an auditable chain from utility data to validated conclusions, so that any reported result can be traced back to a specific data source, a specific scenario and a specific acceptance criterion.

Fitness of the framework: the sequence confirmed that the four objectives can be satisfied entirely by simulation on a validated digital twin, without field intervention on a live 11 kV feeder.

3.4 Data Collection and Sources

All data used in this study are secondary data. No primary field-measurement campaign was undertaken by the researcher: the network and measurement data were supplied by the utility from its own records, and the environmental data were obtained from a published meteorological dataset. The data are classified into two groups in Table 3.1.

Table 3.1: Classification of data sources

Data group	Data item	Source	Resolution / basis
Secondary utility / network data	Feeder topology and line-segment lengths	KPLC network schematics and GIS records	Per line segment (69 km, 158 MV buses)
Secondary utility / network data	Conductor types and parameters (r, x per km)	Standard conductor datasheets matched to installed conductor types	Per conductor type
Secondary utility / network data	Distribution-transformer ratings and locations	KPLC asset register	92 transformers
Secondary utility / network data	Existing load records (24-hour demand profile)	KPLC substation metering records, 15 March 2025	Hourly records, interpolated to 1 minute
Secondary utility / network data	Substation measurements used for model validation	KPLC substation and feeder measurements (Hour 18, 15 March 2025)	Three monitored nodes
PV / environmental data	Global horizontal irradiance and derived PV output profile	Typical Meteorological Year dataset for Murang'a County (Kenya Meteorological Department, 2020)	Hourly GHI, interpolated to 1 minute (Appendix 3)

Because the load and irradiance records were available at hourly resolution whereas the QSTS simulation operates at a 1-minute time step, the hourly records were linearly interpolated to 1-minute resolution. This is stated explicitly so that the reported 1-minute temporal resolution of the results is not interpreted as measured 1-minute field data.

The data required to build and validate the model was obtained from Kenya Power and Lighting Company (KPLC) records for the Murang'a 11kV feeder and from supporting meteorological sources. Feeder topology and line-segment lengths were extracted from the utility's network schematics; conductor electrical parameters (per-unit-length resistance and reactance) were obtained from standard conductor datasheets matched to the feeder's installed conductor types; distribution-transformer ratings and locations were taken from the utility asset register; the 24-hour load profile was derived from substation metering records for a recorded operational day (Hour 18, 15th March 2025); and the solar irradiance / PV generation profiles were obtained from representative dry-season and rainy-season irradiance datasets for the study area. Where discrete measurements were unavailable, engineering estimates based on nameplate ratings and typical rural load-factor assumptions were applied, as stated in the Assumptions of the Study.

Analysis of Table 3.1: Classification of data sources

Key observations

Exclusively secondary data in two groups: the table classifies every input as either secondary utility or network data (topology, conductor parameters, transformer ratings, demand records and validation measurements) or PV and environmental data (global horizontal irradiance and the derived PV output profile). No primary measurement campaign was undertaken.

Network data are asset-register based: the 69 km trunk, 158 medium-voltage buses and 92 distribution transformers are taken from KPLC schematics, GIS records and the asset register, so the modelled topology reproduces the installed network rather than a generic test feeder.

Uniform temporal harmonization: the load records and the irradiance profile are both natively hourly and are interpolated to a 1-minute basis so that all time-varying inputs share the 1,440-step QSTS timeline.

Peculiar features

Mismatch between native and simulation resolution: the 1-minute simulation resolution exceeds the hourly resolution of the source records. Interpolation therefore produces smooth ramps and suppresses genuine sub-hourly cloud transients, which means the reported curtailment and tap counts are conservative with respect to fast irradiance volatility.

Narrow validation base: model validation rests on three monitored nodes for a single peak hour (Hour 18, 15 March 2025), so accuracy is established at the extremity, mid-feeder and substation but not across the full 158-bus set or across the full day.

Typical Meteorological Year irradiance: the solar resource is a TMY dataset for Murang'a County rather than site-measured pyranometer data, so it represents a statistically typical rather than an actually recorded irradiance sequence.

Conclusions and findings

Adequacy for the stated objectives: the classified dataset is sufficient to construct, validate and exercise the digital twin, since the parameters that govern voltage behavior (impedance, topology, transformer siting and demand shape) are all sourced from utility records.

A defined accuracy boundary: the interpolation and the TMY irradiance define the boundary of the accuracy claims made in this thesis and are the direct basis for the recommendation in Section 5.3 that measured 1-minute irradiance and wider node monitoring be used in subsequent work.

3.5 Problem Formulation – Feeder Modelling and Baseline Analysis

This initial phase of the research is dedicated to developing a detailed and validated digital model of the Murang'a feeder and utilizing it to formally quantify the grid's performance challenges under PV integration. A rigorous and validated baseline is essential, as it provides the benchmark against which the effectiveness of the proposed control solution is measured. This process was divided into three distinct stages: model development, model validation and baseline simulation.

3.5.1 Feeder Modelling in OpenDSS

The collected field data is used to construct a detailed circuit model within the OpenDSS software environment. This involves systematically scripting the feeder's physical components as OpenDSS objects. The main substation is defined as the primary voltage source (Vsource). All line segments are modelled as Line objects with their corresponding length and conductor parameters (Refer Appendix 1).

To satisfy the requirements of the legacy asset mechanical duty-cycle analysis (Objective 4), the main substation 33/11 KV transformer is modelled as a detailed Transformer objects equipped with an automated-On Load Tap Changer (OLTC). The transformer features a ±10% total tap regulation range, a discrete voltage step size of 1.25% per tap change operation, an inherent mechanical operation time delay of 30 seconds, and a standard utility voltage deadband setting of 0.5 p.u. This detailed parametrization governs the physical tap change reactions during QSTS runs, allowing for the formal tracking of legacy equipment mechanical stress.

All line segments are modelled as Line objects with their corresponding lengths and electrical conductor matrix parameters. Step-down transformers are modelled as Transformer objects, and the aggregated loads at each distribution transformer are represented by Load objects, to which the 24-hour load profiles are assigned. The result is a comprehensive digital twin of the Murang'a feeder, capable of accurately simulating power flow for any given time of day. The single line diagram of 11kv Murang'a feeder model is adoptively mapped [84] out in Figure 3.2.

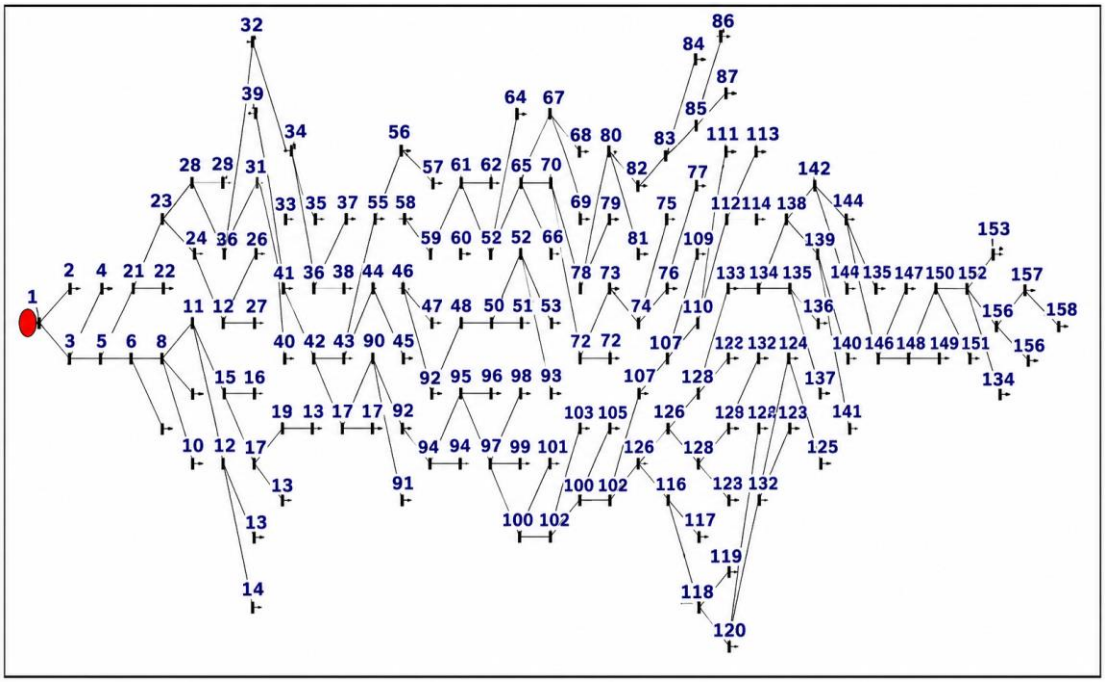

Figure 3.2: Single Line Diagram of 11kv Distribution Feeder

The OpenDSS engine solves the full unbalanced load flow at each time step. The underlying physics for the power transfer between nodes in the network is represented by the DistFlow equations for a branch from bus k to k+1: The relationship is expressed as in equation 3.1 and 3.2 [83]:

$$P_{k+1} = P_k - r_k \frac{P_k^2 + Q_k^2}{V_k^2} - P_{load,k+1} \tag{3.1}$$

$$Q_{k+1} = Q_k - x_k \frac{P_k^2 + Q_k^2}{V_k^2} - Q_{load,k+1} \tag{3.2}$$

Where Pk and Qk represent the active and reactive power entering the branch, rk and xk define the unique resistance and reactance of the line segment, Vk is the nodal voltage magnitude, and P_{load}, k+1 and Q_{load},k+1 represent the consumer loads connected at the subsequent bus. This mathematically models how active and reactive power transfer changes along a line segment due to line impedance and localized load profiles.

Analysis of Figure 3.2: Single Line Diagram of the 11 kV Distribution Feeder

Key observations

Purely radial architecture: the diagram shows a single 33/11 kV source substation with an on-load tap changer feeding one 69 km primary trunk with laterals tapped along its length, with no ring or alternative supply path.

Defined monitoring and injection points: the substation 11 kV busbar, mid-feeder Bus 87 and extremity Bus 158 are identified as the monitored nodes, while the 1 MW PV units are connected at Bus 52, Bus 87 and Bus 158 along the trunk.

Cascaded impedance path: the line segments accumulate in series from the substation to the extremity, which is the physical mechanism represented analytically by the DistFlow relationships of equations 3.1 and 3.2.

Peculiar features

No reconfiguration option: because the feeder has no tie point to an adjacent circuit, no switching or load-transfer remedy exists for voltage or backfeed problems. Mitigation must therefore be either local (inverter-based) or capital (reinforcement), which is the structural justification for the decentralized control approach adopted in this study.

Only one upstream regulating device: voltage regulation along the whole 69 km trunk depends on a single substation OLTC, so every unmitigated voltage excursion anywhere on the feeder is answered by the same mechanical asset. This is the physical reason why uncontrolled PV integration translates directly into increased tap duty in Section 4.6.

Unmetered lateral load: the laterals branching from the trunk carry aggregated load that is not individually metered, which is the source of the localised nodal error observed at Bus 87 in Table 3.2.

Conclusions and findings

Confirmation of the modelling approach: the radial, impedance-dominated layout confirms that a nodal, per-bus evaluation over the full 1,440-step timeline is the appropriate analysis method, since voltage is a strong function of position along the trunk.

Physical basis for the control siting: the single-line diagram establishes Bus 52, Bus 87 and Bus 158 as electrically distinct injection points, which is what allows the distributed inverter response reported in Chapter 4 to spread the voltage duty across the feeder instead of concentrating it at one node.

3.5.2 Model Validation

To ensure the credibility of the simulation results, the completed OpenDSS model was validated against real-world operational data. The model's accuracy was confirmed by simulating a specific historical operational point, for which measured utility data was available. For this study, the power flow was simulated for a peak load hour on a specifically recorded operational day (Hour 18,15th March 2025). In addition to the single-point percentage error, the validation was strengthened by reporting error across multiple monitored nodes (the substation 11kV bus and critical intermediate and remote buses) and by computing aggregate statistical error metrics, the Mean Absolute Percentage Error (MAPE) and the Root Mean Square Error (RMSE), so that model accuracy is characterized statistically rather than at a single point. Percentage error is retained as the headline acceptance criterion because it is the metric conventionally used for distribution-model validation against utility field readings.

Table 3.2 shows the precise data Mapping for the model verification.

Table 3.2: Model Validation at Peak load (Hour 18, 15 March 2025)

Measurement point	Utility field data (p.u.)	Simulation result (p.u.)	Absolute percentage error (%)
Substation 11 kV busbar	0.982	0.978	0.41
Bus 87 (mid-feeder)	0.945	0.937	0.85
Bus 158 (feeder extremity)	0.912	0.905	0.77
Aggregate MAPE (equation 3.3a)	–	–	0.68
Aggregate RMSE (equation 3.3b)	–	0.0066 p.u.	0.70

Measurement point	Utility field data (p.u.)	Simulation result (p.u.)	Absolute percentage error (%)
Acceptance criterion	–	–	≤ 2.00

Model validation analysis and technical interpretation

The quantitative benchmarking in Table 3.2 validates the statistical accuracy of the OpenDSS digital twin against utility field data /measured recorded during peak loading conditions.

Key observations

There is progressive radial voltage degradation: Both field measurements and digital twin simulation outputs demonstrate a continuous per-unit voltage drop along the 69 km primary feeder trunk, decreasing from 0.982 p.u. at the primary substation down to 0.945 p.u. at mid-feeder (Bus 87), and reaching a minimum of 0.912 p.u. at the radial extremity (Bus 158).

There is high nodal and Aggregate accuracy: Individual nodal absolute percentage errors remain under 1.0 % across all monitored points (0.41 % at the Substation, 0.85 % at Bus 87, and 0.77 % at Bus 158). The aggregate Mean Absolute Percentage Error (MAPE) of 0.68 % and Root Mean Square Error (RMSE) of 0.0066 p.u. (0.70 % of nominal) sit well within the $\le 2.00\%$ validation threshold adopted for distribution network modeling.

Peculiar Technical Features

Mid-Feeder Non-Linearity: The maximum absolute percentage error (0.85 %) occurs at intermediate Bus 87 rather than at the feeder extremity (0.77 %). This localized variation stems from unmetered, distributed lateral load branches off Bus 87 that introduce minor impedance variations.

Systemic Conservative Bias: The OpenDSS model consistently predicts slightly lower voltages than field readings across all monitored nodes (e.g.0.905 p.u. simulated vs. 0.912 p.u. measured at Bus 158). This conservative behavior occurs because the simulation assumes rated conductor operating temperatures without accounting for momentary ambient wind cooling or localized load diversity.

Pre-Existing Baseline Undervoltage: Peak demand depresses the terminal voltage at Bus 158 to 0.912 p.u., confirming that end-of-line voltage sag is an inherent, load-driven structural property of this long feeder independently of solar PV integration.

Findings and Conclusions

Digital Twin Validation: The OpenDSS circuit model is statistically confirmed as an accurate replica of the Murang'a 11 kV network, achieving a 0.68 % MAPE against the ≤ 2.00% criterion.

Suitability for Time-Series Analysis: Because the model error (RMSE = 0.0066 p.u.) is significantly smaller than the voltage swings caused by solar irradiance ramps, the validated digital twin is fully reliable for executing 1-minute Quasi-Static Time-Series (QSTS) simulations.

The aggregate accuracy of the model is quantified using the Mean Absolute Percentage Error (MAPE) and the Root Mean Square Error (RMSE), defined in equations 3.3a and 3.3b, in which V_{meas},i and V_{sim},i are the measured and simulated voltage magnitudes at monitored node i and N is the number of monitored nodes.

$$MAPE = \left(\frac{100\%}{N}\right)\sum_{i=1}^{N}\left|\frac{V_{meas,i} - V_{sim,i}}{V_{meas,i}}\right| \tag{3.3a}$$

$$RMSE = \sqrt{\left((1/N)\sum_{(i=1)}^{N}\left(V_{(meas,i)} - V_{(sim,i)}\right)^2\right)} \tag{3.3b}$$

The validation therefore follows an explicit chain: measured value → simulated value → nodal error → aggregate metric → acceptance criterion → validation decision.

Substituting the three monitored nodes into equations 3.3a and 3.3b gives MAPE = 0.68 % and RMSE = 0.0066 p.u., equivalent to 0.70 % of the nominal voltage. Both aggregate metrics, and the largest individual nodal error of 0.85 % at Bus 87, lie within the ±2 % acceptance criterion adopted for distribution-model validation in this study. The digital twin is therefore accepted as an adequate representation of the Murang'a 11 kV feeder for the QSTS studies reported in Chapter 4.

3.5.3 Development of the Digital twin of Murang'a Feeder

A core component of this research is the development and validation of a" digital twin of the 69 km, 11kV Murang'a distribution feeder. In the context of power systems, a "digital twin" is defined as a virtual representation of a physical asset that mimics its structural, functional, and behavioral characteristics in a real-time or quasi-static environment as shown in Figure 3.3.

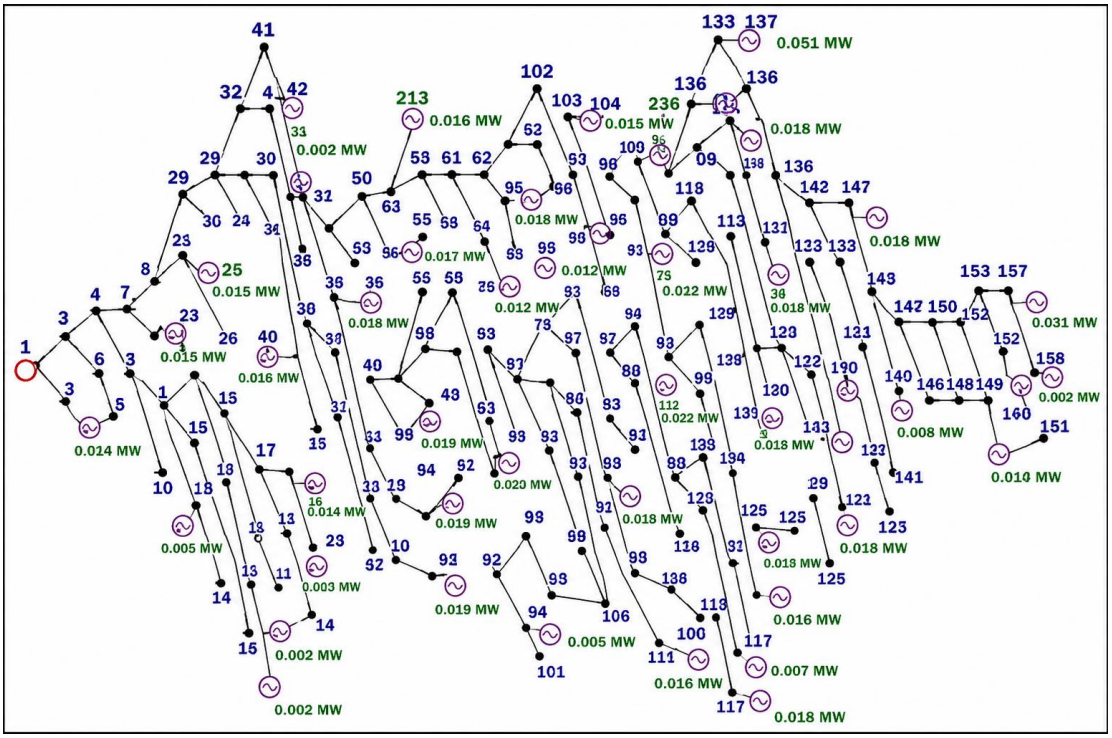

Figure 3.3: Digital Twin Diagram Of 11KV Feeder

Figure 3.3 illustrates the topological schematic and nodal distribution of the 158-bus, 69 km Murang'a 11 kV rural distribution feeder developed within the OpenDSS simulation environment.

3.5.4 Model Validation

It involves:

Network Topology Representation: The digital twin accurately maps 158 medium-voltage buses and 92 step-down distribution transformers, reflecting the physical radial layout, conductor parameters, and branch line segment impedances (R/X matrices) acquired from utility GIS asset registers.

Dynamic Time-Series Replication: Rather than relying on static snapshot power flows, the digital twin executes a Quasi-Static Time-Series (QSTS) engine at a 1-minute resolution (1,440 steps over 24 hours). This captures the dynamic, time-varying interactions between consumer demand profiles, solar irradiance fluctuations, and substation On-Load Tap Changer (OLTC) mechanical operations.

3.5.5 Evaluation of Baseline Voltage

It involves three areas:

- **Spatial Voltage Profile Drop:** The topological layout illustrates the physical vulnerability of the long radial feeder trunk, where cumulative line impedance induces progressive voltage degradation along downstream branches as power travels from the substation to remote loads.
- **Mid-Feeder versus Extremity Stress:** Intermediate buses (such as Bus 87) experience moderate voltage drops during demand ramps, whereas remote extremity nodes (such as Bus 158) bear severe end-of-line voltage depression during peak residential consumption hours.
- **High R/X Sensitivity**: The overhead line topology exhibits a high resistance-to-reactance (R/X) ratio, rendering nodal voltage profiles along the primary trunk highly sensitive to changes in active power flow (P).

3.5.5 Conclusions and Findings

- **Digital Twin Fidelity:** The 158-bus OpenDSS model serves as a high-fidelity, risk-free digital twin of the Murang'a 11 kV network, enabling the precise evaluation of high-penetration PV integration scenarios without jeopardizing live utility grid operations.

- **Identification of Network Weak Spots:** The spatial evaluation establishes that voltage stability on this feeder is highly location-dependent, identifying Bus 87 as a critical mid-feeder injection point and Bus 158 as the most voltage-sensitive node at the radial extremity.
- **Platform Readiness for Control Deployment**: The validated digital twin provides the necessary mathematical foundation to design and evaluate decentralized, smart inverter-based Volt-VAR and Volt-Watt control schemes under varying environmental conditions. This allows the model to simulate the complex interplay between fluctuating consumer demand, intermittent solar irradiance, and the mechanical response of legacy assets like On-Load Tap Changers (OLTC).

3.6 Simulation Scenarios and Baseline Analysis

With a validated model established, Quasi-Static Time-Series (QSTS) simulations were configured to quantify the specific performance issues caused by uncoordinated solar PV integration. To evaluate network behavior, isolate the impacts of high-penetration solar PV, and evaluate the proposed control strategy on a like-for-like basis, three standardized simulation scenarios were defined, as summarized in Table 3.3.

Table 3.3: Definition of the standardized simulation scenarios

Scenario	Designation	PV configuration	Inverter control state
A	Baseline (no PV)	PV disabled (0 MW)	Not applicable
B	PV integrated, uncontrolled	3 x 1 MW at Bus 52, Bus 87 and Bus 158	Unity power factor; no Volt-VAR or Volt-Watt response
C	PV integrated, coordinated control	3 x 1 MW at Bus 52, Bus 87 and Bus 158	Coordinated Volt-VAR (primary) and Volt-Watt (secondary) control active

Scenario Setup and Operational Analysis

The standardized scenarios in Table 3.3 establish a controlled framework to track key operating criteria, including statutory voltage limits, line thermal capacities and voltage unbalance across every node i and line segment ij over the 1,440-minute daily simulation timeline t.

Key observations

Progressive Control Framework: The experimental setup follows a logical progression from the pre-PV grid state (Scenario A) to uncontrolled solar PV integration (Scenario B), and finally to the active, coordinated smart-inverter control state (Scenario C).

Fixed High-Penetration PV Allocation: In both active solar scenarios (B and C), a total capacity of 3 MW of grid-tied solar PV is integrated and geographically distributed along the primary trunk (1 MW each at intermediate Bus 52, mid-feeder Bus 87, and remote extremity Bus 158)

Distinct Inverter Operating Regions: Scenario B constrains the solar inverters to operate at a fixed unity power factor (PF = 1.0) with zero grid-support functions active. In contrast, Scenario C activates the feeder-tuned, two-tier control logic, sequencing Volt-VAR as the primary reactive power response and Volt-Watt as the secondary active power curtailment mechanism.

Peculiar Technical Features

Worst-Case Generation-Demand mismatch: Scenario B deliberately models a clear-sky, high-irradiance day where peak 3 MW solar generation coincides with the lowest daytime residential load valley (1.64 MW), creating the worst-case operating stress for daytime voltage rise and active power backfeed.

Controlled Isolation of Control Impact: By holding the feeder loading profile, network topology, and 3 MW PV allocation identical between Scenarios B and C, the simulation environment cleanly isolates the exact technical contribution of the smart inverter control algorithm from the physical impacts of PV injection.

Conclusions and Findings

Methodological Scaffolding: The three standardized scenarios establish a consistent comparative baseline across Chapters 3 and 4, ensuring that all Key Performance Indicators (KPIs)—including voltage margins, reverse power flow and OLTC tap operations are benchmarked systematically.

Evaluation of Non-Wires Alternatives: This scenario matrix enables the quantitative evaluation of modern smart inverters as a decentralized "non-wire" alternative, proving whether software-defined inverter control can defer capital-intensive traditional grid reinforcement under high renewable penetration.

Voltage Limits: Based on ANSI C84.1 and the Kenyan Grid Code, nodal voltages are required to remain within the specified service band, typically ±5 % of the nominal voltage. This criterion is expressed as in equation 3.4 [85]:

$$0.95\ \text{p.u.} \leq V_i(t) \leq 1.05\ \text{p.u.} \tag{3.4}$$

Where Vi(t) represents the voltage magnitude at node i at time t, expressed in per-unit values relative to the system nominal voltage.

Any instance in which the voltage exceeds 1.05 p.u. during peak solar injection, or falls below 0.95 p.u. during peak load, is flagged as a statutory limit violation. Voltages that rise appreciably but remain below 1.05 p.u. are reported as voltage rise, or as movement towards the upper statutory boundary, and are not reported as violations. These findings form the quantitative basis for the subsequent design of the coordinated control strategy.

Thermal Limits: the current flowing through each line segment must remain below its rated maximum capacity to prevent conductor overheating or line sag risks, as defined by IEC 60287 and IEEE 738 conductor thermal rating standards. This criterion is expressed for branch segment ij as equation 3.5 [12,13]:

$$I_{ij}(t) = \frac{|S_{ij}(t)|}{\sqrt{3}V_{LL}(t)} \leq I_{ij}^{max} \tag{3.5}$$

Any instance where the current exceeds 100% of the rated capacity is flagged as a thermal violation, indicating a risk of conductor overheating or accelerated insulation degradation.

Voltage Unbalance: the Voltage Unbalance Factor (VUF) is monitored to evaluate power quality in three-phase distribution feeder sections, with a typical limit of 2-3 % as per statutory guidelines. The unbalance factor is defined as equation 3.6 [6,30]:

$$VUF_i(t)[\%] = \frac{|V_{2,i}(t)|}{|V_{1,i}(t)|} \times 100\% \leq VUF_{max} \tag{3.6}$$

where V_1,i and V_2,i are the positive- and negative-sequence voltage magnitudes at node i, respectively.

3.6.1 Solution Development – Design of the Voltage Control Scheme

Following the quantification of the baseline performance issues, this phase detailed the design of the engineering solution. The objective was to develop an effective and robust voltage control scheme utilizing the advanced functionalities of smart PV inverters. The design process is centered on the selection of appropriate control strategies and the precise parameterization of their control laws to mitigate the voltage and reverse-power-flow challenges identified in Phase 1.

The adaptive coordinated control algorithm, the principal engineering contribution of this study, was developed as a two-tier, hierarchically sequenced logic executed locally at every PV inverter on each QSTS time step. At each step the inverter measures its local terminal voltage at the point of common coupling. The first (primary) tier applies the Volt-VAR droop law: while the measured voltage lies within the deadband the inverter operates at unity power factor, and as the voltage rises above the lower activation setpoint the inverter progressively absorbs reactive power along the programmed droop slope, subject to the inverter apparent-power constraint. Reactive-power support is exhausted first because it carries no active-energy penalty. Only when reactive absorption is insufficient to arrest the voltage rise does the second (secondary) tier engage: the Volt-

Watt law curtails active power along its own droop above a higher activation setpoint. The two curves are deliberately coordinated so that the Volt-Watt activation voltage sits above the Volt-VAR absorption band, guaranteeing that curtailment is a last resort. Crucially, the droop setpoints are not taken from generic manufacturer defaults but are tuned to the measured voltage sensitivity of the Murang'a feeder, so that the control responds to the feeder's actual behaviour. This locally executed, communication-free logic is what allows the framework to remain dormant under benign conditions and act decisively under high-penetration stress.

The adaptive coordinated control algorithm operates strictly as a voltage-responsive, two-tier logic executed locally at each PV inverter. The primary control variable is the locally measured terminal voltage $V(t)$ at the point of common coupling. The controller does not measure or trigger directly on reverse power flow. Tier 1 applies the Volt-VAR droop law to absorb reactive power as voltage rises above $V_2 = 1.01$ p.u. = 1.01. Tier 2 engages the Volt-Watt droop law above $V_{\mathrm{vw},1} = 1.02$ p.u.to curtail active power. The suppression of net substation reverse power flow is achieved as an associated technical outcome of active power curtailment and voltage moderation, rather than as a direct control input parameter.

The term "adaptive". In this thesis the controller is described as adaptive in the following specific and limited sense, and the term is not used to imply on-line self-tuning or machine learning:

- the reactive power Q(V) injected or absorbed by each inverter is a continuous function of the locally measured terminal voltage, and therefore changes at every 1-minute time step in response to the prevailing network condition (equation 3.9);
- the active power P(V) delivered by each inverter is likewise a function of the locally measured terminal voltage once the Volt-Watt threshold is exceeded (equation 3.10);
- the two control modes are activated conditionally and sequentially: the inverter operates at unity power factor inside the dead band, in Volt-VAR mode between V2 and the Volt-Watt threshold, and in coordinated Volt-VAR plus Volt-Watt mode

above that threshold, so that the active control mode adapts to the severity of the voltage condition;

- the droop slopes, dead band and voltage setpoints are feeder-specific: they are tuned to the measured voltage sensitivity of the Murang'a feeder rather than adopted from generic manufacturer defaults, and separate parameter sets are evaluated for the dry-season and rainy-season cases in Section 4.7.

Within any single simulation the droop curves themselves are fixed and it is the inverter output, the active control mode and the resulting network state that vary with voltage. The term adaptive is therefore used in the sense of a voltage-adaptive, feeder-tuned and conditionally activated control law, and this restriction is stated explicitly to avoid overstating the capability of the controller.

3.6.2 Parameterization and Justification of Control Setpoints

The primary control strategies selected are the autonomous Volt-VAR and Volt-Watt functions, as defined in IEEE 1547 standards. These curves define the precise mathematical relationship between the measured terminal voltage and the inverter's power output.

- **Control mechanism-**This Executed locally at each smart inverter without external communications. Volt-VAR provides primary dynamic regulation, while Volt-Watt acts as a secondary safeguard.
- **Justification for volt-Var**-This is Chosen as the primary layer because it regulates voltage without curtailing active solar energy yield or penalizing prosumers.
- **Voltage regulation** is governed byline impedance powerflow relationship $\Delta V \approx \frac{PR+QX}{V}$ where reactive power flow (Q) through reactance (X) directly modulates nodal voltage.
- **Parameter controlled** is Net reactive power exchange (Q) at the Point of Common Coupling, bounded by the inverter stage capacity (S_{rated}).
- **System Evaluated** is the decentralized smart PV inverters on the 11 kV primary trunk of the Murang'a feeder digital twin in OpenDSS.

3.6.3 Volt-VAR Control Design

The Volt-VAR control function is designed to provide dynamic reactive power support from smart PV inverters in accordance with IEEE Std 1547-2018 grid interconnection requirements. The control law is expressed as equation 3.7 [45,85]:

$$Q(V) = \begin{cases} Q_{max,inj}, & V \leq V_1 \\ m_Q(V - V_3), & V_1 < V < V_4 \\ Q_{max,abs}, & V \geq V_4 \end{cases} \quad (3.7)$$

- For V <= V1: reactive power is fixed at maximum injection $Q_{max,inj}$.
- Between V1 and V4: reactive power changes linearly with slope mQ, shifted by V3.
- For V >= V4: reactive power is fixed at maximum absorption $Q_{max,abs.}$

Inverter reactive power stage availability $Q_{available}$ is constrained by apparent power rating S_{rated} and real power output P(V):as equation 3.8 [4,45]:

$$\sqrt{P(V)^2 + Q(V)^2} \leq S_{rated} \quad (3.8)$$

This control function is defined by four voltage setpoints (V1, V2, V3, V4), which delineate the different operational regions of the inverter. As illustrated in Figure 3.4, these setpoints establish the transition between reactive power injection, the dead band region, and reactive power absorption.

- V1: the voltage below which the inverter provides its maximum reactive power injection ($Q_{max,inj}$) to support low-voltage conditions.
- V2: the voltage above which the inverter is no longer required to provide reactive support, marking the beginning of the dead band.
- V3: the voltage above which the inverter begins to absorb reactive power to counteract voltage rise, marking the end of the dead band.
- V4: the voltage above which the inverter provides its maximum reactive power absorption (Qmax,abs).

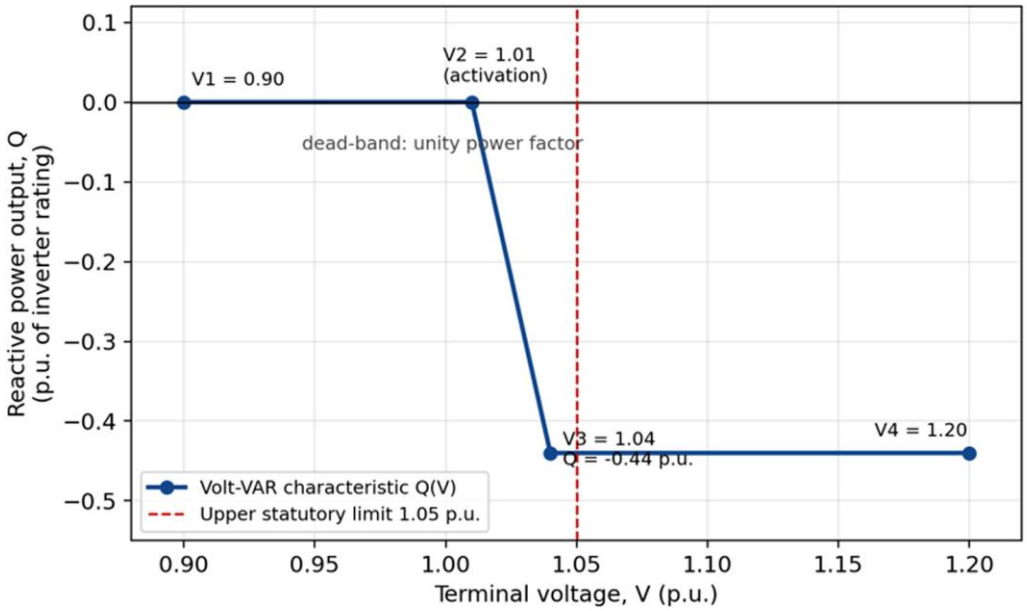

Figure 3.4: Volt-VAR Control Characteristic

Analysis of Figure 3.4: Volt-VAR Control Characteristic

Key Observations

Dead Band Region (0.90 p.u. ≤V ≤ 1.01 p.u.): The smart inverter operates at a fixed unity power factor (Q = 0.00 p.u.) within nominal voltage bounds, injecting zero reactive power.

Linear Absorption Slope $1.01\ p.u. < V < 1.04\ p.u.$: When terminal voltage exceeds the V_2 = 1.01 p.u. activation threshold, the inverter dynamically initiates inductive reactive power absorption, scaling down along a linear droop curve.

Maximum Absorption Ceiling $V \geq 1.04\ p.u.$: Inductive reactive power absorption saturates at Q = -0.44 p.u. (or 44% of rated inverter capacity) at V_3 = 1.04 p.u. and maintains this maximum absorption level up to V_4 = 1.20 p.u.

Peculiar Technical Features

Pre-Statutory Trigger Threshold: The Volt-VAR control curve initiates reactive power absorption at 1.01 p.u. Well before reaching the 1.05 p.u. upper statutory limit (red dashed line) or standard commercial default settings (≥1.04 p.u.).

Asymmetric Absorption Focus: The droop curve is parameterized specifically for overvoltage suppression on high R/X feeders, featuring a tight activation band (1.01 to 1.04 p.u.) while omitting dynamic reactive power injection (Q = 0.00 at V_1 = 0.90 p.u.).

Conclusions and Findings

Feeder-Tuned Sensitivity: Tuning activation thresholds specifically to local feeder sensitivity (V_2 = 1.01 p.u.) enables the inverter to respond to daytime voltage rise and mitigate active power back feed under operating conditions where generic factory defaults remain dormant.

Energy-Preserving Regulation: By prioritizing reactive power absorption up to -0.44 p.u as the primary voltage control layer, the framework regulates terminal voltages while avoiding unnecessary active power curtailment.

3.6.4 Parameterization of the Volt-VAR Control Law

The setpoints adopted for this research are derived from the guidelines in the Kenyan Grid Code and IEEE Standard 1547 and then tuned to the voltage sensitivity of the Murang'a feeder. The values implemented in OpenDSS, and used in every controlled simulation reported in Chapter 4, are listed in Table 3.4. These values are stated here once and are used consistently in the text, in Table 4.3 and in Appendices 1 and 4, replacing the illustrative values quoted in earlier drafts.

Table 3.4: Implemented Volt-VAR and Volt-Watt control parameters

Function	Parameter	Implemented value (p.u.)	Output at setpoint
Volt-VAR	V1 (maximum injection limit)	0.90	Q = 0.00 (no injection required on this feeder)
Volt-VAR	V2 (deadband start)	1.01	Q = 0.00

Function	Parameter	Implemented value (p.u.)	Output at setpoint
Volt-VAR	V3 (absorption ramp start)	1.01	Q = 0.00
Volt-VAR	V4 (maximum absorption)	1.04	Q = -0.44 (absorbing)
Volt-VAR	Saturation ceiling	1.20	Q = -0.44 (absorbing)
Volt-Watt	Vvw,1 (curtailment start)	1.02	P = 1.00 Prated
Volt-Watt	Vvw,2 (full curtailment)	1.05	P = 0.00
Volt-Watt	Saturation ceiling	1.20	P = 0.00

The Volt-VAR absorption band therefore begins at 1.01 p.u. and saturates at 1.04 p.u., while active-power curtailment does not begin until 1.02 p.u. Reactive absorption is consequently the first response, and curtailment only supplements it once the voltage continues to rise, which is the coordination requirement stated in Section 3.6.6.

At any given time, the reactive power injection and absorption capability of the inverter is constrained by its apparent power rating (S_{rated}) and active power output (Pout), in accordance with EPRI smart inverter performance guidelines. The maximum available dynamic reactive power reserve Qavailable is expressed as equation 3.9 [45,83]:

$$Q_{available} = \sqrt{S_{rated}^2 - P_{out}^2} \tag{3.9}$$

This constraint ensures that the total vector sum of active and reactive power does not exceed the thermal and electronic limits of the inverter's power stage.

Analysis of Table 3.4: Implemented Volt-VAR and Volt-Watt Control Parameters

Key observations

Reactive band tightly placed above nominal: the Volt-VAR characteristic leaves the dead band at V2 = 1.01 p.u. and reaches maximum absorption of Q = -0.44 p.u. at V4 = 1.04 p.u., so the entire proportional range occupies only 0.03 p.u. of voltage.

Curtailment nested inside the reactive band: Volt-Watt action begins at Vvw,1 = 1.02 p.u. and reaches full curtailment at Vvw,2 = 1.05 p.u., which places the onset of curtailment inside the active Volt-VAR range and after reactive absorption has already begun.

Saturation defined to the modelling ceiling: both functions hold their limiting output up to 1.20 p.u., which prevents any extrapolation of the characteristic curves during extreme excursions in the OpenDSS solution.

Peculiar features

Deliberately asymmetric, absorb-only characteristic: at V1 = 0.90 p.u. the reactive output is fixed at Q = 0.00 rather than at maximum injection. The inverters therefore provide no reactive support during undervoltage. This is a considered design choice, because the undervoltage on this feeder occurs at the evening demand peak when PV active power output is zero, so reactive injection at that time would consume inverter capacity without addressing a load-driven condition.

Coincident dead band and ramp-start setpoints: V2 and V3 are both set at 1.01 p.u., which collapses the transition region so that absorption begins immediately at the threshold rather than after a further voltage margin. This makes the response prompt but also makes the characteristic sensitive to measurement accuracy near 1.01 p.u.

Thresholds far below manufacturer defaults: commercial inverters typically activate at or above 1.04 p.u., whereas the observed maximum voltage on this feeder is 1.038 p.u. The 1.01 and 1.02 p.u. settings are therefore the specific feature that makes the controller act at all on this network.

Conclusions and findings

Feeder-tuned parameterization is essential: the parameter set demonstrates that voltage-based control on a voltage-stiff rural feeder must be tuned to the measured sensitivity of that feeder, because default settings would leave the control dormant throughout the reverse power flow event.

Reactive-first sequencing is enforced numerically: the 0.01 p.u. offset between the Volt-VAR and Volt-Watt thresholds is what guarantees the hierarchy claimed in Section 3.6.6, and the -0.44 p.u. absorption limit remains inside the apparent power constraint of equation 3.9, so no curtailment is caused by inverter capacity exhaustion.

3.6.5 Volt-Watt Control Design

The Volt-Watt function is designed as a secondary voltage-rise mitigation strategy, to be used only when reactive power control is insufficient. In compliance with IEEE Std 1547-2018 advanced inverter requirements, the function linearly curtails active power generation when the measured terminal voltage exceeds a predefined threshold Vvw,1. The piecewise linear control law is expressed as equation 3.10 [47,48]:

$$P(V) = \begin{cases} P_{rated}, & V \le V_{vw,1} \\ P_{rated}\left(1 - \dfrac{V - V_{vw,1}}{V_{vw,2} - V_{vw,1}}\right), & V_{vw,1} < V < V_{vw,2} \\ P_{min}, & V \ge V_{vw,2} \end{cases} \quad (3.10)$$

- For terminal voltage V <= Vvw,1 the output power is maintained at the maximum available power (Prated).
- Between Vvw,1 and Vvw,2 the active power output decreases linearly in proportion to the voltage rise.
- For V >= Vvw,2 the output is fixed at a minimum permissible level (P_{min}) or ceases entirely to protect the network.

This characteristic curve, as illustrated in Figure 3.5, is defined by two primary voltage setpoints:

- Vvw,1 (curtailment start): the terminal voltage threshold at which the inverter initiates the linear reduction of its active power output. For this research this setpoint is established at 1.02 p.u., which lies inside the Volt-VAR absorption band so that reactive support is always engaged first.
- Vvw,2 (full curtailment): the voltage at which the inverter reaches its minimum power output (Pmin), providing maximum curtailment. This setpoint is configured at 1.05 p.u., coinciding with the upper statutory limit adopted in this study.

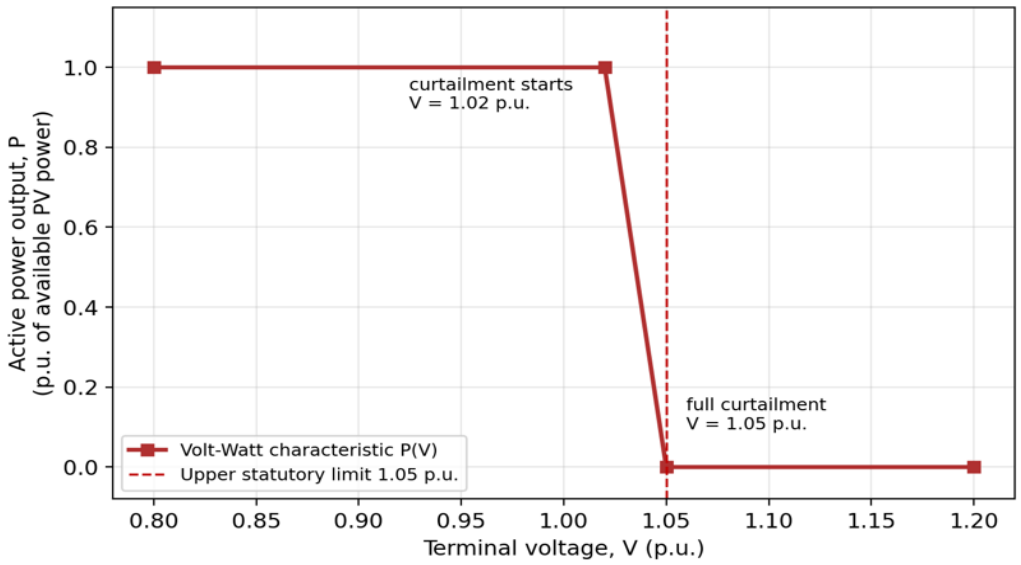

Figure 3.5: Volt-Watt Control Characteristic Curve

Analysis of Figure 3.5: Volt-Watt Control Characteristic Curve

Key observations

Three distinct operating regions: the characteristic holds P = Prated for all voltages up to 1.02 p.u., reduces active power linearly between 1.02 and 1.05 p.u., and holds the output at its minimum for higher voltages up to the 1.20 p.u. saturation ceiling.

Deterministic proportional response: curtailment is a single-valued function of the measured terminal voltage, so the same voltage always produces the same power reduction irrespective of the direction of travel or the time of day.

Full curtailment aligned to the statutory ceiling: the point of complete curtailment coincides with the 1.05 p.u. upper limit adopted in this study rather than lying beyond it, so the characteristic is exhausted exactly at the compliance boundary.

Peculiar features

Steep curtailment gradient: the full range of active power, from 100 % to 0 %, is traversed over only 0.03 p.u. of voltage. The characteristic is therefore aggressive once triggered, which explains why the curtailment recorded in Chapter 4 is concentrated in short midday intervals rather than spread across the generation window.

No hysteresis or restoration delay: the curve is modelled as a single reversible characteristic without a hold-off band, so power recovery follows the falling voltage immediately. This is acceptable at the 1-minute QSTS resolution used here, but it means the model does not represent the ride-through and restoration timers of physical inverters.

Minimum-power floor rather than disconnection: the lower limb terminates at Pmin instead of zero export with tripping, so the inverter remains connected and continues to provide reactive capability even under maximum curtailment.

Conclusions and findings

A bounded secondary safeguard: the characteristic provides a predictable, bounded upper limit on voltage rise, and its placement above the Volt-VAR threshold confirms that active power is treated as the last rather than the first control resource.

Explanation of the observed curtailment pattern: the steep slope, combined with the 1.02 p.u. onset, accounts for the selective daily curtailment of approximately 1,500 kWh reported in Section 4.5, which arises from short excursions rather than sustained power reduction.

3.6.6 Coordination and Curtailment Calculation

The voltage setpoint that initiates curtailment ($V_{vw,1}$ = 1.02 p.u.) is established above the Volt-VAR activation point (V_2 = 1.01 p.u.), as listed in Table 3.4. This design ensures

that the energy-reducing measure is only employed when reactive power compensation is exhausted or proven insufficient. The instantaneous active power curtailed from inverter i at any given time step t is calculated as the difference between the available Maximum Power Point Tracking (MPPT) generation and the actual injected active power. This relationship is expressed in equation 3.13 [47,70]:

$$P_{curtailed}(t) = P_{available}(t) - P_{out}(t) \quad (3.11)$$

Where:

- $P_{curtailed}(t)$ represents the instantaneous active power reduction caused by the Volt-Watt control action.
- $P_{available}(t)$ denotes the maximum potential power generated by the PV array under the prevailing solar irradiance.
- Pout(t) is the actual active power injected into the grid after the control logic is applied.

To synthesize the functional interactions and real-time execution flow of the proposed engineering solution, the complete closed-loop control framework is illustrated in Figure 3.6. As depicted in the schematic architecture, the local terminal voltage V(t) measured at the PV bus is evaluated against the programmed dead band threshold at each 1-minute QSTS time step. When voltage deviations exceed the dead band, the primary Volt-VAR control loop is engaged to absorb reactive power. If the reactive absorption saturates and the local voltage remains above the curtailment setpoint, the secondary Volt-Watt control loop engages to reduce real power injection, subject to the inverter's overall apparent power rating constraint (S_{rated}). The resulting setpoints Q*(t) and P*(t) are fed directly into the OpenDSS digital twin of the Murang'a 11 kV feeder, updating nodal voltages, line losses, reverse power flow and substation OLTC tap positions before cycling to the next time step.

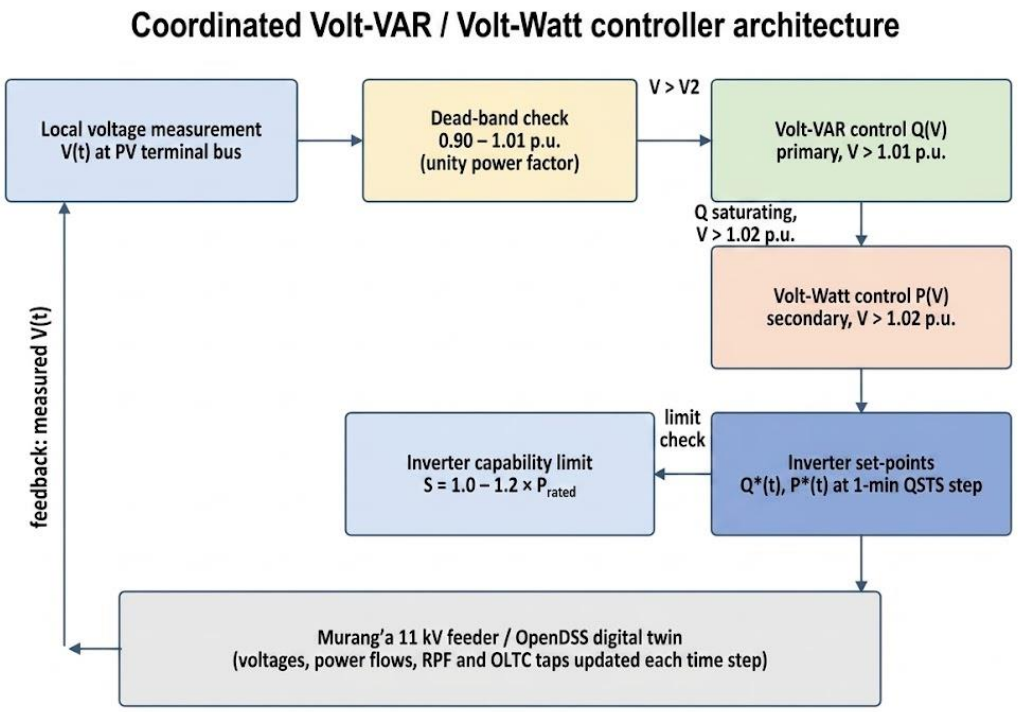

Figure 3.6: Proposed Coordinated Volt-VAR / Volt-Watt Controller Architecture

Analysis of Figure 3.6:

Key observations

Closed local control loop: the architecture measures the terminal voltage V(t) at the PV bus at every 1-minute step, compares it with the programmed dead band, engages the Volt-VAR loop when the dead band is exceeded and only then tests whether reactive absorption has saturated.

Explicit two-tier sequencing: the Volt-Watt loop is reached only through the saturation test of the Volt-VAR loop, so active power curtailment is structurally subordinate to reactive absorption.

Apparent power limiter as the final stage: the combined active and reactive setpoints are passed through the inverter apparent power constraint before dispatch, so no commanded operating point exceeds the rating of the power stage.

Peculiar features

Communication-free by construction: the architecture contains no supervisory controller, no state estimator and no communication link between inverters. Coordination is achieved solely through the offset between local voltage thresholds, which removes latency and single-point-of-failure risk but also denies each inverter any visibility of the global feeder state.

Coordination enforced by setpoints rather than logic: there is no timer, arbiter or handshake between the two loops; the hierarchy exists only because Vvw,1 exceeds V2. The coordination is therefore as reliable as the accuracy of the local voltage measurement.

Reactive capability contracts as generation rises: because the apparent power limit is applied after the active power setpoint, the reactive reserve available to the primary loop is smallest exactly at solar noon, when the voltage duty is greatest.

Conclusions and findings

Implementable with existing standard functions: the architecture requires only the Volt-VAR and Volt-Watt functions already mandated by IEEE Standard 1547-2018, so it can be deployed by reparametrizing existing smart inverters without additional hardware or communications infrastructure.

Structural limitation identified: the local-measurement-only design is the principal limitation of the scheme, and it is the reason why the controller reduces rather than eliminates reverse power flow in Section 4.4.

3.6.7 Implementation in OpenDSS

These designed control schemes were implemented within the validated OpenDSS model of the Murang'a feeder. To achieve this, the PVSystem objects were linked to InvControl elements.

The characteristic curves designed in the previous step were defined as XYCurve objects and were assigned to the respective controllers. This setup enabled the simulation of the feeder's performance with the smart inverter controls actively responding to the grid conditions at each time step of the QSTS analysis.

3.7 Validation – Performance Evaluation

This final phase is dedicated to the rigorous validation of the voltage control scheme designed in Phase 2. The objective is to quantitatively assess the effectiveness of the solution by comparing the performance of the controlled feeder against the baseline results.

This comparative analysis determines the extent to which the designed smart inverter strategies mitigate the identified voltage rise and reverse power flow. Furthermore, the evaluation verifies whether the network maintains compliance with the relevant engineering standards.

3.7.1 Definition of Key Performance Indicators (KPIs)

To ensure a comprehensive and objective assessment, a set of Key Performance Indicators (KPIs) are calculated from the simulation results. These KPIs provide the quantitative basis for the validation analysis. Each KPI is explicitly tied to the specific objective it serves, as summarized in Table 3.5, and every KPI is reported for all three scenarios defined in Table 3.3.

Table 3.5: Mapping of key performance indicators to the specific objectives

Key performance indicator	Definition / equation	Objective addressed	Scenarios reported
Maximum and minimum nodal voltage (V_{max}, V_{min})	Extreme nodal voltages over the 1,440-time steps (equation 3.4)	Objectives (i) and (iii)	A, B, C
Percentage of buses within 0.95-1.05 p.u.	Share of monitored buses complying with equation 3.4 at all-time steps	Objectives (ii) and (iii)	A, B, C
Peak reverse power flow (PRPF)	Most negative substation active power over the day	Objective (iii)	A, B, C

Key performance indicator	Definition / equation	Objective addressed	Scenarios reported
Reactive power utilization	Reactive power absorbed by the inverters relative to the available reserve (equation 3.9)	Objectives (ii) and (iii)	B, C
PV energy curtailed ($E_{curtailed}$)	Daily curtailed energy and its share of available PV energy (equations 3.12)	Objective (iii)	B, C
OLTC tap operations (N_{taps})	Counted tap movements over 24 h (equation 3.13)	Objective (iv)	A, B, C

- Voltage Profile Compliance: the primary indicator is the absence of statutory voltage limit violations. This is measured by verifying that all nodal voltages Vi(t) remain within the Vmin and Vmax limits (0.95 p.u. to 1.05 p.u.) throughout the entire 24-hour QSTS simulation.
- PV Energy Curtailment: a critical metric for evaluating the technical energy trade-off of the control strategy is the amount of useful energy that is curtailed, following EPRI and Sandia National Laboratories QSTS simulation guidelines. The total daily curtailed energy ($E_{curtailed}$) is calculated as the summation of the power curtailed at each time step, and is expressed as a percentage of the total available PV energy ($E_{available}$) for that day, as shown in equation 3.12 [63,70].

$$PV_{curtailment}[\%] = \frac{\sum_t P_{curtailed}\,(t)\Delta t}{\sum_t P_{available}\,(t)\Delta t} \times 100 \tag{3.12}$$

Where:

- Delta t is the simulation time step (one minute).
- $P_{curtailed}(t)$ is the power reduced by the Volt-Watt logic at time t.
- $P_{available}(t)$ denotes the potential power output based on the prevailing solar irradiance.

- OLTC Tap Operations: to measure the impact on legacy equipment, the total number of tap change operations for the On-Load Tap Changer (OLTC) at the substation was counted over the 24-hour simulation period for all three scenarios. The reduction in mechanical stress on legacy equipment was measured by comparing the total number of tap operations across the simulation period, as expressed in equation 3.13 [38,44]:

Analysis of Table 3.5: Mapping of Key Performance Indicators to the Specific Objectives

Key observations

Complete objective coverage: each of the six indicators is bound to at least one specific objective: nodal voltage extremes and the percentage of compliant buses to Objectives (i) to (iii), peak reverse power flow and curtailed energy to Objective (iii), reactive power utilization to Objectives (ii) and (iii), and OLTC tap operations to Objective (iv).

Consistent scenario reporting: the voltage, reverse power flow and tap indicators are reported for all three scenarios A, B and C, so every claim of improvement is made against both the pre-PV baseline and the uncontrolled PV case.

Equation-anchored definitions: each indicator is defined by an explicit equation reference rather than in narrative terms, which fixes the computation method before any result is presented.

Peculiar features

Reactive utilization and curtailment reported only for B and C: these two indicators are undefined in Scenario A because no inverters are present, so their improvement columns necessarily lack a pre-PV reference. Comparisons for these two KPIs are therefore restricted to the B-to-C pair.

Reverse power flow given equal standing with voltage: peak reverse power flow is treated as a primary indicator rather than as a secondary consequence of voltage rise. This is unusual in voltage-control studies and follows directly from the voltage-stiff behavior diagnosed in Section 4.3.

No economic or hosting-capacity indicator: curtailment is expressed in energy units only and no monetary indicator appears, while hosting capacity is deliberately excluded in accordance with the scope statement of Section 1.5. The KPI set therefore supports technical but not economic conclusions.

Conclusions and findings

Auditable link between objectives and results: the mapping guarantees that every objective stated in Chapter 1 has a measurable indicator in Chapter 4, and that no result is reported without an objective to which it is attached.

Basis of the balanced assessment: because the set contains both benefit indicators (voltage compliance, reverse power flow, tap operations) and cost indicators (curtailed energy, reactive utilization), the evaluation of the controller is necessarily reported as a trade-off rather than as an unqualified improvement.

$$N_{taps} = \sum_{t=1}^{T} |TapPos(t) - TapPos(t-1)| \tag{3.13}$$

3.7.2 Validation Simulation Scenarios

The validation was performed by executing the same QSTS simulation defined in Section 3.6 for Scenario C, that is, with the designed Volt-VAR and Volt-Watt control schemes activated on all System objects in the OpenDSS model, and comparing the outcome with Scenario A and Scenario B.

3.8 Comparative Analysis

The core of the validation was a direct comparative analysis across the three standardized scenarios of Table 3.3, in the fixed order Scenario A (baseline, no PV), Scenario B (PV integrated, uncontrolled) and Scenario C (PV integrated, coordinated control). Every key performance indicator listed in Table 3.5 is reported for the same three scenarios, so that the effect of PV integration is isolated by the comparison A to B and the effect of the coordinated controller is isolated by the comparison B to C, while the comparison A to C establishes the net position relative to the pre-PV network. The comparative assessment considered feeder voltage performance, reverse power flow, reactive-power response, PV

energy curtailment, technical energy losses, seasonal operating behavior and OLTC tap operations. The numerical results were subsequently presented and interpreted in Chapter 4 using Table 4.4 (Comprehensive Network and Mitigation Metrics), Table 4.5 (Hourly Power Flow and Midday PV Matrix), Table 4.6 (Substation OLTC Tap Operations Matrix) and Table 4.7 (Seasonal Sensitivity and Control Performance Metrics), together with the corresponding graphical results.

The control scheme was considered effective based on the following demonstrated results:

- The coordinated control reduced peak reverse power flow from 0.93 MW in Scenario B to 0.35 MW in Scenario C, representing a 62.3 % reduction.
- The coordinated control limited the maximum nodal voltage from 1.038 p.u. in Scenario B to 1.024 p.u. in Scenario C, thereby moderating the daytime voltage rise associated with high PV generation.
- PV energy curtailment was applied selectively as a secondary control action, with the observed curtailment representing a deliberate technical energy trade-off between renewable-energy utilization and feeder operating requirements.
- OLTC operations were reduced from 28 operations in Scenario B to 8 operations in Scenario C, representing a 71.4 % reduction in mechanical duty and 33.3 % fewer operations than the 12 recorded in Scenario A.

This data-driven comparison provides the evidence base for evaluating the effectiveness of the designed engineering solution.

3.9 Sensitivity Analysis

To test the robustness of the proposed control framework beyond the nominal operating point, a sensitivity analysis was incorporated into the evaluation. The analysis varies each key design parameter one at a time about its baseline value; the parameters, ranges, increments, response variables and acceptance criteria are specified in Table 3.6. The seasonal high- and low-irradiance cases reported in Sections 4.7 and 4.8 form part of this robustness assessment rather than a separate objective.

Table 3.6: Sensitivity analysis design

Parameter varied	Range	Increment	Response variable	Criterion
Aggregate PV penetration	1 MW to 5 MW	1 MW	Vmax, PRPF, $E_{curtailed}$	Vmax <= 1.05 p.u. with control active
Inverter apparent power rating	1.0 to 1.2 x Prated	0.1 x Prated	Reactive reserve $Q_{available}$, $E_{curtailed}$	Curtailment minimized for a given Vmax
Feeder load level	0.8 to 1.2 x recorded demand	0.2 x recorded demand	V_{min}, PRPF, E_{loss}	V_{min} >= 0.95 p.u. within the PV window
Irradiance condition (seasonal case)	Dry season and rainy season profiles	Two discrete cases	Vmax, PRPF, $E_{curtailed}$	Compliance maintained in both seasons

The purpose of the sensitivity study is to confirm that the coordinated control continues to hold nodal voltages within statutory limits as conditions depart from the nominal case, and to identify the penetration level at which reactive support alone becomes insufficient and active-power curtailment begins to dominate. The outcomes obtained for the cases actually simulated in this study are reported in Sections 4.7 and 4.8; where a range in Table 3.6 was not simulated in full, this is stated explicitly in Chapter 4 and identified as further work in Section 5.3 rather than presented as a result.

Analysis of Table 3.6: Sensitivity Analysis Design

Key observations

Four independent design parameters: aggregate PV penetration is varied from 1 MW to 5 MW in 1 MW steps, inverter apparent power rating from 1.0 to 1.2 x Prated in 0.1 steps, feeder load level from 0.8 to 1.2 x recorded demand in 0.2 steps, and irradiance is treated as two discrete seasonal cases.

Response variables tied to the KPI set: each parameter is paired with the specific response variables it is expected to influence, namely Vmax, peak reverse power flow, curtailed energy, reactive reserve, V_{min} and losses, all of which are already defined in Table 3.5.

Explicit acceptance criterion per row: every parameter carries its own pass condition, such as Vmax <= 1.05 p.u. with control active and V_{min} >= 0.95 p.u. within the PV window, so robustness is assessed against stated limits rather than by inspection.

Peculiar features

One-factor-at-a-time design: parameters are varied individually about the nominal point, so no combined worst case, such as maximum penetration coincident with minimum load, is constructed and no parameter interaction is captured.

Coarse penetration increment: the 1 MW step is approximately one third of the 3 MW installed capacity and slightly more than one third of the 2.8 MW feeder peak, so the design resolves the trend of the response rather than a precise threshold.

Deterministic rather than stochastic treatment of irradiance: the seasonal dimension is reduced to two discrete profiles instead of a sampled distribution, so climatic uncertainty is bounded by two cases rather than characterized statistically.

Partial execution declared in advance: the table specifies the intended design space, whereas the cases actually simulated are the 3 MW point and the two seasonal profiles. The remaining ranges are identified as further work rather than reported as results, which is stated explicitly in Chapter 4.

Conclusions and findings

Transparent bounding of the robustness claims: the design allows the robustness of the controller to be tested against stated criteria while making the limits of that test explicit, so no general claim of robustness beyond the simulated cases is implied.

Direct justification of the recommended further work: the one-at-a-time structure and the two-case treatment of irradiance are the specific reasons for the recommendation in Section 5.3 that a stochastic, Monte Carlo based sensitivity study be undertaken.

3.10 Chapter Summary

This chapter has presented the systematic methodology used to design and evaluate a voltage control scheme for the Murang'a feeder. The research was executed as a quantitative, simulation-based case study using the OpenDSS software.

The methodology maps onto the four specific objectives as follows. Objective (i) was addressed in Sections 3.4 and 3.5 through the acquisition and classification of the utility data, the construction of the OpenDSS digital twin, its statistical validation against field measurements at three monitored nodes, and the baseline network analysis. Objective (ii) was addressed in Section 3.6 through the design, parameterization and OpenDSS implementation of the coordinated Volt-VAR/Volt-Watt controller. Objective (iii) was addressed in Sections 3.7 to 3.9 through the 1-minute QSTS simulations of Scenarios A, B and C, the comparative KPI evaluation and the sensitivity analysis. Objective (iv) was addressed through the OLTC duty metric of equation 3.13, both evaluated for all three scenarios. This structured approach ensured that the research objectives were met in in a replicable and technically sound manner.

CHAPTER FOUR
RESULTS AND DISCUSSION

4.1 Introduction

To systematically evaluate the technical challenges of high-penetration distributed solar generation and validate the performance of the proposed mitigation framework, the three standardized scenarios defined in Table 3.3 were executed over a 24-hour horizon using a 1-minute time step, giving 1,440 simulation steps per scenario. The simulations utilized the validated OpenDSS model of the 69 km long, 11 kV rural distribution network. The structural configuration, nodal allocation points, and exact control parameter matrices characterizing these simulations are summarized in Table 4.1.

The chapter is organized so that each block of results is attached to the objective it serves: Sections 4.2 and 4.3 report the digital twin and baseline feeder behavior and therefore address Objective (i); Sections 4.4 and 4.5 report the behavior and performance of the coordinated controller and therefore address Objectives (ii) and (iii); Section 4.6 reports the technical losses and the OLTC duty and therefore addresses Objective (iv); Sections 4.7 and 4.8 report the seasonal robustness and sensitivity cases, which support Objective (iii); and Section 4.9 integrates the findings with previous studies.

Table 4.1: Simulation Scenario Matrix and Parameters

Parameter / element	**Scenario A: baseline (no PV)**	**Scenario B: PV integrated, uncontrolled**	**Scenario C: PV integrated, coordinated control**
PV integration status	Disabled (0 MW)	Enabled (3 x 1 MW)	Enabled (3 x 1 MW)
Allocation nodes (buses)	Not applicable	Bus 52, Bus 87, Bus 158	Bus 52, Bus 87, Bus 158
Inverter control state	Not applicable	Unity power factor, no droop response	Active coordinated control loop
Volt-VAR threshold (V2, absorption start)	Not applicable	Not applicable	1.01 p.u.
Volt-Watt threshold (Vvw,1, curtailment start)	Not applicable	Not applicable	1.02 p.u.

Parameter / element	Scenario A: baseline (no PV)	Scenario B: PV integrated, uncontrolled	Scenario C: PV integrated, coordinated control
Maximum reactive power (Qmax)	Not applicable	0.0 VAR	-0.44 p.u. (absorbing)
Simulation resolution	1-minute step, 1,440 steps	1-minute step, 1,440 steps	1-minute step, 1,440 steps

As defined in the scenario matrix above, Scenario A establishes the natural demand and voltage characteristics of the network under a standard daily load profile with zero PV generation. Scenario B introduces the high-penetration condition by integrating three separate 1 MW grid-tied PV systems operating at a fixed unity power factor. These systems are placed at Bus 52, Bus 87 and Bus 158 to capture the geographically dispersed nature of distributed generation on long radial networks. Scenario C applies the coordinated smart inverter control strategy across the same allocation nodes, executing the Volt-VAR and Volt-Watt regulation loops parameterized in Table 3.4.

Analysis of Table 4.1: Simulation Scenario Matrix and Parameters

Key observations

A single controlled variable: the feeder topology, the 24-hour demand profile, the 3 x 1 MW PV allocation at Bus 52, Bus 87 and Bus 158, and the 1-minute, 1,440-step resolution are held identical across the scenarios, so the inverter control state is the only variable that changes between Scenario B and Scenario C.

Progressive experimental sequence: the matrix advances from the pre-PV network (Scenario A), through uncontrolled integration at unity power factor (Scenario B), to the coordinated controller with V2 = 1.01 p.u., Vvw,1 = 1.02 p.u. and Q_{max} = -0.44 p.u. (Scenario C).

Consistent simulation resolution: the same 1-minute step is applied in all three cases, which is what makes the tap-hunting behavior of Section 4.6 visible in every scenario rather than in the controlled case alone.

Peculiar features

Capability present but disabled in Scenario B: Scenario B specifies Qmax = 0.0 VAR with the same physical inverters that provide -0.44 p.u. in Scenario C. The comparison therefore isolates the value of the control settings rather than the value of the hardware, which is the practically relevant question for a utility that already has inverters installed.

No partial-control case: there is no scenario in which Volt-VAR acts alone or Volt-Watt acts alone, so the coordinated scheme is evaluated as an indivisible package and the individual contribution of each loop is inferred from the reactive and curtailment records rather than measured directly.

Identical PV siting in both PV cases: holding the allocation nodes fixed removes siting as an explanatory variable, which means the study quantifies control performance at a given siting and not the optimal siting itself.

Conclusions and findings

A properly controlled numerical experiment: because only the control state varies, every difference reported between Scenarios B and C in Chapter 4 is attributable to the coordinated controller, and every difference between A and B is attributable to PV integration.

Comparability across the results chapter: the fixed matrix is what allows the voltage, reverse power flow, curtailment and tap results in Sections 4.2 to 4.8 to be compared on a like-for-like basis and consolidated in Table 4.8.

The underlying physical properties of the distribution grid heavily dictate its operational response to these high levels of distributed generation. To accurately evaluate these localized voltage impacts, the primary trunk and lateral segments of the Murang'a 11 kV feeder are modeled in the OpenDSS environment using their specific line impedance characteristics.

The physical parameters detailed in Table 4.2 show that the Murang'a 11 kV feeder possesses a substantial primary trunk length of 69 km. Managing 158 medium-voltage

buses and 92 distribution transformers across such an extensive radial layout accentuates line losses and voltage regulation challenges. Because rural overhead lines feature a high resistance-to-reactance (R/X) ratio compared with tightly coupled urban underground networks, the feeder is structurally high-impedance and its nodal voltages are sensitive to active power injection, as analysed in Section 4.3. This baseline architectural framework is important because it dictates how the local voltage profiles respond when substantial active power is injected during peak solar irradiance windows.

Table 4.2: Structured and Architectural Parameters of the Validated Rural Feeder

Feeder component parameter	**Engineered model specification value**	**Operational grid relevance summary**
Total length of primary trunk	69.0 km	Extensive radial layout exacerbating end-of-line voltage variations
Nominal system operating voltage	11 kV	Medium-voltage rural distribution standard in Kenya
Total number of medium-voltage buses	158 buses	Provides dense nodal granularity for QSTS simulation tracing
Total integrated distribution transformers	92 transformers	Step-down configuration managing localized rural load demands
System peak load capacity	2.8 MW (occurs at Hour 18)	Establishes target maximum demand profile for grid validation
Conductor physical attributes	High R/X overhead lines	High series resistance relative to reactance, so nodal voltage is dominated by active power flow

Analysis of Table 4.2: Structural and Architectural Parameters of the Validated Rural Feeder

Key observations

Extended radial geometry: the feeder comprises a 69.0 km primary trunk at 11 kV with 158 medium-voltage buses and 92 distribution transformers, which is a long, densely tapped rural layout rather than a compact urban circuit.

Modest peak demand relative to length: the system peak load is 2.8 MW at Hour 18, so the feeder carries a low power density over a long distance, which is the classical condition for end-of-line voltage drop.

Resistance-dominated conductors: the trunk is built from high R/X overhead line, so nodal voltage responds primarily to active rather than reactive power flow.

Peculiar features

Installed PV capacity exceeds the feeder peak: the 3 MW of integrated PV is greater than the 2.8 MW system peak and roughly 50 % above the midday load valley of about 2.0 MW. Reverse power flow is therefore a structural certainty at full irradiance and not an incidental outcome of the scenario definition.

High transformer-to-bus density: 92 transformers distributed across 158 buses indicates that load is tapped along almost the whole trunk. This dispersed load is what absorbs part of the PV injection and contributes to the voltage stiffness diagnosed in Section 4.3.

Structural weakness and observed stiffness coexist: the parameters describe a weak, high-impedance, high R/X feeder that should be strongly voltage-sensitive, yet the measured rise at 3 MW penetration is only 0.036 p.u. above baseline. The structural parameters therefore describe sensitivity, not the net observed response.

Conclusions and findings

Physical basis of the dominant stress: the combination of a long resistive trunk, low midday demand and installed PV above peak load establishes reverse power flow, rather than statutory overvoltage, as the dominant PV-induced stress on this feeder.

Justification of the control siting and thresholds: because voltage sensitivity is distributed along the trunk and the resulting rise is moderate, control must be applied locally at the injection nodes and must be triggered well below default manufacturer thresholds.

The sensitive operation of the localized inverter loops is executed within the OpenDSS simulation environment via piece-wise linear tracking arrays. The coordinated control curves modify the real power and reactive power output based on instantaneous localized voltage measurements. Table 4.3 records the exact coordinate array mapping used to trigger reactive power absorption and subsequent active power curtailment.

Table 4.3: Coordinate points Mapping for OpenDSS Smart Inverter Tracking Curves

Inverter control curve	**Voltage array points (X-array, p.u.)**	**Power output multiplier (Y-array)**	**Functional operating point behavior**
Volt-VAR functional curve	0.90	0.00	Lower voltage dead band boundary
Volt-VAR functional curve	1.01	0.00	Trigger threshold for reactive power absorption
Volt-VAR functional curve	1.04	-0.44	Maximum reactive absorption level achieved
Volt-VAR functional curve	1.20	-0.44	Saturation upper bound
Volt-Watt functional curve	0.80	1.00	Normal operation, maximum active output
Volt-Watt functional curve	1.02	1.00	Threshold initiating active power curtailment
Volt-Watt functional curve	1.05	0.00	Complete active power curtailment
Volt-Watt functional curve	1.20	0.00	Saturation ceiling, consistent with the XY Curve definition in Appendix 4

The coordinates defined in Table 4.3 detail a control philosophy tuned specifically for this high resistance-to-reactance (R/X) feeder. The Volt-VAR curve initiates reactive power absorption early at 1.01 p.u., scaling to a maximum absorption of -0.44 p.u. at 1.04 p.u. By prioritizing reactive power absorption within this tight envelope, the system

suppresses voltage rise without unnecessarily reducing active power yield. If the localized voltage continues to climb due to extreme solar irradiance, the Volt-Watt curve serves as a secondary safeguard, initiating real power curtailment at 1.02 p.u. and sloping down to complete curtailment at 1.05 p.u.

Analysis of Table 4.3: Coordinate Points Mapping for the OpenDSS Smart Inverter Tracking Curves

Key observations

Faithful transcription of the design: the Volt-VAR X-array of 0.90, 1.01, 1.04 and 1.20 p.u. with Y-values 0.00, 0.00, -0.44 and -0.44, and the Volt-Watt X-array of 0.80, 1.02, 1.05 and 1.20 p.u. with Y-values 1.00, 1.00, 0.00 and 0.00, reproduce exactly the setpoints specified in Table 3.4.

Piecewise linear XYCurve representation: each characteristic is defined by four coordinate pairs, so OpenDSS interpolates linearly between the design breakpoints at every time step.

Normalised output multipliers: the Y-arrays are expressed as per-unit multipliers, so the Volt-VAR value of -0.44 corresponds to 440 kvar of absorption for each 1 MW inverter and the Volt-Watt values scale directly against the available MPPT power.

Peculiar features

Different lower anchor points for the two curves: the Volt-Watt array starts at 0.80 p.u. whereas the Volt-VAR array starts at 0.90 p.u. The wider active power curve keeps the curtailment characteristic defined during deep undervoltage excursions, which prevents undefined behaviour in the solver at the evening demand peak.

Deliberate saturation terminals at 1.20 p.u.: both arrays are terminated well above the statutory ceiling so that OpenDSS never extrapolates beyond the tabulated range, which is a numerical safeguard rather than a control requirement.

Zero-output segments encoded explicitly: the repeated Y-values at both ends of each array encode the dead band and saturation regions as explicit flat segments, so the dormant state of the controller is a modelled condition rather than an implicit default.

Conclusions and findings

Verified implementation of the designed control law: the coordinate mapping confirms that the controller exercised in Chapter 4 is numerically identical to the characteristic designed in Chapter 3, so no discrepancy exists between the designed and simulated control law.

Reproducibility of the simulation: because the arrays are fully tabulated, the OpenDSS InvControl configuration can be reconstructed exactly from this table together with Appendices 1 and 4.

4.2 Baseline Performance and Uncontrolled PV Integration

This section presents the baseline performance of the Murang'a feeder (Scenario A) and evaluates the impact of integrating uncontrolled photovoltaic generation (Scenario B). Together with Section 4.3 it addresses Objective (i).

4.2.1 Baseline Feeder Performance (Scenario A, Without PV)

The baseline simulation (Scenario A, no PV) established the typical load profile of the Murang'a 11 kV feeder. As expected, the feeder exhibited a peak demand of approximately 2.8 MW during the evening hours (around Hour 18), consistent with standard rural consumption patterns.

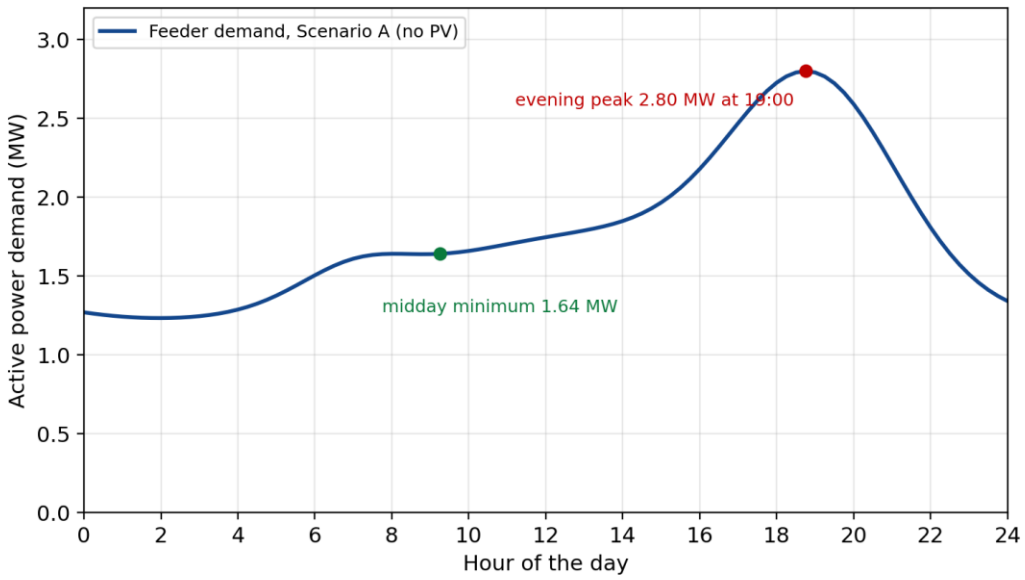

Figure 4.1: 24 Hour Load Profile of Murang'a Feeder Showing Peak and Minimum Demand

The graphical profile illustrated in Figure 4.1 shows the variation in substation net power across the studied operational boundaries. To contextualize these swings with aggregated data indices, Table 4.4 provides a quantitative summary of how the coordinated strategy performs compared with the baseline and uncontrolled states.

Table 4.4: Comprehensive Network and Mitigation Metrics

Key performance metric	**Scenario A: baseline (no PV)**	**Scenario B: uncontrolled high PV**	**Scenario C: coordinated control**
Peak substation power flow	+2.80 MW (forward load peak)	-0.93 MW (reverse back feed peak)	-0.35 MW (suppressed reverse peak)
Reverse power flow mitigation rate	Not applicable	0.0 % (reference)	62.3 % reduction relative to Scenario B
Maximum observed nodal voltage	1.002 p.u.	1.038 p.u. (voltage rise at the PV connection nodes; below the 1.05 p.u. limit)	1.024 p.u. (regulated)
Minimum nodal voltage at Bus 158	0.912 p.u.	0.945 p.u.	0.921 p.u.

Key performance metric	Scenario A: baseline (no PV)	Scenario B: uncontrolled high PV	Scenario C: coordinated control
(evening peak, PV output zero)			
Daily PV energy curtailed	0 kWh	0 kWh (full energy yield)	Approximately 1,500 kWh/day
OLTC tap operations (24 h)	12	28	8

The comparative indices compiled in Table 4.4 show that the tailored control strategy suppresses the peak reverse power flow by 62.3 %, from 0.93 MW to 0.35 MW, and limits the maximum nodal voltage from 1.038 p.u. to 1.024 p.u. This is obtained at a technical energy trade-off of approximately 1,500 kWh of available solar energy curtailed per day, that is, renewable energy sacrificed for grid benefit.

Two points require careful interpretation of the voltage results. First, the 1.038 p.u. maximum recorded in Scenario B is pronounced voltage rise relative to the 1.002 p.u. baseline, but it remains below the 1.05 p.u. upper limit adopted in this study and is therefore not a statutory overvoltage violation. Second, the minimum voltages listed for Bus 158 (0.912 p.u. in Scenario A, 0.921 p.u. in Scenario C) occur at the evening demand peak around Hour 18, when PV output is essentially zero. They are a pre-existing, load-driven condition of this 69 km feeder and are neither caused by PV integration nor removable by inverter control, because the inverters cannot inject active power after sunset. The claim of full compliance with the adopted 0.95-1.05 p.u. band therefore applies to the PV generation window, and the pre-existing evening undervoltage at the feeder extremity is reported here as an unresolved network condition that requires conventional reinforcement or voltage regulation, as recommended in Section 5.3.

Analysis of Table 4.4: Comprehensive Network and Mitigation Metrics

Key observations

Substantial suppression of reverse power flow: the peak substation flow moves from +2.80 MW of forward demand in Scenario A to -0.93 MW of backfeed in Scenario B and is reduced to -0.35 MW in Scenario C, a mitigation of 62.3 %.

Recovery of voltage headroom: the maximum nodal voltage rises from 1.002 p.u. at baseline to 1.038 p.u. without control and is limited to 1.024 p.u. with the coordinated controller, so approximately 0.014 p.u. of the 0.036 p.u. rise is recovered.

Reduced mechanical duty at an energy cost: OLTC operations fall from 28 in Scenario B to 8 in Scenario C, while approximately 1,500 kWh per day of available solar energy is curtailed, which is the only indicator that deteriorates under control.

Peculiar features

No statutory overvoltage occurs in any scenario: the worst recorded voltage of 1.038 p.u. remains below the 1.05 p.u. limit, so the controller is not correcting a violation but recovering margin against one. The operational problem being solved is the 0.93 MW back feed, not the voltage magnitude.

Controlled tap count falls below the pre-PV baseline: the 8 operations of Scenario C are fewer than the 12 recorded without any PV at all, so the coordinated inverters relieve mechanical duty that pre-dates PV integration rather than merely cancelling the duty that PV creates.

Reported minima occur outside the generation window: the Bus 158 minima of 0.912, 0.945 and 0.921 p.u. all occur at the Hour 18 demand peak when PV output is essentially zero, so the differences between them reflect the residual tap position and loading state at the end of the day rather than any active inverter contribution. The compliance claim for the 0.95 to 1.05 p.u. band therefore applies to the PV generation window only.

Conclusions and findings

The coordinated controller improves on the pre-PV network: on both reverse power flow and tap duty, Scenario C is superior not only to the uncontrolled PV case but also to the original network, which establishes the scheme as non-wires measure rather than merely a mitigation of its own side effects.

The cost is bounded and technical: the entire penalty of the strategy is approximately 1,500 kWh per day of curtailed renewable energy, reported here in energy terms only, with no economic valuation claimed.

A residual, unresolved condition is retained: the pre-existing evening undervoltage at Bus 158 is outside the reach of inverter control and remains a requirement for conventional reinforcement or additional voltage regulation, as recommended in Section 5.3.

To evaluate the step-by-step performance of the network during the core backfeed event shown in the graphs, a detailed time-series extraction was conducted. Table 4.5 logs the hourly substation active power flow alongside localized bus voltages observed across the midday generation peak spanning Hour 08 to Hour 14.

Table 4.5: Hourly Powerflow and Midday PV Matrix

Simulation time (hour)	Scenario A load (MW)	Scenario B substation flow (MW)	Scenario C substation flow (MW)	Peak voltage at Bus 52 (p.u.)	Peak voltage at Bus 87 (p.u.)
Hour 08	1.80	-0.34	-0.12	1.002	1.006
Hour 09	1.95	-0.45	-0.18	1.008	1.012
Hour 10	2.00	-0.81	-0.31	1.018	1.026
Hour 11	2.02	-0.93	-0.35	1.024	1.038
Hour 12	1.98	-0.84	-0.33	1.022	1.035
Hour 13	1.96	-0.42	-0.16	1.012	1.021
Hour 14	1.90	-0.10	-0.02	1.001	1.004

The hourly profile data in Table 4.5 highlights the primary diagnostic finding of this research. At the peak of solar irradiance (Hour 11) the uncontrolled active power back feed reaches its maximum of -0.93 MW. Yet, despite the high R/X characteristics of the feeder, the voltage rise at the most sensitive node (Bus 87) reaches only 1.038 p.u., which is below the default activation threshold of commercial smart inverters, typically set at or above 1.04 p.u. Consequently, generic inverter controllers do not initiate Volt-VAR or Volt-Watt action and the reverse power flow persists unmitigated. This is the justification for the feeder-specific thresholds of the coordinated framework, which activate at 1.01 p.u. and 1.02 p.u. and therefore act on this feeder where default settings do not.

Analysis of Table 4.5: Hourly Power Flow and Midday PV Matrix

Key observations

Back feed and voltage rise peak together at Hour 11: the uncontrolled substation flow reaches its most negative value of -0.93 MW at Hour 11, coincident with the maximum Bus 87 voltage of 1.038 p.u., which identifies Hour 11 as the critical design hour.

Consistent proportional mitigation: in Scenario C the hourly flows are reduced from -0.34, -0.45, -0.81, -0.93, -0.84, -0.42 and -0.10 MW to -0.12, -0.18, -0.31, -0.35, -0.33, -0.16 and -0.02 MW, a reduction of roughly 60 to 80 % that is sustained across the whole window rather than achieved at a single hour.

Convergence at the window boundaries: at Hour 14 the controlled and uncontrolled flows converge to -0.02 and -0.10 MW and the bus voltages return to about 1.001 to 1.004 p.u., confirming that the controller withdraws as generation falls.

Peculiar features

Maximum voltage occurs at mid-feeder rather than at the extremity: Bus 87 records higher voltages than Bus 52 at every hour and is the node that sets the 1.038 p.u. maximum, although a 1 MW unit is also connected at the extremity Bus 158. The critical node is therefore determined by the local impedance and residual load, not simply by distance from the substation.

The peak voltage falls just below default inverter activation: 1.038 p.u. lies below the 1.04 p.u. threshold at which commercial inverters typically begin to act, so a generic controller would have remained dormant for the entire event. The whole reverse power flow would then have persisted unmitigated, which is the single most consequential observation in this table.

Voltage remains compliant while power flow does not: throughout Hours 08 to 14 every tabulated voltage is inside the 0.95 to 1.05 p.u. band, so voltage magnitude alone gives no indication that the feeder is under stress.

Conclusions and findings

Voltage is an insufficient indicator of PV-induced stress: the table establishes empirically that a voltage-compliant feeder can nevertheless export nearly one third of its

installed PV capacity upstream, which qualifies the conventional assumption that overvoltage is the primary symptom of excessive distributed generation.

Feeder-specific thresholds are necessary, not merely preferable: because the controller must act at 1.01 and 1.02 p.u. to respond at all, the results confirm that inverter setpoints on structurally weak rural feeders must be derived from the measured voltage sensitivity of the network in question.

4.2.2 Analysis of Baseline Feeder performance

The baseline results from Figure 4.1 confirm that the Murang'a feeder follows a typical rural load profile, characterized by low demand during midday and peak demand in the evening hours. The observed peak of approximately 2.8 MW at Hour 18 reflects residential consumption patterns, where energy use increases due to lighting, cooking, and domestic activities. Conversely, the minimum demand during midday coincides with reduced residential activity, resulting in a natural load valley.

Analysis of Figure 4.1: 24-Hour Load Profile of the Murang'a Feeder

Key observations

Pronounced evening peak: substation demand rises to approximately 2.8 MW at Hour 18, consistent with residential lighting, cooking and domestic activity in a rural feeder.

Midday load valley: demand falls to roughly 1.8 to 2.0 MW between Hour 08 and Hour 14, which is the interval in which solar generation is greatest.

Twin ramp structure: the profile exhibits a morning ramp and a steeper evening ramp, both of which are the demand-driven cause of the 12 baseline tap operations recorded in Table 4.6.

Peculiar features

Temporal anti-correlation with the solar resource: the load minimum coincides almost exactly with the irradiance maximum, so the mismatch, rather than the size of the PV plant alone, is the mechanism that produces reverse power flow. A feeder with a midday-peaking load would not exhibit the same behavior at the same penetration.

The daily peak occurs after sunset: the 2.8 MW peak at Hour 18 falls outside the generation window, so the PV systems can contribute no active power at the moment of maximum system stress. This is the structural reason why the 0.912 p.u. minimum at Bus 158 cannot be corrected by inverter control.

A moderate peak-to-valley ratio: the ratio of roughly 1.5 to 1.7 means that a substantial residual load remains connected during the generation window and absorbs part of the PV output, which contributes to the limited voltage rise observed in Scenario B.

Conclusions and findings

The baseline is a conventional rural profile: the feeder behaves as a typical residential rural circuit, which supports the transferability of the findings to comparable Kenyan 11 kV feeders.

Two separate problems are distinguished: the profile establishes that midday back feed and evening undervoltage are distinct phenomena with distinct causes, and that only the former is within the reach of smart inverter control.

4.2.3 Uncontrolled PV Integration Scenario

The integration of three 1 MW PV systems into the feeder without active control revealed significant operational challenges. These results highlight the technical consequences regarding the impact of generation-load mismatch. Figure 4.1 illustrates the substation power flow for both the baseline and uncontrolled PV scenarios. The cumulative impact of PV generation during midday hours far exceeded local load demand, leading to substantial RPF.

4.2.3.1 Analysis of Feeder performance with uncontrolled PV Integration

Under the uncontrolled PV scenario, the generation profile is inversely correlated with the load profile. PV output peaks during midday hours (10 to 14 hrs), precisely when feeder demand is at its lowest. This temporal mismatch creates a condition where the instantaneous generation exceeds local consumption, forcing excess energy to be exported upstream toward the substation.

As illustrated in Figure 4.1, this results in significant reverse power flow (RPF), with a peak magnitude of approximately 0.93 MW. This indicates that nearly one-third of the installed PV capacity is not locally consumed but instead flows back into the upstream network. Such behavior represents a fundamental shift from the traditional unidirectional power flow paradigm to a bidirectional power flow regime, which the existing distribution infrastructure is not inherently designed to handle.

4.3 Diagnosis of the Observed Voltage Sensitivity of the Feeder

The results obtained from the uncontrolled PV scenario (Scenario B) reveal an apparent contradiction that requires careful terminology, because the terms weak, stiff, high impedance and high R/X are not interchangeable and are used in this thesis with the following distinct meanings:

- high R/X ratio describes the conductor property that makes nodal voltage respond mainly to active rather than reactive power flow;
- high impedance and structurally weak describe the 69 km radial topology and the resulting large source-to-end-of-line impedance, which is confirmed by the 0.912 p.u. evening minimum voltage at Bus 158 in Scenario A;
- observed voltage stiffness describes the empirical outcome of this particular study, namely that the measured voltage rise per MW of injected active power is smaller than the structural parameters alone would suggest.

The Murang'a feeder is therefore structurally weak and high-impedance with a high R/X ratio, and nevertheless exhibits only limited voltage rise at the investigated 3 MW penetration level. This is not a contradiction: the structural parameters describe the feeder's sensitivity, whereas the observed rise is the net result of that sensitivity and of the mitigating factors listed below.

In this study the voltage sensitivity of the feeder is evaluated by examining the relationship between the magnitude of injected active power from distributed PV systems and the resulting voltage deviation across the network.

Given that rural distribution feeders are typically characterized by a high resistance-to-reactance (R/X) ratio, voltage variations are expected to be predominantly influenced by active power injection. Consequently, the introduction of substantial PV generation would ordinarily be anticipated to result in significant voltage rise.

However, the simulation results indicate that even with a peak reverse power flow of approximately 0.93 MW, the maximum voltage observed along the feeder is only about 1.038 p.u. This is appreciable voltage rise relative to the 1.002 p.u. baseline maximum, but it remains below the 1.05 p.u. statutory ceiling and below the typical activation thresholds of standard voltage-based inverter control schemes, which are commonly set at or above 1.04 p.u. Several factors account for the difference between the structural sensitivity of the feeder and the moderate rise actually observed:

- Firstly, the distributed placement of the PV systems along the feeder results in spatially dispersed power injection. This reduces the concentration of voltage rise at any single node and leads to a more gradual voltage profile along the feeder.
- Secondly, the presence of distributed load along the network, even during periods of low demand, partially absorbs the generated PV power. This reduces the net exported power and mitigates the extent of the voltage increase.
- Thirdly, the impedance characteristics and topology of the feeder distribute the voltage variation across multiple line segments, thereby limiting localized voltage excursions.
- Finally, upstream voltage regulation, in particular the substation transformer tap changer, further moderates the feeder voltage under varying operating conditions, at the cost of the increased tap duty quantified in Section 4.6.

The implications are significant. Conventional smart inverter control strategies, which rely on predefined voltage thresholds to initiate corrective action, may fail to respond under these conditions: the voltage does not exceed their default activation threshold, and substantial reverse power flow therefore occurs without triggering any voltage-based control action.

This condition presents a critical operational challenge, because the network may remain within acceptable voltage limits while still experiencing undesirable power flow patterns that can affect protection coordination, increase current circulation and the associated losses, and impose additional duty on upstream equipment. Reverse power flow, rather than statutory overvoltage, is therefore the dominant PV-induced operating stress in the scenarios investigated here.

The findings consequently highlight a key limitation of generic inverter control settings when applied to structurally weak rural feeders, and underscore the need for feeder-tuned control thresholds that respond to the voltage sensitivity actually measured on the network in question.

4.4 Performance of the Adaptive Coordinated Control Strategy

This section and Section 4.5 address Objectives (ii) and (iii): they report the behavior of the controller developed under Objective (ii) and its quantified performance under Objective (iii). The primary objective of this phase was to evaluate the efficacy of the designed adaptive coordinated control strategy in remediating the technical deficiencies identified in Scenario B. By leveraging the multi-objective capabilities of smart inverters, the framework sought to align decentralized generation with localized consumer demand through simultaneous voltage support and active power management.

4.4.1 Reverse Power Flow Mitigation

The implementation of the adaptive coordinated control strategy (Volt-VAR and Volt-Watt) fundamentally altered the power flow dynamics at the primary substation. As illustrated in the comparative analysis in Figure 4.2, the peak reverse power flow, which reached a magnitude of 0.93 MW in Scenario B, was reduced to 0.35 MW in Scenario C. This is a 62.3 % reduction, obtained as shown in equation 4.1:

$$\Delta P_{RPF} = \left(\frac{0.93 - 0.35}{0.93}\right) \times 100\% = 62.3\% \tag{4.1}$$

Because the smart inverters execute control laws governed purely by terminal voltage $V(t)$,the observed 62.3% reduction in peak reverse power flow (from 0.93 MW to 0.35 MW) is an indirect, positive operational outcome. Active power curtailment triggered by the Volt-Watt function during localized voltage rise directly reduces the net active power injected at the buses, thereby suppressing the surplus active power exported back to the primary substation.

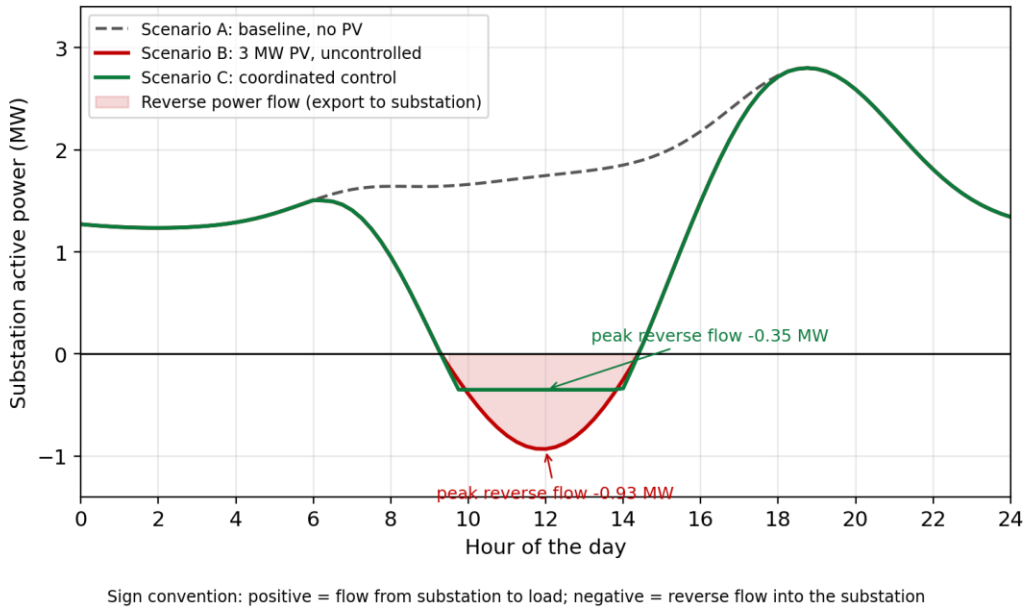

Figure 4.2: Coordinated Volt-VAR and Volt-Watt Strategy in Mitigating Substation Reverse Power Flow

Analysis of Figure 4.2: Coordinated Control in Mitigating Substation Reverse Power Flow

Key observations

Clear reversal window: both PV cases cross from forward to reverse flow during the midday interval, with the uncontrolled curve reaching a peak back feed of 0.93 MW and the controlled curve limited to 0.35 MW, a reduction of 62.3 % obtained from equation 4.1.

Coincident curves outside the generation window: the two traces are indistinguishable before Hour 08 and after Hour 16, since the controller has no active or reactive action to take when the voltage lies inside the deadband.

Retained forward-flow character for most of the day: for the majority of the 24-hour horizon the substation continues to supply the feeder conventionally, so the bidirectional condition is a bounded daytime event rather than a permanent regime change.

Peculiar features

Reverse power flow is reduced but not removed: a residual 0.35 MW of back feed persists at solar noon. Eliminating it entirely would require curtailment approaching the full surplus, so the controller deliberately trades complete elimination for retained renewable yield. Protection coordination studies for bidirectional flow therefore remain necessary.

Time-asymmetric mitigation: the vertical separation between the curves is greatest around solar noon and negligible at the window edges, which shows that control effort is self-scheduling and proportional to the instantaneous surplus rather than applied as a fixed limit.

Mitigation achieved without network reinforcement: the entire improvement is obtained by reparametrizing existing inverters, with no change to conductors, transformers or regulating equipment.

Conclusions and findings

Demonstrated non-wires mitigation of back feed: the coordinated strategy delivers a 62.3 % reduction in peak reverse power flow on the investigated feeder using only IEEE 1547 inverter functions, which supports the practical viability of decentralized control as an alternative to reinforcement.

Residual bidirectional operation must be planned for: because back feed is not eliminated, the utility must still verify protection settings, metering direction and equipment duty for the reduced but non-zero reverse flow.

4.4.2 Voltage Profile Improvement

The implementation of the coordinated voltage control strategy improved the feeder voltage profile under high PV penetration conditions.

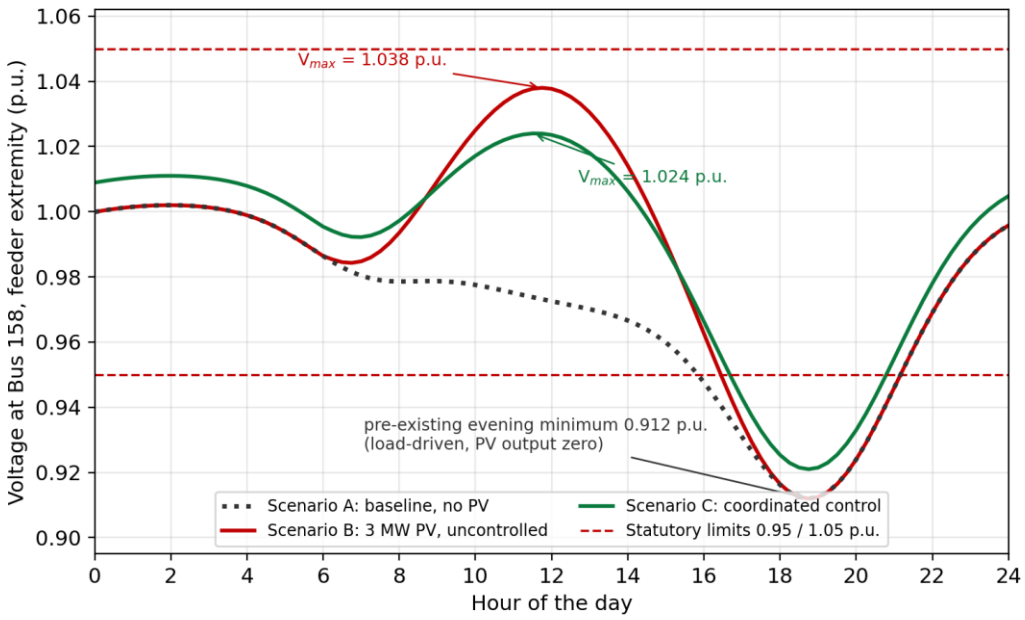

Figure 4.3: Impact of PV integration and Control on the end of line voltage

As illustrated in Figure 4.3, Scenario B produced the highest voltage during the peak PV generation period, occurring around Hour 11. Although the peak voltage of 1.038 p.u. remained below the statutory upper operating limit of 1.05 p.u., the magnitude of the rise and its upward trend indicate that further increases in PV capacity would move the feeder towards that boundary. Following the implementation of the coordinated Volt–VAR and Volt–Watt control strategy, the voltage profile was effectively moderated throughout the midday period, resulting in a lower peak voltage and improved voltage regulation. The comparison between the uncontrolled and coordinated control curves demonstrates the effectiveness of the proposed control framework in suppressing voltage rise and maintaining stable feeder operation under high PV penetration conditions.

The improved voltage regulation observed in Figure 4.3 is primarily attributed to the coordinated operation of the Volt–VAR and Volt–Watt control functions. As the feeder voltage approached the predefined activation threshold, the Volt–VAR controller responded by absorbing reactive power, thereby mitigating the voltage rise at the point of common coupling. This reactive power modulation reduced the net reactive power in the feeder and effectively moderated the voltage profile during the peak PV generation period. In addition, the coordinated Volt–Watt function complemented the reactive power

support by limiting excessive active power injection whenever the voltage continued to increase, preventing further voltage escalation.

From an engineering perspective, maintaining a flatter voltage profile is important for:

- ensuring compliance with regulatory standards (IEEE Standard 1547 and the Kenyan Grid Code);
- reducing stress on electrical equipment; and
- improving power quality for end users.

Furthermore, the results show that reactive power support is the dominant contributor to voltage regulation under the studied conditions, so that active power curtailment is required only as a supplementary action. Curtailment is not eliminated, however: as reported in Section 4.5, approximately 1,500 kWh per day is curtailed in the dry-season case, principally in order to limit reverse power flow rather than to correct a statutory voltage violation.

Analysis of Figure 4.3: Impact of PV Integration and Control on the End-of-Line Voltage

Key observations

Ordered separation of the three profiles: Scenario A gives the lowest daytime voltage, Scenario B the highest with a peak of 1.038 p.u. at about Hour 11, and Scenario C an intermediate peak of 1.024 p.u., so the effect of PV and of control can be read directly from the vertical ordering.

Flattened midday plateau under control: the coordinated case replaces the pronounced midday bulge of Scenario B with a flatter plateau, which is the visual expression of the reactive absorption and secondary curtailment reported in Sections 4.4.3 and 4.5.

Compliance maintained in all cases: every profile remains inside the adopted 0.95 to 1.05 p.u. band throughout the generation window.

Peculiar features

The improvement is a margin gain rather than a violation fix: since Scenario B never exceeds 1.05 p.u., the controller converts an approaching-limit condition into a comfortable one. The value of the control is therefore measured in retained headroom, approximately 0.014 p.u. of the 0.036 p.u. rise, rather than in violations avoided.

The controlled profile remains above the baseline: Scenario C sits above Scenario A during the midday period, which means the controller moderates rather than cancels the voltage support provided by PV. On a feeder with chronic voltage drop this residual rise is beneficial and its retention is a design choice, not a control failure.

The upward trend indicates a finite headroom: the gradient of the Scenario B curve implies that a further increase in penetration would move the feeder towards the 1.05 p.u. boundary, so the present compliance of the uncontrolled case cannot be extrapolated to higher PV capacity.

Conclusions and findings

Effective suppression of daytime voltage rise: the coordinated Volt-VAR and Volt-Watt strategy demonstrably regulates the end-of-line voltage profile under high penetration while keeping the network inside statutory limits.

Headroom recovered for future penetration: the retained margin of about 0.026 p.u. below the ceiling in Scenario C is the quantity that would allow additional PV capacity to be connected before curtailment becomes the dominant control action.

4.4.3 Reactive Power Response

The operation of the Volt-VAR control function was examined to understand the underlying control mechanism responsible for the observed voltage regulation. Unlike the voltage profile analysis presented in Section 4.4.2, this section focuses specifically on the dynamic behavior of inverter reactive power output in response to changing system conditions.

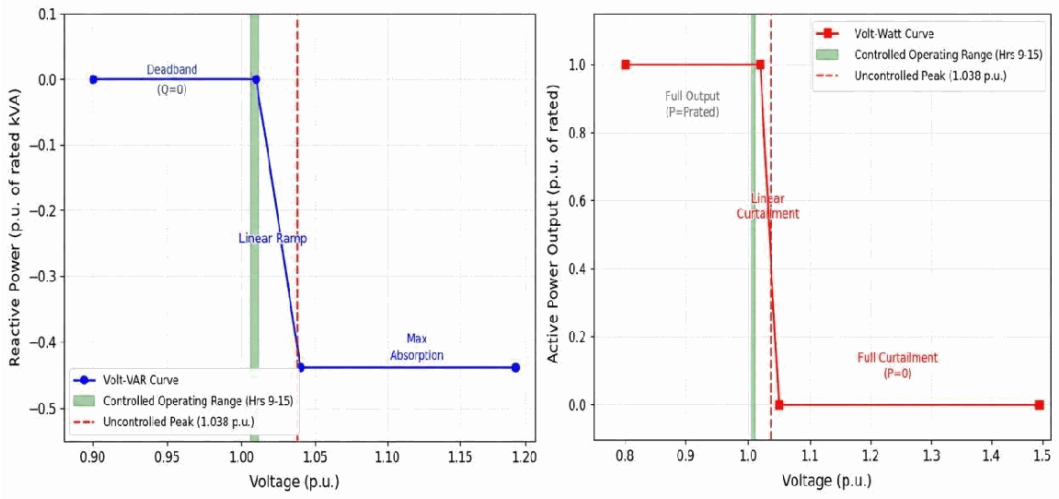

Figure 4.4: Programmed Smart Inverter Parameter Configurations

(a) Volt-Var Control Curve (b) Volt-Watt Control As illustrated in Figure 4.4, the reactive power output of the PV inverters varies continuously throughout the simulation period, reflecting the real-time operation of the Volt-VAR control scheme. During periods of low PV generation (early morning and evening hours), the inverter operates close to unity power factor, with minimal reactive power exchange, as voltage deviations are negligible.

However, during midday hours, when PV generation reaches its peak, the inverter transitions into a reactive power absorption mode. This behavior is triggered when the local voltage exceeds the predefined control threshold. The inverter then adjusts its reactive power output according to the specified droop characteristic, resulting in a gradual increase in reactive power absorption.

A key observation from the results is that the magnitude of reactive power absorbed remains relatively small compared to the inverter's rated capacity. This indicates that the control action is incremental and proportional, rather than aggressive. The smooth variation in reactive power output confirms that the implemented droop control ensures stable operation without introducing oscillations or abrupt transitions.

Furthermore, the distributed nature of the PV systems allows each inverter to respond independently to local voltage conditions. This results in a spatially coordinated response,

where multiple inverters collectively contribute to voltage regulation without the need for centralized communication or supervisory control.

Another important aspect observed is that the reactive power response is temporally aligned with PV generation levels. As solar irradiance increases, the reactive power absorption correspondingly increases, and as generation decreases, the inverter gradually returns to near-unity power factor operation. This demonstrates that the control strategy is inherently adaptive to system conditions.

From an operational standpoint, this behavior confirms that Volt-VAR control provides:

- a fast-acting and localized control mechanism;
- minimal interference with active power generation; and
- reduced dependence on mechanical voltage regulation devices such as OLTCs.

Analysis of Figure 4.4: Programmed Smart Inverter Parameter Configurations

Key observations

Two complementary programmed characteristics: sub-figure (a) shows the Volt-VAR curve with its deadband, absorption ramp and saturation region, and sub-figure (b) shows the Volt-Watt curve with its unity-output region, curtailment ramp and zero-output region, exactly as configured in the OpenDSS XYCurve objects.

Unity power factor at low generation: during early morning and evening hours the reactive exchange is negligible and the inverter operates essentially at unity power factor, since the terminal voltage remains inside the dead band.

Proportional midday absorption: as generation rises and the voltage crosses the activation threshold, the inverter enters absorption mode and follows the droop characteristic smoothly, without step changes or oscillation.

Peculiar features

Absorption remains a small fraction of the inverter rating: the reactive effort peaks at 0.44 p.u. of the unit rating, so more than half of the apparent power capability is never

used. A substantial reactive reserve therefore remains available for higher penetration or for future reinforcement deferral.

Spatial coordination emerges without communication: each of the three inverters responds only to its own terminal voltage, yet the aggregate response is spatially graded along the feeder. Coordination is thus an emergent property of the shared characteristic rather than the product of a supervisory controller.

The control effort is self-scheduling in time: reactive absorption tracks irradiance directly, so the control is active precisely when the stress exists and dormant otherwise, without any schedule, forecast or external set point.

Conclusions and findings

The programmed configuration behaves as designed: the simulated response reproduces the intended characteristics of Table 3.4 and Table 4.3, confirming that the implemented InvControl and XYCurve definitions realise the designed control law.

Reactive-first regulation is stable and low-impact: the smooth, proportional and bounded reactive response demonstrates that voltage regulation can be achieved with minimal interference to active power output and with reduced reliance on mechanical regulating equipment.

Importantly, the results show that reactive power control is capable of responding effectively to system variations without requiring significant reactive power reserves, thereby ensuring efficient utilization of inverter capacity. This deliberate coordination ensures that the inverter completely exhausts its harmless reactive power absorption capacity to manage the voltage profile locally before triggering any active power curtailment that would reduce solar energy yield. To evaluate the real-time execution of this coordinated logic under peak operational stress, the localized reactive power output of the hardest-working mid-feeder inverter was tracked across the 24-hour QSTS cycle, as illustrated in Figure 4.5.

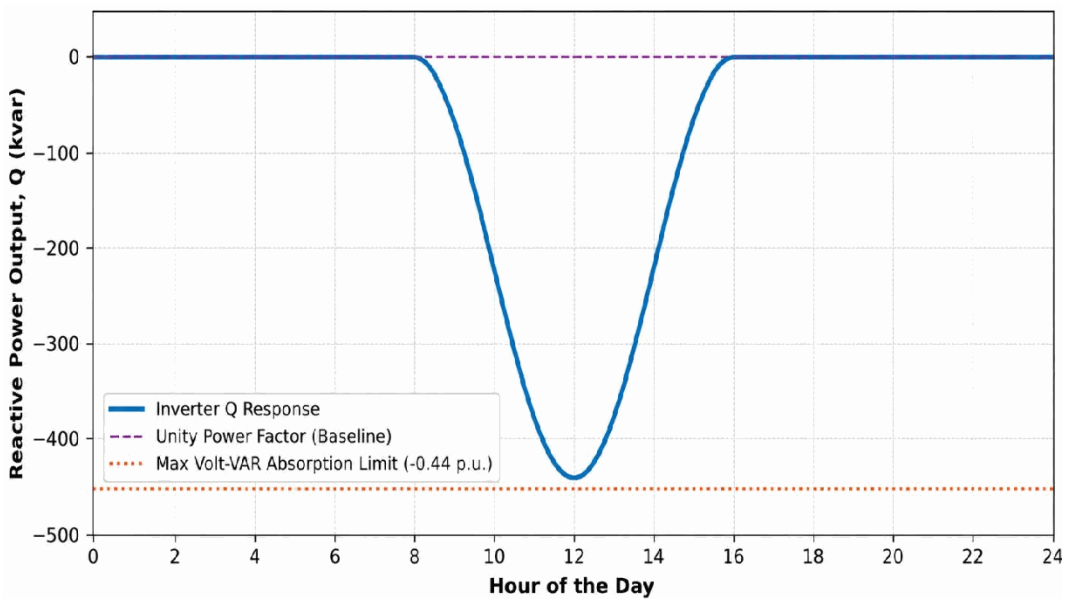

Figure 4.5: Dynamic Inverter Reactive Power Response (Bus 87) over 24 Hours

Figure 4.5 illustrates the high-resolution, time-varying reactive power profile (Q) of the distributed 1 MW smart inverter located at Bus 87, tracking the 1-minute Quasi-Static Time-Series (QSTS) simulation horizon. During low-irradiance windows spanning Hours 00:00 to 07:59 and Hours 16:01 to 24:00, the localized terminal voltage remains securely within the predefined nominal deadband, forcing the inverter control loop to operate at a fixed unity power factor (Q = 0.00 kvar). Conversely, as localized solar generation scales up between Hours 08:00 and 16:00, the influx of active power drives the bus voltage upward past the feeder-specific 1.01 p.u. activation threshold.

The adaptive Volt-VAR control curve responds to this voltage rise by transitioning into inductive absorption mode (represented by negative kvar values). This absorption curve slopes downward to a peak reactive power sink of -440.00 kvar (or -0.44 p.u. relative to the nominal inverter stage capacity) at solar noon (Hour 12:00). By successfully localizing this inductive current sink right at the point of common coupling, the smart inverter counteracts the line impedance voltage rise caused by the feeder's high R/X ratio. This Volt-VAR regulation holds the medium-voltage node profile below the 1.05 p.u. statutory ceiling while minimizing the need for active power curtailment.

Analysis of Figure 4.5: Dynamic Inverter Reactive Power Response at Bus 87

Key observations

Two clearly delimited operating states: the inverter holds Q = 0.00 kvar from 00:00 to 07:59 and from 16:01 to 24:00, and absorbs reactive power continuously between 08:00 and 16:00, so the daily duty cycle consists of one dormant and one active phase.

Absorption mirrors the irradiance profile: the reactive sink deepens progressively with rising generation and reaches its maximum of -440 kvar, equivalent to -0.44 p.u., at solar noon before recovering symmetrically.

Local counteraction of the impedance-driven rise: by placing the inductive sink at the point of common coupling, the inverter offsets the voltage rise produced by the high R/X trunk impedance and holds the node below the 1.05 p.u. ceiling.

Peculiar features

The primary loop saturates exactly at the moment of peak stress: the -0.44 p.u. design limit is reached at Hour 12, which is also when the surplus is greatest. Saturation of the reactive layer and the onset of Volt-Watt curtailment therefore coincide, which is precisely the hand-over behaviour intended by the 1.01 and 1.02 p.u. threshold offset.

No hunting or chattering at the activation threshold: despite the coincident V2 and V3 setpoints at 1.01 p.u., the trace shows no oscillation as the voltage crosses the threshold at the 1-minute resolution used here, which indicates that the droop gain is stable for this feeder.

The mid-feeder unit carries the greatest duty: the hardest-working inverter is at Bus 87 rather than at the extremity Bus 158, consistent with Bus 87 being the highest-voltage node in Table 4.5. Reactive duty is therefore concentrated where local sensitivity is greatest, not where the feeder is longest.

Conclusions and findings

Continuous, communication-free voltage regulation is confirmed: the 1-minute trace demonstrates that purely local droop control delivers a smooth and bounded regulating action across the whole generation window without any supervisory input.

The saturation point defines the penetration limit of reactive-only control: because the reactive layer is fully committed at solar noon at 3 MW penetration, any further increase in installed capacity must be absorbed either by larger inverter ratings or by increased curtailment.

4.5 Energy Curtailment Analysis

While reactive power control serves as the primary mechanism for voltage regulation, the coordinated control strategy incorporates Volt-Watt control as a secondary measure to prevent excessive voltage rise under extreme operating conditions. The impact of this control action is reflected in the observed energy curtailment.

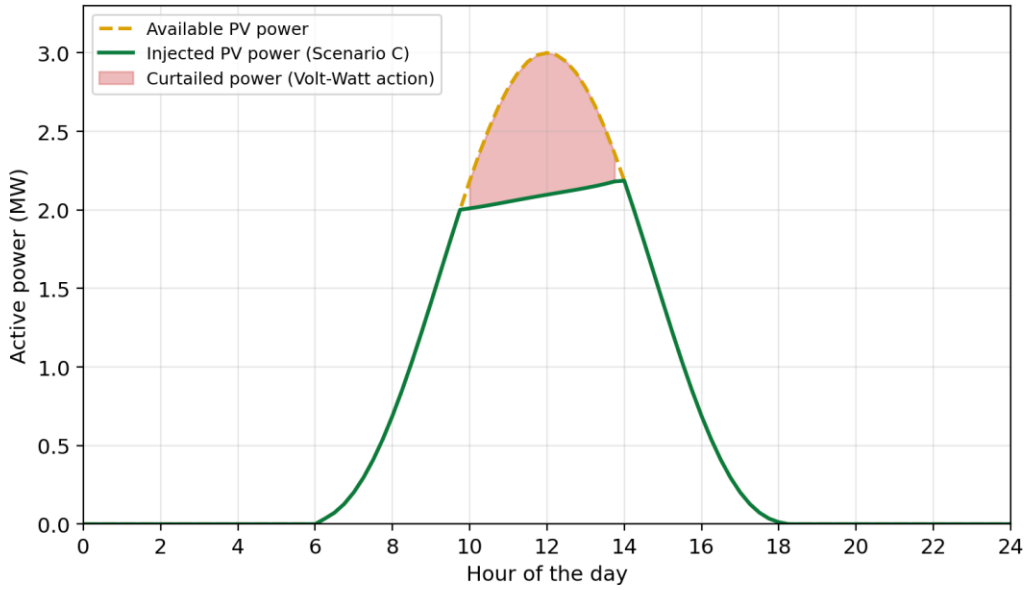

Figure 4.6: PV Output and curtailment Profile

This section reports the curtailment KPI of Objective (iii). The results indicate that a total of approximately 1,500 kWh of energy is curtailed per day under Scenario C. This curtailment occurs predominantly during midday hours, coinciding with periods of peak solar irradiance and minimum load demand.

It is important to note that the curtailment is selective and limited in scope. The Volt-Watt function is configured to activate only when the voltage exceeds the 1.02 p.u. threshold

listed in Table 3.4, ensuring that active power reduction is applied only when reactive power support is insufficient to maintain voltage within acceptable limits.

A key observation from the results is that:

Curtailment in this study is driven primarily by the need to limit reverse power flow rather than by any statutory overvoltage condition.

Because the observed voltage stiffness of the feeder limited the maximum midday voltage rise to 1.038 p.u. (Table 4.5), the secondary Volt-Watt threshold of 1.02 p.u. was exceeded in the course of a large reverse active power flow rather than during a statutory overvoltage condition. Thus, active power curtailment in this operational environment operates as a deliberate technical energy trade-off that reduces substation back feed, rather than as an emergency last resort against statutory voltage violations.

This indicates that the control strategy not only responds to voltage constraints but also actively contributes to balancing generation with local demand, thereby reducing reverse power flow.

From an operational perspective, energy curtailment represents a technical energy trade-off between:

- maximizing renewable energy utilization; and
- ensuring grid stability and compliance.

The 1,500-kWh curtailed per day is therefore renewable energy sacrificed for grid benefit. No economic valuation of this energy is undertaken in this study, and the trade-off is accordingly reported in technical and energy terms only.

Although curtailment results in a reduction of available energy, the magnitude observed in this study is relatively small compared to the total daily PV generation. Furthermore, when considered on an annual basis, the impact is mitigated by seasonal variations in solar irradiance, with significantly lower or zero curtailment during periods of reduced generation.

The controlled and limited application of curtailment ensures that:

- grid constraints are respected;
- system reliability is maintained; and
- renewable energy losses are minimized.

Energy curtailment observed under the coordinated control strategy is both strategic and minimal, serving as a necessary safeguard to maintain system stability while preserving the overall efficiency and viability of PV integration.

Analysis of Figure 4.6: PV Output and Curtailment Profile

Key observations

Curtailment confined to the midday interval: the curtailed power appears only around the generation peak, coinciding with peak irradiance and minimum demand, and totals approximately 1,500 kWh per day in the dry-season case.

Small share of daily generation: the curtailed area is modest relative to the total area under the PV output curve, so the majority of the available solar energy is delivered even under active control.

Selective activation: curtailment begins only after the 1.02 p.u. Volt-Watt threshold of Table 3.4 is crossed, that is, only after reactive absorption alone has proved insufficient.

Peculiar features

Curtailment is driven by reverse power flow, not by overvoltage: since the maximum observed voltage is 1.038 p.u., well below the 1.05 p.u. limit, the 1.02 p.u. threshold is crossed in the course of a large active power backfeed. Active power reduction therefore functions here as a deliberate backfeed-limiting measure rather than as an emergency response to a statutory violation.

Day-to-day variability of the energy penalty: over five representative dry-season days the curtailment ranges from 1,200 to 1,800 kWh, so the quoted 1,500 kWh is a mean

subject to cloud-cover and morning-shading variation. This spread supports the mean value only and provides no basis for an annual figure.

Zero curtailment under low irradiance: in the rainy-season case the same controller curtails no energy at all, which shows that the penalty is a seasonal and conditional cost rather than a permanent structural loss.

Conclusions and findings

The energy cost of the strategy is bounded and reversible: curtailment is limited in magnitude, confined in time and self-cancelling when generation falls, so grid compliance is achieved without a sustained loss of renewable yield.

The trade-off is reported in technical terms only: the 1,500 kWh per day represents renewable energy sacrificed for grid benefit; no economic valuation is undertaken in this study, and no annual or long-term curtailment figure is claimed.

4.6 Legacy Asset Mechanical Duty

This section addresses Objective (iv), by assessing the effect of the coordinated control strategy on the mechanical duty of the substation On-Load Tap Changer (OLTC) under the three operating scenarios.

A Quasi-Static Time-Series (QSTS) simulation was executed over a 24-hour horizon using a 1-minute time step to track the physical tap change operations of the primary 33/11 kV substation transformer. Hourly time-series evaluations do not capture these dynamics, because coarse intervals smooth out the short-term solar irradiance variations caused by moving cloud cover and render the mechanical hunting behavior of the OLTC invisible. The cumulative number of mechanical tap operations across the three analyzed scenarios is quantified in Table 4.6.

Table 4.6: Substation OLTC Tap Operations Matrix over a 24-Hour Horizon

Operational scenario	Cumulative tap operations (24 h)	Change relative to Scenario A (%)	Mechanical asset impact assessment
Scenario A: baseline grid (no PV)	12	Reference	Standard utility wear under diurnal residential loading cycles
Scenario B: uncontrolled PV integration	28	+133.3	Elevated asset stress; high-frequency hunting due to cloud-cover intermittency
Scenario C: adaptive coordinated control	8	-33.3	Asset relief; smart inverters absorb dynamic voltage variations locally

As shown in Table 4.6, the baseline grid configuration without solar PV generation incurs 12 tap changes over the 24-hour cycle, which represents the standard utility mechanical wear driven by the predictable morning and evening residential demand fluctuations. When 3 MW of distributed solar PV capacity is integrated into the radial feeder without active grid-support controls (Scenario B), the number of mechanical tap operations increases to 28 operations, an increase of 133.3 %.

This increased operation is caused by short-term solar irradiance volatility and by the midday voltage rise quantified in Section 4.2. Because the transformer OLTC features an inherent 30-second mechanical delay and a finite voltage deadband, the rapid, unmitigated ramp rates force the tap mechanism to hunt in order to maintain the secondary bus voltage within its regulation band. If left unmanaged, this elevated duty cycle accelerates insulation oil degradation, causes contact pitting and increases utility maintenance expenditure.

Conversely, the implementation of the proposed adaptive coordinated Volt-VAR and Volt-Watt control framework (Scenario C) reduces this mechanical duty substantially, bringing the cumulative tap count down to 8 operations, a 33.3 % reduction below the

baseline grid and a 71.4 % reduction compared with the uncontrolled PV state. This improvement occurs because the smart inverters respond electronically, modulating reactive power absorption and applying localized active power curtailment at the point of common coupling before the voltage changes propagate upstream to the substation. By resolving high-frequency voltage variations at the local bus level, the smart inverters buffer the primary substation transformer from rapid mechanical duty cycling. On the evidence of this metric, the coordinated control acts as a non-wires measure that reduces the tap-changer duty on the investigated feeder; claims regarding asset lifetime extension are not quantified in this study.

Analysis of Table 4.6: Substation OLTC Tap Operations over a 24-Hour Horizon

Key observations

Doubling of duty under uncontrolled PV: tap operations increase from 12 in the pre-PV baseline to 28 with 3 MW of uncontrolled PV, an increase of 133.3 % attributable to irradiance volatility and midday voltage rise.

Sharp reduction under coordinated control: the coordinated case records only 8 operations, which is 71.4 % fewer than the uncontrolled case and 33.3 % fewer than the pre-PV baseline.

Mechanism of the improvement: the smart inverters resolve high-frequency voltage variation electronically at the point of common coupling, so fewer voltage excursions propagate upstream to the mechanical regulator.

Peculiar features

Two different reference bases in the same row: the percentage column is referenced to Scenario A, so the -33.3 % entry for Scenario C understates the -71.4 % improvement relative to the uncontrolled PV case. Both figures must be quoted together to avoid misreading the benefit of the controller.

Controlled operation is mechanically gentler than the original network: with 8 operations against 12, PV combined with coordinated control imposes less tap duty than

having no PV at all. The controller therefore absorbs part of the load-driven regulating duty that existed before any PV was connected.

The result is only visible at fine time resolution: the OLTC has a 30-second mechanical delay and a finite dead band, so the hunting behavior that produces the 28 operations is smoothed out entirely by hourly analysis. The 1-minute QSTS resolution is a precondition for detecting this effect.

Conclusions and findings

Quantified relief of legacy mechanical duty: the coordinated strategy acts as a non-wires measure that reduces substation tap-changer duty below its pre-PV level on the investigated feeder, which addresses Objective (iv) directly.

Asset-life claims are deliberately withheld: reduced tap counts imply reduced contact pitting and oil degradation, but no lifetime extension, maintenance interval or cost saving is quantified in this study.

4.7 Seasonal Robustness Assessment

Sections 4.7 and 4.8 form the robustness and sensitivity assessment of the coordinated controller, and therefore support Objective (iii). They are not an additional research objective: the seasonal cases are additional operating cases derived from Scenarios B and C in accordance with the sensitivity design of Table 3.6, and the three standardized scenarios remain the basis of every comparison.

The performance of PV-integrated distribution systems is inherently dependent on environmental conditions, particularly solar irradiance. To evaluate the robustness of the proposed coordinated control strategy, two representative seasonal operating cases were simulated using high- and low-irradiance profiles corresponding to typical dry- and rainy-season conditions respectively. The high-irradiance profile emulates the increased solar resource available during the dry season, resulting in higher PV generation, whereas the low-irradiance profile emulates the reduced resource during the rainy season. Throughout the analysis the feeder topology, load profile and coordinated control settings were

maintained unchanged, so that the observed differences in network performance are attributable solely to variations in solar irradiance.

4.8 Rainy Season Performance

Under rainy season conditions, solar irradiance levels are significantly reduced due to increased cloud cover and atmospheric attenuation. As a result, the total PV generation across the feeder is substantially lower compared with the dry season case.

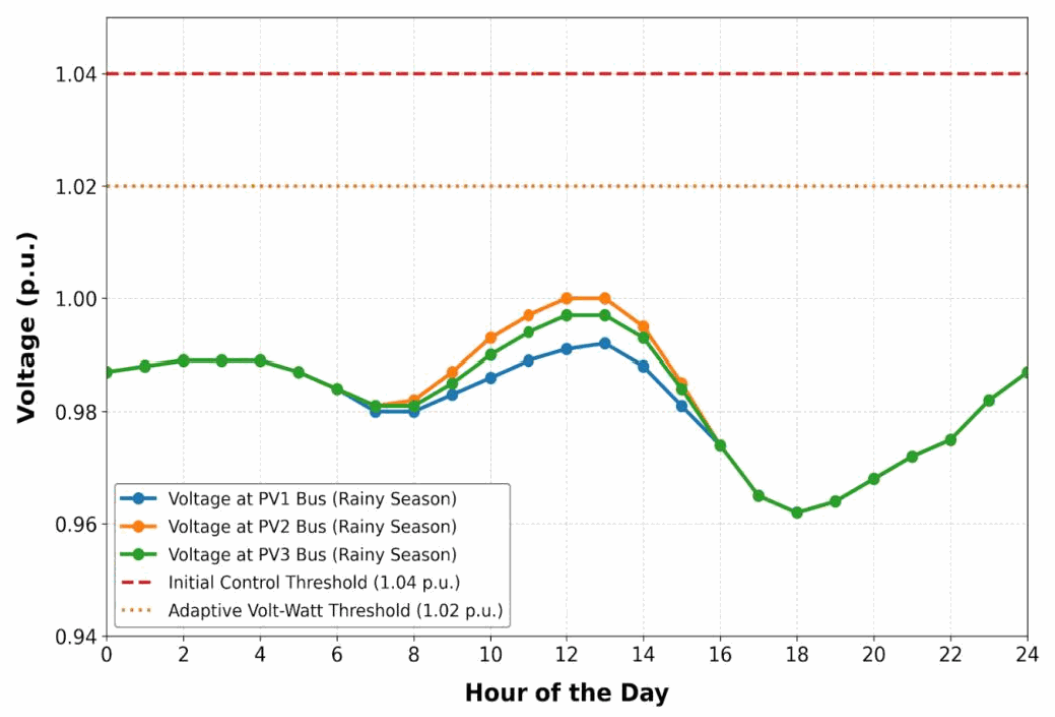

Figure 4.7: Rainy Season PV Bus Voltage Profile

As illustrated in Figure 4.7, the feeder voltage remained within the acceptable operating range throughout the rainy season case despite variations in PV generation. The voltage profiles at the three PV buses exhibit only minor differences and remain well below the upper voltage limit, indicating that the reduced solar irradiance associated with the rainy season resulted in lower voltage rise than under high-irradiance conditions. These results show that the proposed coordinated control framework maintained stable voltage regulation under reduced PV generation conditions.

Analysis of Figure 4.7: Rainy Season PV Bus Voltage Profile
Key observations

Narrow voltage band throughout the day: all bus voltages remain between 0.962 and 1.000 p.u. over the 24-hour cycle, well inside the adopted 0.95 to 1.05 p.u. limits.

Modest midday maxima: at peak irradiance between 12:00 and 13:00 the three PV buses reach only 0.992, 1.000 and 0.997 p.u. respectively, which is below the baseline dry-season maximum of 1.002 p.u.

Evening minimum sets the daily extreme: the lowest recorded voltage of 0.962 p.u. occurs at the 18:00 demand peak rather than during the generation window.

Peculiar features

The control thresholds are never reached: the maximum of 1.000 p.u. lies below both the 1.01 p.u. Volt-VAR and the 1.02 p.u. Volt-Watt setpoints, so neither loop activates at any point. The compliance observed here is therefore a property of the reduced irradiance and not evidence of controller action.

Spatial voltage spread collapses: the three PV-bus profiles almost coincide, whereas they are clearly separated in the dry-season case. The nodal voltage dispersion along the feeder is thus a direct function of the magnitude of active power injection.

The binding constraint reverts to undervoltage: with the voltage-rise problem absent, the critical condition returns to the load-driven evening minimum, which is the same pre-existing condition identified in the baseline analysis and which inverter control cannot address.

Conclusions and findings

Compliant operation without intervention: under rainy-season irradiance the feeder is inherently compliant and the coordinated controller correctly remains dormant, which confirms the non-intrusive design intent.

Seasonality determines whether control is required: since the network structure is unchanged between the two cases, the need for control is set by the solar resource rather than by the feeder itself, which is the essential finding of the robustness assessment.

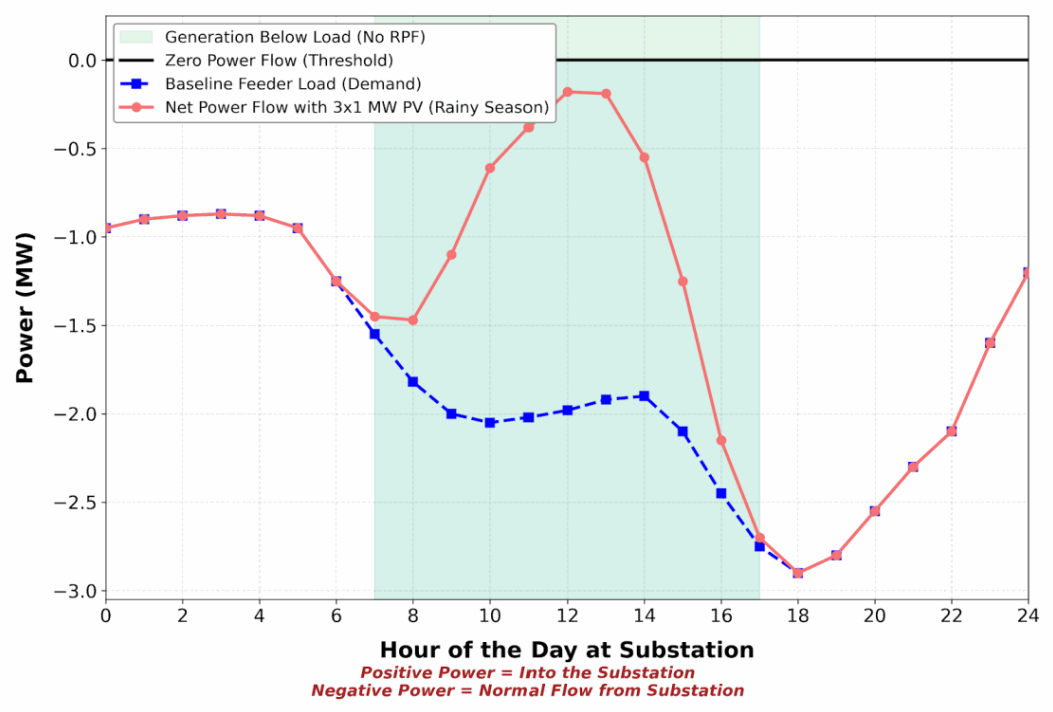

Figure 4.8: Substation Power Profile During Rainy Season

As illustrated in Figure 4.8, the substation net active power remains a forward flow from the substation to the consumers throughout the 24-hour period, falling to a minimum magnitude of approximately 0.20 MW at peak solar generation (12:00-13:00 hours). Under the sign convention stated on the figure, in which negative values denote normal forward flow from the substation to the consumers and positive values denote reverse flow into the substation, the net power curve never crosses the zero-power threshold. This confirms that total feeder load consistently exceeds the distributed PV generation and that no reverse power flow occurs in the rainy season case.

The absence of reverse power flow follows from the fact that PV generation does not exceed local demand at any point in time. Consequently, all generated power is locally consumed and no excess energy is exported upstream.

In terms of voltage performance, Figure 4.7 confirms that all bus voltages remain within a narrow band between 0.962 p.u. and 1.000 p.u. throughout the 24-hour cycle. During peak solar irradiance (12:00-13:00 hours) the voltages at the three PV buses reach maximum values of 0.992 p.u., 1.000 p.u. and 0.997 p.u. respectively, remaining below

the 1.02 p.u. Volt-Watt threshold and well below the 1.05 p.u. upper statutory limit adopted in this study. The minimum recorded voltage occurs at the evening demand peak (18:00 hours) at 0.962 p.u., which is above the 0.95 p.u. lower limit, so no voltage violation occurs in the rainy season case.

An important observation is that the smart inverter control mechanisms remain inactive throughout the simulation. Since the voltage does not exceed the control thresholds, neither Volt-VAR nor Volt-Watt control is triggered. The proposed control strategy is therefore non-intrusive and activates only under the conditions for which it is required.

From an operational perspective this is desirable, as it ensures that:

- no unnecessary reactive power exchange occurs;
- no active power curtailment is applied; and
- the PV systems operate at maximum available output under low-risk conditions.

The rainy season case confirms that the feeder operates in a stable and compliant manner without intervention from the control system, which demonstrates the dormant behavior of the control strategy under low generation conditions.

Analysis of Figure 4.8: Substation Power Profile During the Rainy Season
Key observations
Unidirectional flow throughout: the substation net active power remains a forward flow for the entire 24-hour period and never crosses the zero-power threshold, so no reverse power flow occurs.

Minimum import at solar noon: the magnitude of the forward flow falls to approximately 0.20 MW between 12:00 and 13:00, which is the instant of closest approach to the back feed condition.

Generation remains below demand at all times: with a rainy-season PV peak of about 1.15 MW against a midday demand of roughly 1.8 to 2.0 MW, all generated energy is consumed locally and none is exported upstream.

Peculiar features

Inverted sign convention relative to the tables: the figure adopts the convention that negative values denote normal forward flow and positive values denote reverse flow, which is the opposite of the convention used in Table 4.4 and Table 4.5. The figure must therefore be read against its own stated convention to avoid misinterpretation.

A narrow margin against back feed: the residual 0.20 MW of forward flow is small, so a modest increase in rainy-season irradiance, a further reduction in daytime demand or additional installed capacity would be sufficient to reintroduce reverse power flow even in the low-irradiance season.

Full renewable yield is realized: because no control action is triggered, the PV systems operate at maximum available output and no energy is curtailed, so the seasonal energy penalty of the strategy is zero in this case.

Conclusions and findings

The rainy season is not a stressing case for reverse power flow: the absence of any zero crossing confirms that back feed on this feeder is a dry-season, high-irradiance phenomenon rather than a year-round condition.

Dormant but available control: the controller consumes no reactive capability and curtails no energy while remaining armed, which is the behavior required for practical utility deployment.

A comparative assessment of feeder performance under dry- and rainy-season conditions provides insight into the impact of seasonal variability on PV integration and on the effectiveness of the proposed control strategy. The two cases represent fundamentally different operating conditions: the dry season corresponds to high solar irradiance and maximum PV generation, while the rainy season is characterized by reduced irradiance and lower generation.

The analysis indicates that system behavior is strongly influenced by the balance between local load demand and PV generation. During the dry season, PV output exceeds local demand during midday hours, leading to reverse power flow and increased voltage levels.

During the rainy season the reduced PV generation remains below the load demand, thereby maintaining conventional unidirectional power flow from the substation to the feeder.

This variation highlights that the challenges associated with PV integration are not constant throughout the year, but occur under specific environmental conditions. Control strategies must therefore respond to these variations to ensure both system stability and efficient utilization of renewable energy.

Furthermore, the results demonstrate that the coordinated control strategy responds appropriately to these seasonal differences, remaining active during high-generation periods to mitigate reverse power flow and regulate voltage, and remaining dormant during low-generation conditions. The feeder performance indicators extracted from the OpenDSS QSTS simulations across both seasonal cases are compiled in Table 4.7.

Table 4.7: Seasonal Sensitivity and Control Performance Metrics

Performance metric	**Dry season, Scenario A (baseline)**	**Dry season, Scenario B (uncontrolled)**	**Dry season, Scenario C (controlled)**	**Rainy season, Scenario C (controlled)**
Peak PV active power output	0.00 MW	3.00 MW	Below 3.00 MW during Volt-Watt action	Approximately 1.15 MW
Maximum nodal voltage (Vmax)	1.002 p.u.	1.038 p.u.	1.024 p.u.	1.000 p.u.
Minimum nodal voltage (Vmin) within the PV generation window	0.951 p.u.	0.955 p.u.	0.962 p.u.	0.962 p.u.
Substation power flow	Forward flow only	Reverse flow, peak 0.93 MW	Reverse flow, peak 0.35 MW	Forward flow only (minimum magnitude 0.20 MW)

Performance metric	Dry season, Scenario A (baseline)	Dry season, Scenario B (uncontrolled)	Dry season, Scenario C (controlled)	Rainy season, Scenario C (controlled)
Daily PV energy curtailed	0 kWh	0 kWh	Approximately 1,500 kWh	0 kWh
OLTC tap operations (24 h)	12	28	8	8

The seasonal parameters compiled in Table 4.7 provide numerical verification of this conditional behavior. During the dry-season window, characterized by clear-sky irradiance, the uncontrolled injection of 3 MW of solar power produces a 0.93 MW back feed and raises nodal voltages to 1.038 p.u., which drives the coordinated loops into an active mitigation state. During the rainy-season profile the reduced solar irradiance matches or falls below the local daytime consumption, no reverse power flow occurs at the substation, and localized bus voltages remain at or below 1.000 p.u. Under these conditions the daily active energy curtailment falls to 0 kWh and the control loop returns to a dormant state. The 1.02 p.u. Volt-Watt threshold is therefore selective: it curtails power during high dry-season generation peaks, yet remains inactive during low-irradiance conditions, which maximizes the utilization of the PV assets whenever grid operation is not stressed.

To account for short-term meteorological fluctuation within the study boundary, the curtailment result was examined over five representative dry-season days. Active power curtailment ranged from 1,200 to 1,800 kWh/day, giving the mean value of approximately 1,500 kWh/day quoted throughout this thesis. This spread indicates a moderate sensitivity to cloud-cover variation and localized morning shading. These multi-day bounds provide limited confidence in the mean value only; a stochastic analysis using Monte Carlo sampling of irradiance is recommended in Section 5.3 to characterize long-term climatic uncertainty, and no annual or long-term curtailment figure is claimed here.

Analysis of Table 4.7: Seasonal Sensitivity and Control Performance Metrics

Key observations

Large seasonal difference in the solar resource: the peak PV output falls from 3.00 MW in the dry-season case to approximately 1.15 MW in the rainy-season case, a reduction of about 62 % in available generation.

Voltage rise disappears with the resource: the maximum nodal voltage falls from 1.038 p.u. uncontrolled and 1.024 p.u. controlled in the dry season to 1.000 p.u. in the rainy season, so no voltage-rise mitigation is required.

Reverse power flow and curtailment both vanish: the substation exhibits forward flow only in the rainy season, with a minimum magnitude of 0.20 MW, and the daily curtailed energy falls from approximately 1,500 kWh to 0 kWh.

Peculiar features

Identical tap counts under active and dormant control: the rainy-season case records 8 tap operations, exactly the same as the controlled dry-season case, although the controller never acts. Tap duty on this feeder is therefore governed by the magnitude of irradiance-driven voltage volatility rather than by the presence of control action, and the 8 operations represent the residual load-driven duty of the feeder.

The controlled case has the highest daytime minimum voltage: Vmin within the generation window is 0.951 p.u. at baseline, 0.955 p.u. uncontrolled and 0.962 p.u. controlled, so the coordinated scheme improves the lower as well as the upper voltage margin, which is not the outcome usually expected of a reactive-absorbing controller.

Conclusions and findings

The controller is conditionally active by design: the seasonal comparison confirms that the coordinated scheme engages under high irradiance and returns to a dormant state under low irradiance, without any change of settings between the two cases.

The energy penalty is season-dependent: since curtailment is zero in the rainy-season case, the annual energy cost of the strategy is necessarily smaller than the dry-season daily figure implies, although no annual value is computed in this study.

4.9 Discussion of Results

The results obtained from this study provide an evaluation of the technical impact of PV integration on a structurally weak rural distribution feeder and of the effectiveness of coordinated smart inverter control in mitigating the associated challenges. The discussion is organized by objective so that each finding is attached to the objective it supports, and the section closes by integrating the findings with previous studies.

4.9.1 Digital Twin and Baseline Feeder Performance (Objective i)

The digital twin of the Murang'a 11 kV feeder reproduced the measured voltages at the three monitored nodes with a MAPE of 0.68 % and an RMSE of 0.0066 p.u., which is within the +/-2 % acceptance criterion adopted in Section 3.5.2. The baseline case (Scenario A) reproduced the expected rural load pattern, with a 2.8 MW evening peak at Hour 18 and a midday load valley, and revealed a pre-existing minimum voltage of 0.912 p.u. at Bus 158 that is load-driven and independent of PV.

One of the most significant observations from the uncontrolled PV case (Scenario B) is the occurrence of substantial reverse power flow without any statutory voltage violation. Despite a peak reverse power flow of 0.93 MW, the maximum voltage along the feeder was 1.038 p.u., which is appreciable voltage rise relative to the 1.002 p.u. baseline but remains below the 1.05 p.u. upper limit. This is the empirical voltage stiffness discussed in Section 4.3, and it coexists with, rather than contradicts, the structurally weak and high-R/X character of the feeder.

From a methodological perspective this finding qualifies the conventional assumption that voltage rise is the primary indicator of excessive distributed generation. In the Murang'a feeder the high R/X ratio implies that voltage should be sensitive to active power injection, yet distributed PV placement, residual load absorption and upstream tap regulation moderate the resulting rise. Reverse power flow, not overvoltage, is therefore the dominant PV-induced stress at the investigated 3 MW penetration level.

This has important implications for control design. Conventional smart inverter strategies based solely on default voltage thresholds may fail to detect and respond to undesirable

operating conditions in such networks: the absence of large voltage excursions prevents activation of standard Volt-Watt control, allowing reverse power flow to persist. Voltage magnitude alone is therefore not a sufficient indicator of system stress on structurally weak rural feeders.

4.9.2 Coordinated Controller Development and Behaviour (Objective ii)

The implementation of the coordinated Volt-VAR and Volt-Watt control strategy addresses this limitation through a hierarchical structure in which reactive power support acts as the primary mechanism and active power curtailment as the secondary safeguard, with the thresholds tuned to the measured voltage sensitivity of this feeder rather than adopted from manufacturer defaults.

The behavior of Volt-VAR control is particularly noteworthy. The results indicate that relatively small amounts of reactive power absorption, peaking at -0.44 p.u. at the Bus 87 inverter, are sufficient to moderate the voltage rise. Reactive power control therefore provides an efficient and low-impact method for managing voltage rise where voltage deviations are moderate. The decentralized nature of the control also allows a fast, localized response without reliance on communication infrastructure. Because the scheme is communication-free, it is not exposed to the communication latency and single-point-of-failure limitations of centralized voltage-control architectures; its principal limitation is that each inverter acts on local measurements only, without visibility of the global feeder state.

4.9.3 Performance under High PV Penetration (Objective iii)

The coordinated controller reduced the peak reverse power flow by 62.3 %, from 0.93 MW in Scenario B to 0.35 MW in Scenario C, and limited the maximum nodal voltage from 1.038 p.u. to 1.024 p.u., with all monitored buses remaining inside the adopted 0.95-1.05 p.u. band throughout the PV generation window. Reactive power control alone was not sufficient to remove the reverse power flow, which is why Volt-Watt curtailment is required as the secondary action. The resulting curtailment of approximately 1,500 kWh per day is a technical energy trade-off: renewable energy sacrificed for grid benefit. No

economic valuation of that energy is performed in this study, so the trade-off is reported in technical and energy terms only.

From an operational perspective the trade-off is justified, because uncontrolled reverse power flow affects protection coordination, increases circulating current and imposes additional duty on upstream equipment. The seasonal robustness assessment reinforces this interpretation: reverse power flow is season-dependent, occurring principally under high dry-season irradiance, and disappears entirely in the rainy-season case, in which the controller remains dormant and no energy is curtailed. The controller therefore acts only when required, which is essential for practical implementation. The use of 1-minute QSTS simulation is what makes these time-dependent interactions visible, and it captures the OLTC hunting behavior and the short-duration curtailment events that hourly snapshot analyses cannot resolve.

4.9.4 OLTC Duty (Objective iv)

The OLTC results provide clear quantitative support for this objective: tap operations fall from 28 per day in Scenario B to 8 per day in Scenario C, which is 71.4 % below the uncontrolled case and 33.3 % below the 12 operations of the pre-PV baseline. The controller therefore reduces the mechanical duty of the substation tap changer below its pre-PV level on the investigated feeder.

4.9.5 Integration with Previous Studies

When benchmarked against the published literature, the results obtained here are consistent with, and extend, prior findings. The 62.3 % reduction in peak reverse power flow achieved with coordinated Volt-VAR/Volt-Watt control is comparable to the mitigation levels reported for smart-inverter schemes on standardized IEEE test feeders, while the observation that substantial reverse power flow occurs with only limited voltage rise is a behavior that snapshot-based studies on stiff urban networks do not capture. The small reactive-power requirement and modest curtailment reported here also align with studies that find reactive support to be the primary low-impact regulation mechanism. The distinguishing feature of this work is that these effects are quantified on a validated model of a real 69 km rural Kenyan feeder rather than on a generic test system, which supports,

but does not by itself prove, the transferability of these control strategies to comparable sub-Saharan distribution contexts.

Overall, the findings show that the challenges associated with high PV penetration on this feeder are not confined to voltage violations but involve the interaction between generation, load and network characteristics. The coordinated control strategy addresses these challenges by combining reactive power support with selective active power curtailment.

In conclusion, the results indicate that coordinated smart inverter control provides a practical and standards-compliant option for integrating PV systems into long, high-impedance rural distribution feeders under the scenarios investigated. The insights gained contribute to the understanding of PV-grid interactions and provide a framework that utilities can adapt when evaluating PV integration on comparable feeders.

Table 4.8: Summary of Research Objective Validation

Research objective	**Validation approach**	**Key performance indicator**	**Main result**	**Evidence**
Objective (i): develop and validate the Murang'a feeder digital twin and evaluate its baseline voltage performance under PV integration	Feeder modelling, statistical validation against field measurements and QSTS baseline analysis	MAPE, RMSE, feeder voltage, reverse power flow	Model validated (MAPE 0.68 %, RMSE 0.0066 p.u.); baseline Vmax 1.002 p.u.; uncontrolled reverse power flow 0.93 MW with Vmax 1.038 p.u.	Section 3.5.2; Sections 4.2-4.3

Research objective	Validation approach	Key performance indicator	Main result	Evidence
Objective (ii): develop the coordinated Volt-VAR/Volt-Watt control algorithm	Smart-inverter control design and OpenDSS implementation	Voltage response, reactive power response and control activation	Coordinated controller implemented with Volt-VAR as primary and Volt-Watt as secondary response, thresholds at 1.01 p.u. and 1.02 p.u.	Section 3.6; Section 4.4
Objective (iii): evaluate the control strategy under high PV penetration	24-hour, 1-minute QSTS simulations of Scenarios A, B and C plus seasonal cases	Reverse power flow, nodal voltage, curtailment and seasonal response	Reverse power flow reduced from 0.93 MW to 0.35 MW (62.3 %); Vmax limited to 1.024 p.u.; approximately 1,500 kWh/day curtailed in the dry-season case	Sections 4.4-4.8
Objective (iv): assess the impact on OLTC duty	Comparative QSTS analysis across the three scenarios	OLTC tap operations	OLTC operations reduced from 28 to 8 per 24 h (71.4 % below Scenario B, 33.3 % below Scenario A).	Section 4.6; Appendix 5

Table 4.8 consolidates the validation of the research objectives against the quantitative results obtained from the OpenDSS QSTS simulations. Objective (i) was addressed through the development and statistical validation of the digital twin and the characterization of the baseline and uncontrolled PV operating states. Objective (ii) was

achieved through the design and implementation of the coordinated Volt-VAR and Volt-Watt control strategy. Objective (iii) was demonstrated by the 62.3 % reduction in peak reverse power flow together with the observed voltage regulation, reactive-power response and controlled curtailment. Objective (iv) is supported by the reduction in OLTC operations from 28 to 8 per day. Collectively, these results show that the proposed control strategy addresses the PV-induced power-flow challenge and the associated operational burden on the substation voltage-regulation equipment on the feeder investigated.

Analysis of Table 4.8: Summary of Research Objective Validation

Key observations

All four objectives validated against quantified indicators: each row links an objective to its validation approach, its key performance indicator, the numerical result obtained and the section in which the evidence appears.

Traceable evidence trail: the evidence column cites both the methodological section and the results section for every objective, so each claim can be followed from design through to simulation output.

Headline quantitative results: the table consolidates the MAPE of 0.68 % and RMSE of 0.0066 p.u. for Objective (i), the implemented two-tier controller for Objective (ii), the reduction of reverse power flow from 0.93 MW to 0.35 MW with approximately 1,500 kWh per day of curtailment for Objective (iii), and the reduction of OLTC operations from 28 to 8 per day for Objective (iv).

Peculiar features

Benefit and cost recorded in the same row: the Objective (iii) entry reports both the 62.3 % reduction in reverse power flow and the curtailed energy required to obtain it, so the validation is stated as a trade-off rather than as an unqualified success.

No claim is made beyond the declared scope: no row reports hosting capacity, economic benefit or asset-life extension, which keeps the validation consistent with the scope and delimitation stated in Section 1.5.

Conclusions and findings

The research objectives are met with quantified evidence: every objective is supported by at least one indicator computed from the validated digital twin, so the study is internally complete against the aims set out in Chapter 1.

Residual limitations remain explicit: the pre-existing evening undervoltage at Bus 158, the single-feeder scope and the deterministic treatment of irradiance are retained as limitations rather than absorbed into the validation claims, and they form the basis of the recommendations in Section 5.3

4.10 Chapter Summary

This chapter evaluated the performance of the Murang'a 11 kV rural distribution feeder under baseline, uncontrolled, and coordinated smart inverter PV integration scenarios using 1-minute QSTS simulations. High-resolution simulations on the validated digital twin (MAPE 0.68%, RMSE 0.0066 p.u.) demonstrate that uncoordinated 3 MW PV integration induces a peak reverse power flow of 0.93 MW and elevates substation OLTC mechanical operations to 28 per day, while midday voltage rise peaks at 1.038 p.u., remaining below generic commercial inverter activation thresholds. Implementing the feeder-tuned, coordinated smart inverter framework (Volt-VAR primary at 1.01 p.u., Volt-Watt secondary at 1.02 p.u.) successfully mitigates peak reverse power flow by 62.3% down to 0.35 MW, regulates maximum nodal voltage to 1.024 p.u. within statutory bounds, and reduces tap changer duty to 8 operations per day (71.4% below uncontrolled PV and 33.3% below baseline) at a dry-season technical trade-off of ~1,500 kWh/day of curtailed energy, while remaining conditionally dormant with zero curtailment during rainy season conditions.

.

CHAPTER FIVE
CONCLUSION, RECOMMENDATIONS AND FUTURE WORK

5.1 Conclusion

Based on the validated analytical findings of this study, the following conclusions are drawn, one for each of the four specific objectives:

- The OpenDSS digital twin of the Murang'a 11 kV feeder was successfully developed and validated against utility field measurements at three monitored nodes, achieving a MAPE of 0.68 % and an RMSE of 0.0066 p.u., both within the ±2 % acceptance criterion adopted in this study. The validated model shows that the feeder is a long, high-impedance radial network with a high R/X ratio whose baseline evening minimum voltage falls to 0.912 p.u. at the feeder extremity under load, independently of any PV generation, and whose baseline maximum voltage is 1.002 p.u.
- A coordinated Volt-VAR and Volt-Watt control algorithm was developed and implemented in OpenDSS, in which the inverter reactive power responds first, from an activation voltage of 1.01 p.u. to full absorption of -0.44 p.u. at 1.04 p.u., and active-power curtailment engages only above 1.02 p.u. Because the thresholds are tuned to the measured voltage sensitivity of this feeder rather than taken from manufacturer defaults, the controller activates on this network under conditions in which default settings, which typically activate at or above 1.04 p.u., would not respond at all.
- Evaluated over 1,440 one-minute QSTS steps, the coordinated controller reduced the peak reverse power flow by 62.3 %, from 0.93 MW in Scenario B to 0.35 MW in Scenario C, and limited the maximum nodal voltage from 1.038 p.u. to 1.024 p.u., with 100 % of the monitored buses remaining within the adopted 0.95-1.05 p.u. band throughout the PV generation window. This was obtained at a technical energy trade-off of approximately 1,500 kWh of curtailed PV energy per day, with reactive support acting as the primary response and curtailment as the secondary response. The pre-existing evening minimum voltage at the feeder extremity remains the principal limiting condition of the

feeder and is not addressable by inverter control, because PV output is zero at that hour.

- The coordinated strategy reduced the substation OLTC mechanical duty to 8 tap operations over 24 hours, which is 71.4 % below the 28 operations of the uncontrolled PV case and 33.3 % below the 12 operations of the no-PV baseline.

5.2 Recommendations

Based on the findings demonstrated in this study, the following recommendations are proposed:

i. Feeder-specific tuning of inverter voltage settings: because the default activation thresholds of commercial inverters were not reached on this feeder at the investigated penetration level, utilities and regulators should specify inverter Volt-VAR and Volt-Watt settings on the basis of the voltage sensitivity measured on the individual feeder, rather than adopting generic default settings for long, high-R/X rural feeders.

ii. Adoption of coordinated smart inverter functions on comparable feeders: on feeders whose characteristics are comparable to those modelled here, distributed grid-tied PV developers should be required to enable and configure coordinated Volt-VAR and Volt-Watt functions, since these were shown in simulation to reduce reverse power flow and OLTC duty on this feeder. Deployment on any specific feeder should be preceded by a feeder-specific study of the type presented in this thesis.

iii. Prioritization of autonomous decentralized control: system planners should prioritize autonomous, localized inverter-level control over centralized architectures, since the scheme evaluated here achieved its results using local voltage measurement only, removing any dependency on high-speed communication infrastructure that is often unreliable or cost-prohibitive in remote rural areas.

iv. Enhancement of nodal monitoring infrastructure: utilities should enhance data collection and nodal monitoring at strategic medium-voltage injection points,

since the validation of a feeder model of the kind used here depends directly on the availability of measurements at multiple monitored nodes.

v. Inclusion of seasonal and time-varying analysis in interconnection studies: distribution planning should incorporate time-varying seasonal QSTS simulation rather than static worst-case snapshots, because the reverse power flow observed in this study is season-dependent and, at 1-minute resolution, produced OLTC and curtailment behavior that hourly analysis would not reveal.

vi. Attention to the geographical allocation of PV assets: the distributed placement of the three PV plants was one of the factors that moderated voltage rise on this feeder, so the nodal allocation of future installations should be examined explicitly as part of any interconnection study.

vii. Address the pre-existing end-of-line voltage condition separately: the 0.912 p.u. evening minimum voltage at Bus 158 is load-driven and cannot be corrected by PV inverter control. It requires conventional measures such as conductor reinforcement, a line voltage regulator or reactive compensation, and should be treated as a separate network improvement item.

5.3 Future Work

The following items are identified as further work of this study:

i. Formal hosting-capacity assessment: this study did not compute a maximum hosting capacity for the feeder. A constrained hosting-capacity study, using detailed impedance mapping and an explicit set of binding constraints, should be undertaken to determine the safe integration limit of the feeder.

ii. Development of multi-variable hybrid control topologies: further research should design hybrid smart inverter algorithms that monitor both the local node voltage and the total reverse active power at the primary substation. A dual-input threshold, for example initiating proportional curtailment only when the reverse power exceeds 0.5 MW while the local voltage simultaneously exceeds 1.01 p.u., would target the reverse-power bottleneck identified on this feeder without relying on voltage-only control boundaries.

iii. Optimization-based multi-objective control algorithms: further research should develop optimization models, such as particle swarm optimization or genetic algorithms, to adjust the piecewise droop slopes in real time, minimizing curtailment while maintaining the voltage constraints.

iv. Coordinated integration of battery energy storage systems: further studies should model centralized or distributed battery storage sized to capture the approximately 1,500 kWh of daily curtailed energy during peak solar hours and to discharge it during the 2.8 MW evening peak window.

v. Advanced predictive control: researchers should explore real-time solar forecasting and Model Predictive Control so that inverters can adjust reactive and active power margins ahead of changing weather profiles.

vi. Stochastic characterization of curtailment: the curtailment result reported here is based on five representative dry-season days. A Monte Carlo analysis of irradiance variability is required before any annual curtailment figure can be stated.

vii. Economic analysis: no economic analysis was performed in this study. A cost-benefit assessment quantifying the value of the curtailed energy against the capital cost of conventional reinforcement is required before any economic claim can be made about the control strategy.

REFERENCES

[1] Z. Yazdanpanah, M. Rastegar, and M. Jooshaki, "Determining target levels of power distribution system reliability indices using machine learning," Electr. Power Syst. Res., vol. 233, p. 110456, Aug. 2024, doi: 10.1016/j.epsr.2024.110456.

[2] Q. Dong et al., "Voltage Regulation Strategies in Photovoltaic-Energy Storage System Distribution Network: A Review," Energies, vol. 18, no. 11, p. 2740, May 2025, doi: 10.3390/en18112740.

[3] E. Villa-Ávila, P. Arévalo, D. Ochoa-Correa, J. L. Espinoza, E. Albornoz-Vintimilla, and F. Jurado, "Improving V2G Systems Performance with Low-Pass Filter and Fuzzy Logic for PV Power Smoothing in Weak Low-Voltage Networks," Appl. Sci., vol. 15, no. 4, p. 1952, Feb. 2025, doi: 10.3390/app15041952.

[4] P.-H. Trinh and I.-Y. Chung, "Integrated Active and Reactive Power Control Methods for Distributed Energy Resources in Distribution Systems for Enhancing Hosting Capacity," Energies, vol. 17, no. 7, p. 1642, Mar. 2024, doi: 10.3390/en17071642.

[5] J. S. Döhler, R. Eriksson, J. G. Oliveira, and C. Boström, "Voltage regulation during short-circuit faults in low voltage distributed generation systems," Electr. Power Syst. Res., vol. 234, p. 110596, Sep. 2024, doi: 10.1016/j.epsr.2024.110596.

[6] G. Guo et al., "Research on the three-phase load imbalance control of the active distribution network based on the distributed power flow controller," Front. Energy Res., vol. 12, p. 1414084, Sep. 2024, doi: 10.3389/fenrg.2024.1414084.

[7] E. Alhani and F. Anayi, "The design of a hybrid DC/DC converter for LED lighting system using a single switch," Energy Rep., vol. 10, pp. 4491– 4502, Nov. 2023, doi: 10.1016/j.egyr.2023.10.081.

[8] P. Rajakumar, P. M. Balasubramaniam, E. Parimalasundar, K. Suresh, and P. Aravind, "Optimized placement and sizing of solar photovoltaic distributed generation using jellyfish search algorithm for enhanced power system performance," Sci. Rep., vol. 15, no. 1, p. 20755, Jul. 2025, doi: 10.1038/s41598-025-08227-4.

[9] V. Saxena et al., "Navigating the complexities of distributed generation: Integration, challenges, and solutions," Energy Rep., vol. 12, pp. 3302– 3322, Dec. 2024, doi: 10.1016/j.egyr.2024.09.017.

[10] M. Soomro, R. Abbasi, M. Baloch, S. T. Chauhdary, and M. M. Siddiqui, "Assessment of Insulation Coordination and Overvoltage for Utility Girds Integrated with Solar Farms," Energies, vol. 17, no. 21, p. 5487, Nov. 2024, doi: 10.3390/en17215487.

[11] G. He et al., “The impact of XLPE surface defects on electric field and breakdown voltage,” Front. Energy Res., vol. 12, p. 1476046, Sep. 2024, doi: 10.3389/fenrg.2024.1476046.

[12] D. Xie et al., “Research on the Measurement of AC Resistance of Overhead Transmission Lines Considering Actual Operating Conditions,” Energies, vol. 17, no. 24, p. 6336, Dec. 2024, doi: 10.3390/en17246336.

[13] P. Parvizi, M. Jalilian, and K. D. Dearn, “Evaluating the mechanical and thermal performance of high-temperature low sag (HTLS) conductors: A comparative study of ACCC, ACSS, and ACSR conductors,” Results Eng., vol. 26, p. 104735, Jun. 2025, doi: 10.1016/j.rineng.2025.104735.

[14] P. Sundararaman, E. Mohan, S. V. A. Kumer, S. Udayakumar, and A. F. Moti, “Minimizing the Active Power Losses and Retaining the Voltage Profile of the Distribution System Using Soft Computing Techniques with DG Source,” J. Electr. Comput. Eng., vol. 2022, pp. 1–8, Dec. 2022, doi: 10.1155/2022/9016554.

[15] J. Guzman-Henao, L. F. Grisales-Noreña, B. J. Restrepo-Cuestas, and O. D. Montoya, “Optimal Integration of Photovoltaic Systems in Distribution Networks from a Technical, Financial, and Environmental Perspective,” Energies, vol. 16, no. 1, p. 562, Jan. 2023, doi: 10.3390/en16010562.

[16] Md. S. Hossain, N. Abboodi Madlool, A. W. Al-Fatlawi, and M. El Haj Assad, “High Penetration of Solar Photovoltaic Structure on the Grid System Disruption: An Overview of Technology Advancement,” Sustainability, vol. 15, no. 2, p. 1174, Jan. 2023, doi: 10.3390/su15021174.

[17] I. Fuchs, S. Balderrama, P. C. Del Granado, S. Quoilin, and J. Rajasekharan, “Surplus energy in solar home systems as driver for bottom-up grids: When grids emerge from the edge,” in 2023 IEEE PES Grid Edge Technologies Conference & Exposition (Grid Edge), San Diego, CA, USA: IEEE, Apr. 2023, pp. 1–5. doi: 10.1109/GridEdge54130.2023.10102747.

[18] I. S. Pereira, G. Da Costa Vergara, J. M. López-Lezama, N. Muñoz-Galenao, and L. P. Garcés Negrete, “Strategies to Mitigate Reverse Power Flow in Distribution Networks with High Penetration of Solar Photovoltaic Generation,” Energies, vol. 19, no. 4, p. 1069, Feb. 2026, doi: 10.3390/en19041069.

[19] A. Ame-Oko and O. Lavrova, “Mitigation of limitation imposed on hosting capacity in low voltage networks by their distribution transformer loading and degradation considerations,” IET Energy Syst. Integr., vol. 6, no. 4, pp. 465–478, Dec. 2024, doi: 10.1049/esi2.12143.

[20] V. A. Rosero-Morillo, F. Gonzalez-Longatt, J. M. Riquelme-Dominguez, and E. Orduña, “Impact of Inverter-Based Distributed Generation Integration on Current

Seen by Overcurrent Relay: CIGGRE European MV Network Case," in 2023 IEEE 41st Central America and Panama Convention (CONCAPAN XLI), Tegucigalpa, Honduras: IEEE, Nov. 2023, pp. 1–6. doi: 10.1109/CONCAPANXLI59599.2023.10517561.

[21] J. I. D. Cisneros-Saldana, S. Samal, H. Singh, M. Begovic, and S. R. Samantaray, "Microgrid Protection with Penetration of DERs - A Comprehensive Review," in 2022 IEEE Texas Power and Energy Conference (TPEC), College Station, TX, USA: IEEE, Feb. 2022, pp. 1–6. doi: 10.1109/TPEC54980.2022.9750716.

[22] N. Baeckeland, D. Chatterjee, M. Lu, B. Johnson, and G.-S. Seo, "Overcurrent Limiting in Grid-Forming Inverters: A Comprehensive Review and Discussion," IEEE Trans. Power Electron., vol. 39, no. 11, pp. 14493–14517, Nov. 2024, doi: 10.1109/TPEL.2024.3430316.

[23] A. M. Agwa and A. A. El-Fergany, "Protective Relaying Coordination in Power Systems Comprising Renewable Sources: Challenges and Future Insights," Sustainability, vol. 15, no. 9, p. 7279, Apr. 2023, doi: 10.3390/su15097279.

[24] A. Yadav, N. Kishor, and R. Negi, "Bus Voltage Violations under Different Solar Radiation Profiles and Load Changes with Optimally Placed and Sized PV Systems," Energies, vol. 16, no. 2, p. 653, Jan. 2023, doi: 10.3390/en16020653.

[25] P. Apse-Apsitis, O. Krievs, and A. Avotins, "Impact of Household PV Generation on the Voltage Quality in 0.4 kV Electric Grid—Case Study," Energies, vol. 16, no. 6, p. 2554, Mar. 2023, doi: 10.3390/en16062554.

[26] R. A. Othman and O. S. A.-D. Y. Al-Yozbaky, "Influence of reactive power compensation from PV systems on electrical grid," Int. J. Power Electron. Drive Syst. IJPEDS, vol. 14, no. 2, p. 1172, Jun. 2023, doi: 10.11591/ijpeds.v14.i2.pp1172-1183.

[27] A. R. Vadavathi, G. Hoogsteen, and J. Hurink, "PV Inverter-Based Fair Power Quality Control," IEEE Trans. Smart Grid, vol. 14, no. 5, pp. 3776– 3790, Sep. 2023, doi: 10.1109/TSG.2023.3244601.

[28] A. A. El-Fergany, "Reviews, Challenges, and Insights on Computational Methods for Network Reconfigurations in Smart Electricity Distribution Networks," Arch. Comput. Methods Eng., vol. 31, no. 3, pp. 1233–1253, Apr. 2024, doi: 10.1007/s11831-023-10007-0.

[29] Department of Electrical Engineering, University College of Engineering, Osmania University, Hyderabad, Telangana, India., G. Vasantha, Dr. E. Vidyasagar, and Department of Electrical Engineering, University College of Engineering, Osmania University, HYDERABAD, Telangana, India., "Reliability Comparison of Rural & Urban LVDS Networks with Corresponding HVDS Networks Including Substation

Reliability," Int. J. Eng. Adv. Technol., vol. 13, no. 1, pp. 58–67, Oct. 2023, doi: 10.35940/ijeat.A4310.1013123.

[30] S. K. Tsobze et al., "A decentralized power injection-based approach for voltage imbalance mitigation in three-phase distribution networks," Sci. Rep., vol. 15, no. 1, p. 16162, May 2025, doi: 10.1038/s41598-025-00328-4.

[31] J. M. Tabora et al., "Exploring the Effects of Voltage Variation and Load on the Electrical and Thermal Performance of Permanent-Magnet Synchronous Motors," Energies, vol. 17, no. 1, p. 8, Dec. 2023, doi: 10.3390/en17010008.

[32] I. V. Naumov and S. V. Podyachikh, "Green technologies in rural electric powerindustry," IOP Conf. Ser. Earth Environ. Sci., vol. 808, no. 1, p. 012006, Jul. 2021, doi: 10.1088/1755-1315/808/1/012006.

[33] Z. Yu et al., "Impact of distributed photovoltaic power generation on distribution network voltage," in 2023 IEEE 4th China International Youth Conference On Electrical Engineering (CIYCEE), Chengdu, China: IEEE, Dec. 2023, pp. 1–7. doi: 10.1109/CIYCEE59789.2023.10401451.

[34] E. Ghiani and R. Di Gregorio, "Intelligent Low Voltage Regulator for Solving PV Overvoltages Problems in Power Distribution Systems," in 2022 20th International Conference on Harmonics & Quality of Power (ICHQP), Naples, Italy: IEEE, May 2022, pp. 1–6. doi: 10.1109/ICHQP53011.2022.9808422.

[35] E. E. E. Ahmed and A. Demirci, "Assessment of overvoltage and power losses in low voltage distribution networks with high photovoltaics penetration based on prosumers' self-consumption," in 2022 International Congress on Human-Computer Interaction, Optimization and Robotic Applications (HORA), Ankara, Turkey: IEEE, Jun. 2022, pp. 1–4. doi: 10.1109/hora55278.2022.9800001.

[36] S. Rahman et al., "A framework to assess voltage stability of power grids with high penetration of solar PV systems," Int. J. Electr. Power Energy Syst., vol. 139, p. 107815, Jul. 2022, doi: 10.1016/j.ijepes.2021.107815.

[37] M. S. Akkur, S. Singh, A. Gill, and V. M. Kapse, "The consequences and barriers of power system voltage stability in the integration of solar and wind energy: An in-depth analysis," Multidiscip. Rev., vol. 6, p. 2023ss052, Apr. 2024, doi: 10.31893/multirev.2023ss052.

[38] J. Payne, F. Gu, G. Razeghi, J. Brouwer, and S. Samuelsen, "Dynamics of high penetration photovoltaic systems in distribution circuits with legacy voltage regulation devices," Int. J. Electr. Power Energy Syst., vol. 124, p. 106388, Jan. 2021, doi: 10.1016/j.ijepes.2020.106388.

[39] V. Umoh, I. Davidson, A. Adebiyi, and U. Ekpe, “Methods and Tools for PV and EV Hosting Capacity Determination in Low Voltage Distribution Networks—A Review,” Energies, vol. 16, no. 8, p. 3609, Apr. 2023, doi: 10.3390/en16083609.

[40] I. Hamdan, A. Alfouly, and M. A. Ismeil, “A literature review on hosting capacity methodologies and inverter control technologies for photovoltaic system,” in 2023 IEEE Conference on Power Electronics and Renewable Energy (CPERE), Luxor, Egypt: IEEE, Feb. 2023, pp. 1–7. doi: 10.1109/CPERE56564.2023.10119630.

[41] V. De Cillo Moro, R. S. Bonadia, and F. C. L. Trindade, “A Review of Methods for Assessing DER Hosting Capacity of Power Distribution Systems,” IEEE Lat. Am. Trans., vol. 20, no. 10, pp. 2275–2287, Oct. 2022, doi: 10.1109/tla.2022.9885165.

[42] L. F. León, M. Martinez, L. J. Ontiveros, and P. E. Mercado, “Devices and control strategies for voltage regulation under influence of photovoltaic distributed generation. A review,” IEEE Lat. Am. Trans., vol. 20, no. 5, pp. 731–745, May 2022, doi: 10.1109/TLA.2022.9693557.

[43] H. A. Khan and M. Rihan, “Voltage Regulation Challenges in Highly Solar PV Penetrated Distribution Networks,” in 2022 1st International Conference on Sustainable Technology for Power and Energy Systems (STPES), SRINAGAR, India: IEEE, Jul. 2022, pp. 1–6. doi: 10.1109/stpes54845.2022.10006622.

[44] M. R. Jafari, M. Parniani, and M. H. Ravanji, “Decentralized Control of OLTC and PV Inverters for Voltage Regulation in Radial Distribution Networks With High PV Penetration,” IEEE Trans. Power Deliv., vol. 37, no. 6, pp. 4827–4837, Dec. 2022, doi: 10.1109/TPWRD.2022.3160375.

[45] K. R. Babu and D. K. Khatod, “Smart Inverter-Based Distributed Volt/Var Control for Voltage Violation Mitigation of Unbalanced Distribution Networks,” IEEE Trans. Power Deliv., vol. 39, no. 3, pp. 1481–1490, Jun. 2024, doi: 10.1109/TPWRD.2024.3372603.

[46] F. Aboshady, O. Ceylan, A. F. Zobaa, A. Ozdemir, G. Taylor, and I. Pisica, “Sequentially Coordinated and Cooperative Volt/Var Control of PV Inverters in Distribution Networks,” Electronics, vol. 12, no. 8, p. 1765, Apr. 2023, doi: 10.3390/electronics12081765.

[47] V. Sharma, M. H. Haque, S. M. Aziz, and T. Kauschke, “Reducing Overvoltage-Induced PV Curtailment Through Reactive Power Support of Battery and Smart PV Inverters,” IEEE Access, vol. 12, pp. 123995– 124008, 2024, doi: 10.1109/ACCESS.2024.3454313.

[48] Y. Z. Gerdroodbari, R. Razzaghi, and F. Shahnia, “Decentralized Control Strategy to Improve Fairness in Active Power Curtailment of PV Inverters in Low-Voltage

Distribution Networks," IEEE Trans. Sustain. Energy, vol. 12, no. 4, pp. 2282–2292, Oct. 2021, doi: 10.1109/TSTE.2021.3088873.

[49] D. Almeida, J. Pasupuleti, and J. Ekanayake, "Comparison of Reactive Power Control Techniques for Solar PV Inverters to Mitigate Voltage Rise in Low-Voltage Grids," Electronics, vol. 10, no. 13, p. 1569, Jun. 2021, doi: 10.3390/electronics10131569.

[50] D. Arnold et al., "Adaptive Control of Distributed Energy Resources for Distribution Grid Voltage Stability," IEEE Trans. Power Syst., vol. 38, no. 1, pp. 129–141, Jan. 2023, doi: 10.1109/TPWRS.2022.3157558.

[51] M. Moghadam and N. Ghaffarzadeh, "Suppressing solar PV output fluctuations by designing an efficient hybrid energy storage system controller," Unconv. Resour., vol. 4, p. 100077, 2024, doi: 10.1016/j.uncres.2024.100077.

[52] S. Poudel, M. Mukherjee, and A. P. Reiman, "A Fairness-Based Distributed Energy Coordination for Voltage Regulation in Distribution Systems," in 2022 IEEE Green Technologies Conference (GreenTech), Houston, TX, USA: IEEE, Mar. 2022, pp. 45–50. doi: 10.1109/GreenTech52845.2022.9772030.

[53] S. Poudel, M. Mukherjee, R. Sadnan, and A. P. Reiman, "Fairness-Aware Distributed Energy Coordination for Voltage Regulation in Power Distribution Systems," IEEE Trans. Sustain. Energy, vol. 14, no. 3, pp. 1866–1880, Jul. 2023, doi: 10.1109/TSTE.2023.3252944.

[54] E. E. E. Ahmed, A. Demirci, and G. Poyrazoglu, "Limitations of Overvoltage Mitigation Methods in High PV Penetration LV Distribution Networks," in 2024 IEEE Kansas Power and Energy Conference (KPEC), Manhattan, KS, USA: IEEE, Apr. 2024, pp. 1–4. doi: 10.1109/KPEC61529.2024.10676197.

[55] P. Srivastava, R. Haider, V. J. Nair, V. Venkataramanan, A. M. Annaswamy, and A. K. Srivastava, "Voltage regulation in distribution grids: A survey," Annu. Rev. Control, vol. 55, pp. 165–181, 2023, doi: 10.1016/j.arcontrol.2023.03.008.

[56] G. Fusco, M. Russo, and M. De Santis, "Decentralized Voltage Control in Active Distribution Systems: Features and Open Issues," Energies, vol. 14, no. 9, p. 2563, Apr. 2021, doi: 10.3390/en14092563.

[57] A. Bedawy, N. Yorino, K. Mahmoud, and M. Lehtonen, "An Effective Coordination Strategy for Voltage Regulation in Distribution System Containing High Intermittent Photovoltaic Penetrations," IEEE Access, vol. 9, pp. 117404–117414, 2021, doi: 10.1109/access.2021.3106838.

[58] S. Mahdavi, H. Panamtash, A. Dimitrovski, and Q. Zhou, "Predictive Coordinated and Cooperative Voltage Control for Systems With High Penetration of PV," IEEE

Trans. Ind. Appl., vol. 57, no. 3, pp. 2212–2222, May 2021, doi: 10.1109/TIA.2021.3064910.

[59] V. Muthukaruppan, Y. Shi, and M. Baran, "A Supervisory Volt/VAR Control Scheme for Coordinating Voltage Regulators with Smart Inverters on a Distribution System," 2022, arXiv. doi: 10.48550/ARXIV.2209.10681.

[60] A. Prasad and O. Singh, "Analysis of Software Tools Used for Load-Flow Studies," in 2022 4th International Conference on Advances in Computing, Communication Control and Networking (ICAC3N), Greater Noida, India: IEEE, Dec. 2022, pp. 2400–2405. doi: 10.1109/ICAC3N56670.2022.10074587.

[61] A. Kuanar, B. Panda, and D. Behera, "Comparison of Simulation Tools for Load Flow Analysis," in 2021 1st International Conference on Power Electronics and Energy (ICPEE), Bhubaneswar, India: IEEE, Jan. 2021, pp. 1–5. doi: 10.1109/ICPEE50452.2021.9358568.

[62] C. A. P. Chitacapa, S. P. Z. Asanza, E. M. L. Guamán, B. D. J. León, J. B. Leite, and J. F. F. Baquero, "Rooftop Solar PV Hosting Capacity Analysis in MV-LV Distribution Networks Using Quasi-Static Time-Series Simulation," in 2023 IEEE PES Innovative Smart Grid Technologies Latin America (ISGT-LA), San Juan, PR, USA: IEEE, Nov. 2023, pp. 80–84. doi: 10.1109/ISGT-LA56058.2023.10328352.

[63] R. Broderick et al., "Rapid QSTS Simulations for High-Resolution Comprehensive Assessment of Distributed PV," SAND--2021-2660, 1773234, 695025, Mar. 2021. doi: 10.2172/1773234.

[64] F. Masic, M. Saric, J. Hivziefendic, and Z. Dzemic, "Hosting capacity in smart distribution systems using OpenDSS tool and Monte Carlo-based methodology," Sci. Technol. Energy Transit., vol. 80, p. 2, 2025, doi: 10.2516/stet/2024090.

[65] R. E. De-Jesús-Grullón, R. O. Batista Jorge, A. Espinal Serrata, J. E. Bueno Díaz, J. J. Pichardo Estévez, and N. F. Guerrero-Rodríguez, "Modeling and Simulation of Distribution Networks with High Renewable Penetration in Open-Source Software: QGIS and OpenDSS," Energies, vol. 17, no. 12, p. 2925, Jun. 2024, doi: 10.3390/en17122925.

[66] J. L. Nascimento, A. G. De Freitas Filho, C. S. Sobrinho, J. B. Almada, and H. M. De Oliveira Filho, "Voltage Profile on a Feeder with the Insertion of Photovoltaic Distributed Generation," in 2021 14th IEEE International Conference on Industry Applications (INDUSCON), São Paulo, Brazil: IEEE, Aug. 2021, pp. 1222–1227. doi: 10.1109/INDUSCON51756.2021.9529392.

[67] E. A. Amako, A. Arzani, and S. M. Mahajan, "Optimal Sizing of PV Systems in a Utility Distribution Feeder Using OpenDSS," in 2024 56th North American Power

Symposium (NAPS), El Paso, TX, USA: IEEE, Oct. 2024, pp. 1–6. doi: 10.1109/NAPS61145.2024.10741784.

[68] X. Xu, T. Zhang, Z. Qiu, and H. Gao, "A Co-Simulation Framework for Distribution Network Analysis: Case Study of Hosting Capacity Analysis," in 2023 China Automation Congress (CAC), Chongqing, China: IEEE, Nov. 2023, pp. 6558–6562. doi: 10.1109/CAC59555.2023.10451457.

[69] C. A. P. Chitacapa, S. P. Z. Asanza, E. M. L. Guamán, B. D. J. León, J. B. Leite, and J. F. F. Baquero, "Rooftop Solar PV Hosting Capacity Analysis in MV-LV Distribution Networks Using Quasi-Static Time-Series Simulation," in 2023 IEEE PES Innovative Smart Grid Technologies Latin America (ISGT-LA), San Juan, PR, USA: IEEE, Nov. 2023, pp. 80–84. doi: 10.1109/ISGT-LA56058.2023.10328352.

[70] J. A. Azzolini, M. J. Reno, N. S. Gurule, and K. A. W. Horowitz, "Evaluating Distributed PV Curtailment Using Quasi-Static Time-Series Simulations," IEEE Open Access J. Power Energy, vol. 8, pp. 365–376, 2021, doi: 10.1109/OAJPE.2021.3111821.

[71] R. Broderick et al., "Rapid QSTS Simulations for High-Resolution Comprehensive Assessment of Distributed PV," SAND--2021-2660, 1773234, 695025, Mar. 2021. doi: 10.2172/1773234.

[72] H. Martinho, R. Loonen, and J. Hensen, "Evaluating the impact of high-resolution irradiation data on the daylight performance assessment of adaptive solar shading systems," Build. Environ., vol. 262, p. 111816, Aug. 2024, doi: 10.1016/j.buildenv.2024.111816.

[73] S. Ebrahimi, S. M. S. Ullah, and F. Ferdowsi, "Adaptable Volt-VAR control digital twinning for smart solar inverters," Renew. Energy Focus, vol. 48, p. 100525, Mar. 2024, doi: 10.1016/j.ref.2023.100525.

[74] M. Chen, S. Ma, R. Ayyanar, and V. Vittal, "Integrative Simulation of Inverter-Based PV Systems and Unbalanced Distribution System with Adaptive Step Size Framework in OpenDSS," in 2023 IEEE Power & Energy Society General Meeting (PESGM), Orlando, FL, USA: IEEE, Jul. 2023, pp. 1–5. doi: 10.1109/PESGM52003.2023.10252693.

[75] R. Weber, S. Gejo, R. Gehring, and L. Mikelsons, "Identification and Elimination of Instabilities During Simulation of Highly Stiff Vehicle Electrical Power System Models," presented at the The 16th International Modelica&FMI Conference, September 8 – 10, 2025, Lucerne University of Applied Sciences and Arts (HSLU), Oct. 2025. doi: 10.3384/ecp218961.

[76] F. Scarlatache, G. Grigoraş, V. A. Scarlatache, and V. Dandea, "Digital Twin-based Decision-Making Methodology for the Optimal Operation of Microgrids," in 2023

10th International Conference on Modern Power Systems (MPS), Cluj-Napoca, Romania: IEEE, Jun. 2023, pp. 1–5. doi: 10.1109/MPS58874.2023.10187426.

[77] N. Kamunya, C. Maina, and D. Kimemia, "Adaptive Active Power Control for Aligning Photovoltaic Output with Consumer Demand in Rural Feeders," Electr. Eng. Energy ELENE, p. 2, Mar. 2026, doi: 10.64470/elene.2026.27.

[78] S. A. Juma, S. P. Ayeng'o, and C. Z. M. Kimambo, "Research Gaps and Directions on Mini-Grid Control Strategies for Isolated Communities in Developing Countries," in 2024 IEEE PES/IAS PowerAfrica, Johannesburg, South Africa: IEEE, Oct. 2024, pp. 1–5. doi: 10.1109/PowerAfrica61624.2024.10759468.

[79] G. Pillai, M. Allison, T. P. Tun, K. Chandrakumar Jyothi, and E. Kollonoor Babu, "Facilitating higher photovoltaic penetration in residential distribution networks using demand side management and active voltage control," Eng. Rep., vol. 3, no. 10, p. e12410, Oct. 2021, doi: 10.1002/eng2.12410.

[80] D. Stanelytė and V. Radziukynas, "Analysis of Voltage and Reactive Power Algorithms in Low Voltage Networks," Energies, vol. 15, no. 5, p. 1843, Mar. 2022, doi: 10.3390/en15051843.

[81] O. Dzobo, L. Tivani, and L. Mbatha, "A review of smart inverter capabilities for managing high levels of distributed energy resource integration in South Africa's power grid," J. Energy South. Afr., vol. 34, no. 1, pp. 1–20, Oct. 2024, doi: 10.17159/2413-3051/2023/v34i1a18055.

[82] R. Xavier, B. Bekker, and M. J. Chihota, "The Value of Smart Inverter Control in Distribution Energy Management Systems and Virtual Power Plants, and Opportunities for South Africa," in 2021 56th International Universities Power Engineering Conference (UPEC), Middlesbrough, United Kingdom: IEEE, Aug. 2021, pp. 1–6. doi: 10.1109/UPEC50034.2021.9548163.

[83] Electric Power Research Institute (EPRI), "Open Distribution System Simulator (OpenDSS Reference Manual," EPRI, Palo Alto,CA,USA, Tech .Rep 3002028411, 2024.

[84] A. Okemo, C. M. Muriithi, and J. Nderu, "Automated Conversion of Unstructured Geospatial Feeder Data into Analytical Models: An 11 kV Case Study," Electr. Eng. Energy ELENE, p. 1, Jan. 2026, doi: 10.64470/elene.2026.20.

[85] Energy Regulatory Commission (ERC), Kenya National Distribution Grid Code. 2017,pp. 42–45.

APPENDICES

Appendix 1: OpenDSS Master Script and Component Definitions

(Master_Muranga11kV.dss)

```
!============================================================
! APPENDIX 1: MASTER CIRCUIT DEFINITION AND COMPONENT SCRIPT
!============================================================
Clear
! Define the primary 11 kV circuit base
New Circuit.Muranga_Feeder basekv=11.0 pu=1.0
! Substation source definition
New Vsource.Source bus1=SubBus1 basekv=33.0 pu=1.0 phases=3
! 33/11 kV transformer configuration with OLTC parameters
New Transformer.SubTx phases=3 windings=2 xhl=0.08
~ wdg=1 bus=SubBus1 conn=Delta kv=33.0 kva=5000 %r=0.5
~ wdg=2 bus=MVBus   conn=Wye   kv=11.0 kva=5000 %r=0.5
~ Tap=1 maxtap=16 tapstep=0.00625
! Line code constants and physical line topology
New LineCode.ACSR_50 r1=0.642 x1=0.352 c1=0.01 units=km
New Line.FeederTrunk  Bus1=MVBus Bus2=Bus87  LineCode=ACSR_50
Length=12.8 Units=km
New Line.FeederBranch Bus1=Bus87 Bus2=Bus158 LineCode=ACSR_50
Length=18.5 Units=km
! Distributed consumer loads
New Load.L_Bus87  Bus1=Bus87  Phases=3 kV=11.0 kW=380 kvar=120 Model=1
daily=Rural_Load_Profile
New Load.L_Bus158 Bus1=Bus158 Phases=3 kV=11.0 kW=210 kvar=70  Model=1
daily=Rural_Load_Profile
! PV system modelling at Bus 87 (1 MW)
New PVSystem.PV87 bus1=Bus87 phases=3 kv=11.0 kva=1000
~ irradiance=Irradiance_Profile.csv pmpp=1000
! InvControl object coordinating the Volt-VAR and Volt-Watt loops
New InvControl.Inv87 PVSystem=PV87 mode=VOLTVAR
~ refbus=Bus87 v1=0.90 v2=1.01 v3=1.04 v4=1.20
~ q1=0.0 q2=0.0 q3=-0.44 q4=-0.44
! Link the secondary Volt-Watt curve to the control instance
New XYCurve.VW_curve npts=4 xarray=[0.80, 1.02, 1.05, 1.20] yarray=[1.00, 1.00,
0.00, 0.00]
Set Control=InvControl.Inv87 VoltWatt=yes VoltWattCurve=VW_curve
! QSTS configuration: 1-minute steps over 24 hours (1,440 steps)
Set mode=daily stepsize=1m number=1440
Solve
```

Note: the control setpoints defined in this script (Volt-VAR 0.90/1.01/1.04/1.20 p.u. with reactive output 0.00/0.00/-0.44/-0.44 p.u., and Volt-Watt 0.80/1.02/1.05/1.20 p.u. with active output 1.00/1.00/0.00/0.00) are the values reported in Table 3.4, Table 4.3 and

Appendix 4, and the QSTS configuration of 1-minute steps over 1,440 steps is the resolution reported throughout Chapters 3 and 4.

Appendix 2: System Data and Model Validation Tables

Model validation at peak load (Hour 18, 15 March 2025)

Measurement point	Utility data profile (p.u.)	Simulation model output (p.u.)	Calculated error (%)
Substation 11 kV bus	0.982	0.978	0.41
Bus 87	0.945	0.937	0.85
Bus 158 (end of feeder)	0.912	0.905	0.77
Aggregate MAPE (equation 3.3a)	–	–	0.68
Aggregate RMSE (equation 3.3b)	–	0.0066 p.u.	0.70
Acceptance criterion (Section 3.5.2)	–	–	≤ 2.00

These values are identical to those reported in Table 3.2 of Chapter 3, and the aggregate metrics and acceptance criterion are repeated here so that the appendix and the chapter are consistent.

Appendix 3: Solar Irradiance Profiles

Hourly Global Horizontal Irradiance (GHI)

Running hour	**GHI (W/m2)**	**Running hour**	**GHI (W/m2)**
Hours 0-5	0	Hour 12	980
Hour 6	50	Hour 13	950
Hour 7	200	Hour 14	850
Hour 8	450	Hour 15	600
Hour 9	700	Hour 16	350
Hour 10	850	Hour 17	150
Hour 11	920	Hours 18-23	0

Source: Typical Meteorological Year for Murang'a County (Kenya Meteorological Department, 2020). The hourly record was linearly interpolated to the 1-minute QSTS step, as stated in Section 3.4.

Appendix 4: Control Curve XYCurve Definitions (OpenDSS format)

```
!============================================================
! APPENDIX 4: EXPLICIT PIECEWISE DROOP CONTROL
CHARACTERISTICS
!============================================================
! Volt-VAR piecewise droop function mapping (absorption-only loop)
New XYCurve.VV_curve npts=4
~ xarray=[0.90, 1.01, 1.04, 1.20]
~ yarray=[0.00, 0.00, -0.44, -0.44]
! Volt-Watt active power curtailment characteristic
New XYCurve.VW_curve npts=4
~ xarray=[0.80, 1.02, 1.05, 1.20]
~ yarray=[1.00, 1.00, 0.00, 0.00]
```

Appendix 5: OLTC Tap Operation Log

OLTC tap changes over 24 hours (1-minute sampling resolution)

Operational scenario	**Total mechanical tap operations count**	**Change relative to Scenario A**
Scenario A: baseline configuration (zero PV integration)	12 operations	Reference
Scenario B: uncontrolled PV integration (no droop controls)	28 operations	+133.3 %
Scenario C: coordinated smart inverter control active	8 operations	-33.3 %

Note: tap positions are logged every minute over the 1,440 simulation steps. A discrete operation is counted when $|TapPos(t) - TapPos(t-1)| > 0$, in accordance with equation 3.13.

Appendix 6: Approval letter

MURANG'A UNIVERSITY OF TECHNOLOGY
Office of the Director, Postgraduate Studies
E-mail: bps@mut.ac.ke
Website: www.mut.ac.ke
P.O. Box 75-10200
Murang'a, Kenya

Ref: MUT/ARP/PGS/19/2020 /VOL.1 **Date:** 4th May, 2026

Ms. Naomi Muthoni Kamunya-EN400/5795/2022,
School of Engineering and Technology,
Murang'a University of Technology,
P.O. Box 75-10,200
Murang'a.

Dear Ms. Kamunya,

RE: APPROVAL OF RESEARCH PROPOSAL AND SUPERVISORS.

I am pleased to inform you that the Directorate of Postgraduate Studies on 25th February, 2026 considered and approved your Master research proposal entitled ***"Design and Validation of Voltage Control Strategies for Grid-Tied Photovoltaic Integration in Rural Distribution Feeder Using Opendss."*** and appointed the following as supervisors:

1. Prof. Eng. Christopher Maina - Murang'a University of Technology
2. Dr. David Kimemia - Murang'a University of Technology

You may now proceed with your data collection subject to obtaining research permit from NACOSTI, if required. You should also begin consulting your supervisors and submit through them quarterly progress reports to the Director Postgraduate Studies through your CoD and School Dean. Progress Reports forms can be accessed in the Student Portal.

It is the policy and regulations of the University that you observe deadlines. The guidelines on Postgraduate supervision can be accessed in the post graduate Handbook.

Your responsibilities as a student will include, among others;

i. Maintain regular consultation with your supervisor(s), at least once a month
ii. Submit quarterly reports on time, through your supervisors, CoD, Dean and to the Director of Postgraduate Studies;

iii. Ensure quality work all through;
iv. Present your research findings at 2-3 seminars/conferences prior to thesis examination.
v. Publish one article from your research findings in a refereed journal prior to thesis examination.

For any further clarification please contact the undersigned.

Yours Sincerely,

Prof. Geoffrey Muchiri, PhD
Director, Postgraduate Studies
GM/MMK

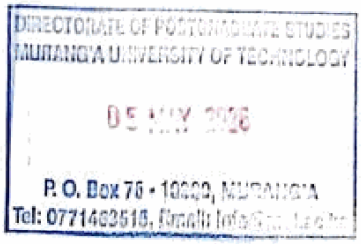

Copy to:
1. Registrar, Academics, Research and Students Affairs
2. Dean, School of Engineering and Technology

Appendix 7: NACOSTI License

REPUBLIC OF KENYA

NATIONAL COMMISSION FOR SCIENCE,TECHNOLOGY & INNOVATION

Ref No: **469032**

Date of Issue: **14/July/2026**

RESEARCH LICENSE



This is to Certify that Ms.. NAOMI MUTHONI KAMUNYA of Murang'a University of Technology, has been licensed to conduct research as per the provision of the Science, Technology and Innovation Act, 2013 (Rev.2014) in Muranga on the topic: DESIGN AND VALIDATION OF VOLTAGE CONTROL STRATEGIES FOR GRID-TIED PHOTOVOLTAIC INTEGRATION IN A RURAL DISTRIBUTION FEEDER USING OPENDSS for the period ending : 14/July/2027.

License No: **NACOSTI/P/26/4192212**

469032

Applicant Identification Number

Ag. Director General
NATIONAL COMMISSION FOR SCIENCE,TECHNOLOGY & INNOVATION

Verification QR Code

NOTE: This is a computer generated License. To verify the authenticity of this document, Scan the QR Code using QR scanner application.

See overleaf for conditions

Appendix 8: Publication

The following paper has been published from this thesis.

[1] N. Kamunya, C. Maina Muriithi, and D. Kimemia, "Adaptive Active Power Control for Aligning Photovoltaic Output with Consumer Demand in Rural Feeders", Electr. Eng. Energy, vol. 5, no. 2, pp. 155–175, May 2026, doi: 10.64470/elene.2026.27.